Blueprints for Smell: Defining the Architecture of the Necklace Olfactory System

Blueprints for Smell: Defining the Architecture of the Necklace Olfactory System

A dissertation presented

by

Taralyn Marie Tan

to

The Division of Medical Sciences

in partial fulfillment of the requirements

for the degree of

Doctor of Philosophy

in the subject of

Neurobiology

Harvard University

Cambridge, Massachusetts

August 2016

Dissertation Advisor: Dr. Sandeep Robert Datta Taralyn Marie Tan

Blueprints for Smell: Defining the Architecture of the Necklace Olfactory System

Abstract

Animals must extract salient information from complex environments in order to generate adaptive behaviors. Mice have evolved multiple olfactory subsystems that enable detection and discrimination of a vast range of chemical stimuli. Although distinct olfactory subsystems detect overlapping subsets of odor space, the specific perceptual functions of each subsystem – and how subsystems interact with one another – remains largely unknown.

The GC-D "necklace" olfactory subsystem detects odorants from mates, predators, and food, suggesting it may play an important role in mediating innate behaviors. However, this subsystem is also required for a specific form of olfactory social learning. Olfactory sensory neurons (OSNs) of the GC-D subsystem detect odorants via molecular mechanisms distinct from those of conventional OSNs. Consistent with a specialized role in olfactory processing, the GC-D subsystem also exhibits atypical anatomical organization: GC-D OSNs are concentrated within isolated regions of the nasal epithelium, and unlike canonical OSNs – whose axons converge onto a small number of isolated foci (called glomeruli) within the olfactory bulb (OB) – GC-D neurons project axons to a "necklace" of 25-40 seemingly interconnected

glomeruli that encircle the caudal OB. The neural circuitry beyond the OB that decodes information from necklace glomeruli is completely unknown.

To define the organizing principles by which this subsystem processes olfactory information, we combined novel surgical approaches and an electroporation cell-labeling technique with retrograde and trans-synaptic viral reagents to trace the connectivity of the necklace glomeruli. We find that individual GC-D glomeruli are presynaptically innervated by spatially dispersed OSN populations and postsynaptically are heavily interconnected with both GC-D and other atypical glomeruli within the OB; these features define physical substrates for integration of peripheral olfactory signals both within the GC-D necklace system and between multiple olfactory subsystems. Centrally, the GC-D subsystem projects to canonical brain targets of the main (but not the accessory) olfactory system; however, it also projects to unique septal targets within the basal forebrain, in part synapsing with cholinergic neurons. The GC-D subsystem is therefore – through peripheral mechanisms to broadly sample sensory channels and privileged access to central behavioral circuits – uniquely poised to direct behavioral responses to ethologically salient cues.

TABLE OF CONTENTS

TABLE OF CONTENTS

ACKNOWLEDGEMENTS

First I would like to thank my advisor, Bob Datta, for giving me the opportunity to work with him the past five-plus years. In the lab, Bob is a brilliant scientist, a fantastic writer, and an incredibly enthusiastic person, and I was lucky to be the beneficiary of all of these traits. Outside of lab, Bob loves haunted houses more than I think is healthy, he is surprisingly gifted at Rock Band, and he is a mediocre Boda Borg player. (Hey, we can't all be perfect.) Bob's commitment to fostering lab camaraderie through lab dinners and recreational outings certainly brought the lab closer together and improved the richness of both scientific and social interactions among lab members.

Bob challenges members of his lab to be creative and fearless, and he provides us resources to pursue even the craziest ideas, knowing that the paths less traveled often reveal the most interesting biology. I have grown so much as a scientist and a person since joining Bob's lab, and I have truly enjoyed the transformation from mentee to colleague. Thank you for everything you've taught me.

Bob should also be credited with assembling a fantastic group of people within the lab without whom graduate school would not have been nearly as enjoyable. As part of the initial cohort to pass through the Datta lab, I have absolutely loved the close relationships with lab members that have developed over the years. My labmates are truly a second family to me, as we talk science together, exercise together, and hang out together. A special shout-out to fellow grad students Stan Pashkovski, Alex Wiltschko, Dan Bear, and Masha Bloom for being great classmates and friends, and for always being available and willing to discuss experimental troubleshooting, science, or

life over a cup of coffee (or a bottle of beer). Thanks also to all of the postdocs – Paul Greer, Andrew Giessel, Giuliano Iurilli, Tatsuya Tsukahara, and Jeff Markowitz – from whom I've learned so much. I would also like to thank the wonderful undergraduate students with whom I've had the privilege to work: Kristen Drummey, Neha Bhagat, Jesse Katon, and Alex Williams. Your enthusiasm is contagious and your hard work has been critical to get this project to where it is today. I couldn't have done it without you. Finally, thanks to Allison Petrosino, Ally Nowlan, and Neha Bhagat for making sure the lab continued to run.

I would like to thank my scientific mentors from Oregon State University, as I would not be where I am today without them. I'd like to thank Fred Stormshak (aka Stormy) for letting me work in his lab as an undergraduate, and for letting me wrangle sheep even though I was the molecular biologist of the group. Stormy always treated me like a graduate student and a scientist in my own right, even as I was just getting started, and his support was a critical factor in my wanting to go to graduate school. Similarly, Kevin Ahern and Indira Rajagopal have been invaluable as mentors and friends throughout my time at OSU and into the present day. Kevin and Indira continue to inspire me with their dedication to education and their love for their students. They have given me more opportunities and supported me in more ways than I can enumerate here. So thank you for everything.

Thank you to the various mentors I've had here at Harvard, too. Thanks to Qiufu Ma for his guidance and mentorship while I was a research technician in his lab. My time in Qiufu's lab instilled in me a love for sensory neurobiology and introduced me to

the wonderful neuroscience community in the Longwood area. Thanks to members of my Dissertation Advisory Committee – Rick Born, Steve Liberles, and Brad Lowell – who have been with me since my qualifying exam and have been incredibly supportive of my science throughout graduate school. Thanks to Rick for staying on as Chair of my Dissertation Exam Committee, and thank you to the members of my Exam Committee – Venkatesh Murthy, Michael Do, and James Schwob – for reading my dissertation and discussing my work with me.

Within the Program in Neuroscience and Department of Neurobiology I have had the opportunity to be mentored by so many wonderful scientists and people. Thanks to Rick, Rachel Wilson, Roz Segal, and David Ginty for their mentorship and friendship, as well as their commitment to all of the students of PiN. Thank you also to Karen Harmin for being a great resource and friend, and for the probably pounds of chocolate that she has provided over the years. PiN students are lucky to have her. A special thanks to Lisa Goodrich, who let me TA for her for three years and who went out of her way to stoke my love of teaching by finding new ways to involve me with the course. Lisa's commitment to her students is inspiring, and I am so impressed by her ability to simultaneously manage a successful research program and lead educational efforts within the graduate program. I am very grateful that I have the opportunity to work with her and learn from her.

Thank you to my classmates and friends who made all of the failed experiments these past six years bearable. I have loved our football parties, board game nights, hiking trips, Friendsgivings, and bowling nights at Jillian's, and I hope our friendships

remain just as strong in the years to come, even as we scatter to the wind after graduate school. Special thanks to Alan Emanuel, Kaori Graybeal, Alex Trott, Leah Kandel, Dan Millman, Milner, Allison Petrosino, Helen Hou, Caroline Wee, Ari Morcos, and Sarah Pease for six years of great memories!

I would also like to thank members of my family (aka the Tan Clan) who have been incredibly loving and supportive throughout my life and during my time in graduate school. Thanks to my parents, Lori and Larry, for all of the sacrifices they've made over the years to be the wonderful parents that they are, and thanks to my fantastic siblings – Jeff, Robbie, Corey, and Sydney – for their friendship and support. To my entire family, thanks for indulging my nerdy tendencies all of these years, and thank you for all of the check-ins and encouraging words throughout this process.

Finally, thanks to the best (or worst, depending on how you look at it) neuroanatomy study partner in the whole world, Ian McLachlan. I may not be an anatomy expert, but I found an amazing person with whom to spend the rest of my life. Ian, you are an incredible friend, husband, and scientist, and I am so lucky to have found such a compatible partner who inspires me, challenges me, and makes everything I do more enjoyable by virtue of your being a part of it. I'm glad your G1 year rumination of, "I don't think I could ever date another neuroscientist" was an empty threat. I love you more than I'll ever be able to adequately express. Thank you so much for being in my life.

LIST OF FIGURES

LIST OF ABBREVIATIONS

2-PT, 2-propylthietane; 2,3-DMP, 2,3-dimethylpyrazine; 2,5-DMP, 2,5-dimethylpyrazine; 2MB, 2-methyl butyric acid; AAA, adeno-associated virus; AC3, adenylate cyclase 3; ACh, acetylcholine; AChE, acetylcholinesterase; aCoA, anterior cortical amygdala; AHN, anterior hypothalamic nucleus; AOB, accessory olfactory bulb; AON, anterior olfactory nucleus; AVP, arginine vasopressin; BAOT, bed nucleus of the accessory olfactory tract; BNST, bed nucleus of the stria terminalis; CAR2, carbonic anhydrase II; ChAT, choline acetyltransferase; ChR2, channelrhodopsin; CNG, cyclic nucleotide-gated; CRFR2, corticotropin-releasing factor receptor 2; CS_2, carbon disulfide; dlPAG, dorsolateral periaqueductal gray; dmPAG, dorsomedial periaqueductal gray; dmVMH, dorsomedial portion of the ventromedial hypothalamic nucleus; dPMN, dorsal premammilary nucleus; Ent, entorhinal cortex; EnvA, envelope A protein; EPL, external plexiform layer; ET, external tufted; FPR, formyl peptide receptor; GC-D, guanylate cyclase D; GG, Grueneberg ganglion; GL, glomerular layer; GnRH, gonadotropin-releasing hormone; GPCR, G protein-coupled receptor; Halo, halorhodopsin; hNDB, horizontal limb of the nucleus of the diagonal band; hPAX-P2, human placental antigen X-P2; HRP, horseradish peroxidase; Hy, hypothalamus; IEG, immediate early gene; IHC, immunohistochemistry; JG, juxtaglomerular; LOT, lateral olfactory tract; LSr, lateral septum; M, mitral; MA, magnocellular nucleus; MCL, mitral cell layer; MeA, medial amygdala; MOB, main olfactory bulb; MOE, main olfactory epithelium; MPN, premammilary nucleus; MS, medial septum; MS4A, membrane-spanning, 4-pass A; MSN, medium spiny neuron; MTMT, (methylthio)methanethiol; NAc, nucleus

accumbens; nAChR, nicotinic acetylcholine receptor; NDB nucleus of the diagonal band; nLOT, nucleus of the lateral olfactory tract; NPY, neuropeptide Y; OB, olfactory bulb; OL, olfactory limbus; OMP, olfactory marker protein; OR, olfactory receptor; OSN, olfactory sensory neuron; OT, olfactory tubercle; OTR, oxytocin receptor; Pcdh21, protocadherin 21; PCtx, piriform cortex; PDE, phosphodiesterase; pdMeA, posterodorsal medial amygdala; PEA, 2-phenylethylamine; PG, periglomerular; plCoA, posterolateral cortical amygdala; pmCoA, posteromedial cortical amygdala; pvMeA, posteroventral medial amygdala; RVG, rabies virus glycoprotein; SA, short axon; SBT, 2-*sec*-butyl-4,5-dihydrothiazole; SO, septal organ; STFP, socially transmitted food preference; T, tufted; TAAR, trace amine-associated receptor; TMR, tetramethylrhodamine; TMT, 2,4,5-trimethyl-3-thiazoline; TRP, transient receptor potential; TT, tenia tecta; V1R, vomeronasal type I receptor; V2R, vomeronasal type II receptor; vlVMH, ventrolateral portion of the ventromedial hypothalamic nucleus; vNDB, vertical limb of the nucleus of the diagonal band; VNO, vomeronasal organ; VP, ventral pallidum; vPMN, ventral premammilary nucleus; VSN, vomeronasal sensory neuron

Page intentionally left blank

CHAPTER 1

Introduction

Animals experience the outside world through sensory systems that – via primary sensory neurons that interface directly with stimuli in the environment and a series of central neural relays that construct an internal representation of the world – guide an animal's behavioral choices towards those that maximize survival. The sense of olfaction is the primary sense used by most animals to interact with the external environment, and mice have evolved a number of olfactory subsystems to detect ethologically important chemical stimuli like those signifying the presence of potential mates, predators and food. These specialized cues induce innate, stereotyped behavioral responses (Hashikawa et al., 2016; Li and Liberles, 2015; Liberles, 2014), suggesting that the neural circuits mediating those behaviors – including their physical connections within the brain – are genetically hard-wired. Olfactory subsystems employ a variety of anatomical and molecular configurations to mediate innate behaviors, and we can exploit these organizational differences to gain insight into the specific neural strategies employed by the mammalian brain to convert sensory signals into reliable, yet flexible, behavioral responses.

This introduction will present the organization of the mammalian peripheral olfactory system and describe a number of the olfactory subsystems known to mediate specific behaviors. It will conclude with a description of our current understanding of the higher-order neural circuits that mediate innate odor-evoked behavioral responses, which to date remains incomplete. Much progress towards establishing the general functional roles of various olfactory subsystems has been made; however, the field overall still has a poor understanding of the exact mechanisms by which ethologically

relevant stimuli are encoded in the periphery and decoded by central circuits to elicit appropriate behavioral responses. As described in this chapter, the mouse olfactory system is characterized both by subsystem-specific anatomical and molecular specializations, but also by seemingly parallel or partially redundant circuitry among the subsystems. We hypothesize that this may reflect the fact that individual subsystems uniquely mediate specific aspects of olfactory perception that together facilitate the full expression of complex, odor-evoked behaviors in a context-appropriate manner. To gain insight into this possibility, we seek to identify the specific functional roles of the guanylate cyclase D (GC-D) necklace olfactory subsystem. Towards that end, this dissertation describes our efforts to better define the peripheral and central architecture of the GC-D subsystem.

BLUEPRINTS FOR THE MAMMALIAN PERIPHERAL OLFACTORY SYSTEM

Despite their unique attributes, the various mammalian olfactory subsystems share peripheral organizational principles. Olfactory sensory neurons (OSNs) located within sensory epithelia in the nose express families of receptor proteins that bind to odorant molecules and initiate odor-evoked intracellular signaling events (Ihara et al., 2013). The receptor proteins confer specific odor-response properties onto the OSNs that express them (Bozza et al., 2002). OSNs project axons to segregated clusters of neuropil within the olfactory bulb (OB) of the brain called glomeruli, where they form synapses with second-order projection neurons called mitral and tufted cells (M/T cells) and local interneurons that mediate intrabulbar inhibition (Mombaerts et al., 1996; Nagayama et al., 2014). M/T cells project broadly ramifying axons to a number of regions in the brain, routing olfactory information to downstream circuits (Haberly and Price, 1977; Scalia and Winans, 1975).

The OB is divided into two domains, the main olfactory bulb (MOB) and the accessory bulb (AOB). The AOB is innervated exclusively by the vomeronasal olfactory subsystem and is described in more detail later in this chapter. The OSNs of the remaining olfactory subsystems project to glomeruli within the MOB, though the subsystems differ in the positions and numbers of glomeruli innervated therein. In general, each glomerulus is innervated by a homogeneous population of OSNs that each expresses the same olfactory receptor protein (Mombaerts et al., 1996; Ressler et al., 1994; Vassar et al., 1994). The activation of different receptors therefore results in activation of the glomeruli innervated by the OSNs expressing those receptors.

Consequently, odors are represented in the OB as stimulus-specific patterns of glomerular activity (Rubin and Katz, 1999).

The MOB is a radial laminated structure composed of (from exterior to interior): the outer nerve layer (ONL), the glomerular layer (GL), the external plexiform layer (EPL), the mitral cell layer (MCL), and the granule cell layer (GCL) (Nagayama et al., 2014). OSN axons travel within the ONL until they innervate their specific glomerulus within the GL. The GL houses three classes of neurons (collectively termed juxtaglomerular (JG) cells) whose cell bodies and processes delineate individual glomeruli: the inhibitory periglomerular (PG) cells and short axon (SA) cells, and the excitatory external tufted (ET) cells. The EPL houses excitatory tufted (T) cells, while the mitral cell layer encompasses both excitatory mitral (M) cells and inhibitory granule (G) cells. The majority of G cells are located within the GCL that comprises the majority of the OB (Cleland, 2014; Ennis and Holy, 2015; Nagayama et al., 2014) **(Fig. 1.1)**. Canonically, each M/T cell extends a single apical dendritic tuft into one glomerulus, and each glomerulus is innervated by a homogeneous population of OSNs. Thus, each glomerulus exists as a segregated channel that processes olfactory information conveyed by a particular sensory neuron type (Mori et al., 1999). A glomerular unit is comprised of thousands of OSN axonal inputs and the dendritic tufts of ~20 M cells, ~50 T cells, and ~1500-2000 JG cells (Ennis and Holy, 2015). Activation of the glutamatergic OSNs results in excitation of the postsynaptic M/T projection neurons; however, the pattern of M/T cell activity is not a perfect copy of OSN activation. Instead, the OSN-to-M/T cell transformation is modulated by other cell types within the OB.

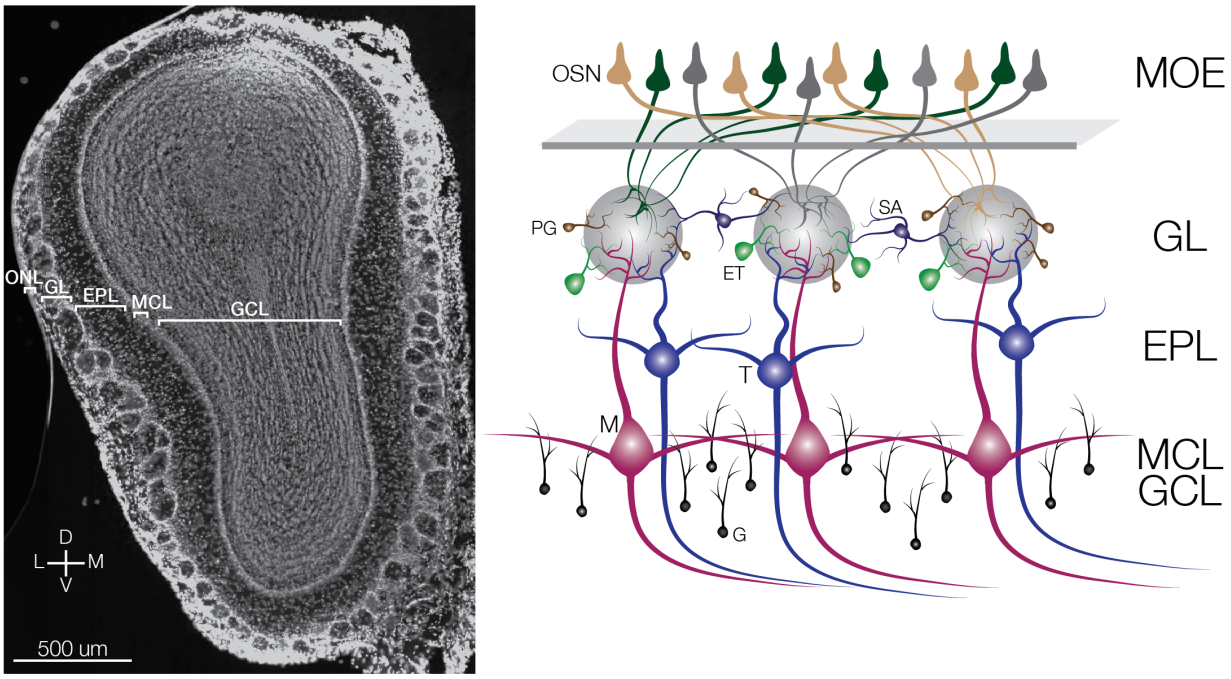

Figure 1.1. Organization and Cell Types of the Main Olfactory Bulb

(Left) Layers of the MOB labeled in a coronal section of the mouse MOB stained with the nuclear marker DAPI. (Right) Schematic of major cell types within the olfactory bulb. Abbreviations: ONL, outer nerve layer; GL, glomerular layer; EPL, external plexiform layer; MCL, mitral cell layer; GCL, granule cell layer; PG, periglomerular cell; ET, external tufted cell; SA, short axon cell; T, tufted cell; M, mitral cell; G, granule cell.

For example, OSNs also synapse onto and activate inhibitory PG interneurons, which in turn inhibit both M/T cells via dendrodendritic synapses and the OSNs themselves. Feed-forward inhibition of M/T cells appears to act as a filtering mechanism to promote M/T firing only in response to strongly activating OSN signals (Cleland, 2014; Shao et al., 2013). At moderate levels of OSN activation, the PG inhibition prevails and can prevent M/T action potentials (Gire and Schoppa, 2009). Notably, this mechanism of contrast enhancement is subject to modulation by centrifugal inputs to the OB, such as cholinergic projections from the basal forebrain (D'Souza and Vijayaraghavan, 2014). Thus, olfactory signals can be modulated in a state-dependent manner even before they are passed to downstream circuits.

M/T responses are further differentiated from their OSN inputs because individual glomerular channels are not completely isolated from one another. M/T cells extend lateral dendrites within the EPL that extend up to 10-12 glomeruli widths (Wilson and Mainen, 2006). During M/T cell activation, these lateral dendrites release glutamate and activate G cells that form reciprocal dendrodendritic synapses with M/T cells. G cells therefore inhibit the initially excited M/T cells and mediate lateral inhibition of M/T cells located a significant distance from the activated glomerulus (Ennis and Holy, 2015). These intrabulbar transformations sparsen the odor-evoked patterns of M/T activity (specifically, changes in firing rates) relative to the primary OSN representation (Cleland, 2014). However, M/T cells exhibit different types of odor-evoked responses, like changes in spike timing (Cury and Uchida, 2010; Shusterman et al., 2011), so the exact transformation that occurs between OSNs and M/T cells is even more nuanced.

UNIQUE ORGANIZATIONS OF MOUSE OLFACTORY SUBSYSTEMS

The mouse olfactory system is comprised of four anatomically segregated subsystems defined by the location of their OSNs within different sensory structures of the nose: the main olfactory epithelium (MOE), the vomeronasal organ (VNO), the septal organ (SO), and the Grueneberg ganglion (GG). Within the MOE and VNO there also exist genetically defined subsystems named for specific molecules expressed by unique populations of OSN. These include the GC-D, trace amine-associated receptor (TAAR), and transient receptor potential (TRP) subsystems within the MOE, and the formyl peptide receptor (FPR) subsystem within the VNO (Fülle et al., 1995; Liberles and Buck, 2006; Liberles et al., 2009; Lin et al., 2007; Omura and Mombaerts, 2014; Rivière et al., 2009). The various olfactory subsystems differ not only in their molecular mechanisms used to detect and transduce specific olfactory signals, but also in their projections to the OB (**Fig. 1.2**, and text). Many of the subsystems are described below, with particular attention given to the two best-studied subsystems – the main and the vomeronasal subsystems – and to the GC-D necklace subsystem, the subject of this dissertation.

The Main Olfactory System

OSNs of the "canonical" mammalian main olfactory system are located within the MOE and detect odorants via the large olfactory receptor (OR) family of G protein-coupled receptors (GCPRs) (Buck and Axel, 1991). The OR family consists of 913 intact genes in mice (Godfrey et al., 2004) and 390 putatively functional ORs in humans

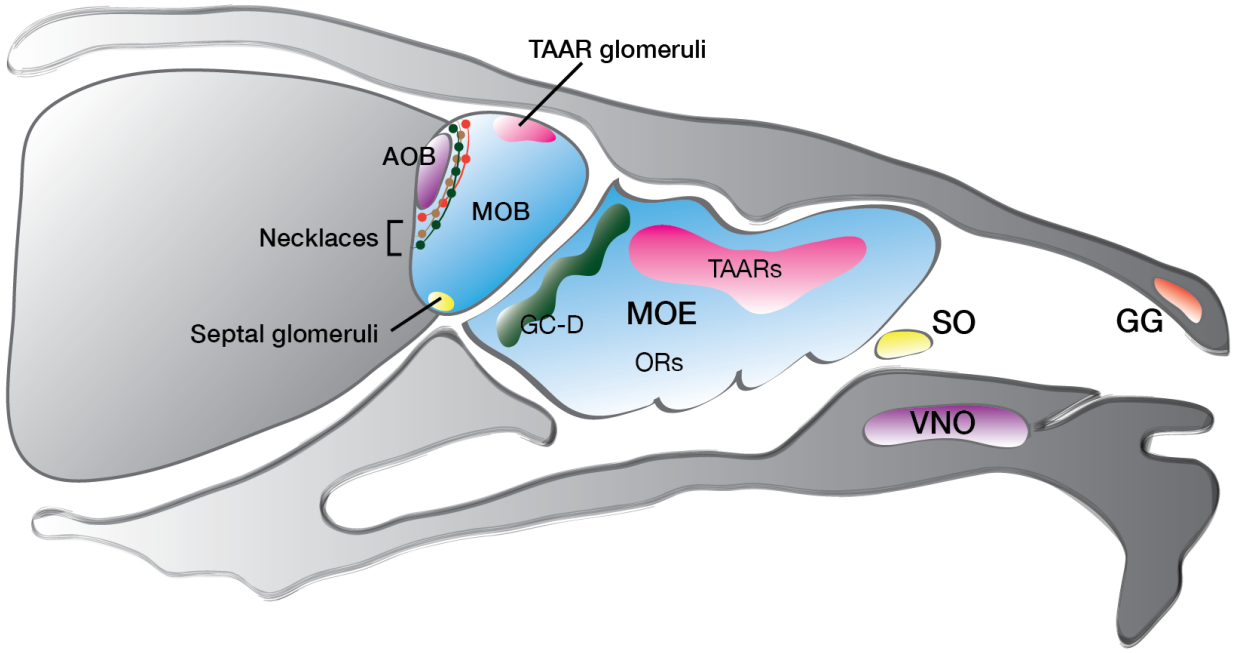

Figure 1.2. Olfactory Subsystems of the Mouse

Schematic of the peripheral organizations of the anatomically segregated olfactory subsystems – the MOE, VNO, GG and SO – and the molecularly distinct GC-D and TAAR subsystems located within the MOE. Note that each subsystem projects to a stereotyped region of the olfactory bulb. Shown in the necklace region of the olfactory bulb are the necklaces corresponding to the GC-D and GG subsystems, as well as the atypical cholinergic glomeruli (tan) whose sensory neurons are unknown.

(Adipietro et al., 2012). The OR proteins localize to specialized cilia endings of the OSN dendrite – the site of odor binding and signal transduction – and they also localize to OSN axon terminals, where they play an instructive role guiding OSN axons to their glomerular targets in the OB (Wang et al., 1998). ORs couple to an olfactory-specific G protein alpha subunit, $G_{\alpha olf}$. Activation of an OR by the binding of an odorant molecule results in an adenylate cyclase-mediated increase in intracellular cAMP and subsequent depolarization of the cell through the activation of a cyclic nucleotide-gated (CNG) nonselective cation channel. Expression of the CNGA2 subunit of this channel is a defining molecular feature of all OSNs within the MOE, with the exception of cells expressing GC-D.

Each OSN expresses only a single allele of a single OR gene (Chess et al., 1994), and this monoallelic pattern of expression ensures that only a single OR species is present in any given cell. Thus, the olfactory receptive field of an individual OSN is entirely defined by the ligand-binding properties of a single type of OR protein. Individual ORs (and therefore individual OSNs) are activated by multiple odorants, as demonstrated by single-unit recordings of OSNs *in vivo* (Duchamp-Viret, 1999) and by calcium imaging in dissociated OSNs (Malnic et al., 1999; Nara et al., 2011). Similarly, individual odorants activate multiple receptor species. Within the MOE, cells that express a given OR are confined within large, circumscribed zones that are roughly organized along the dorsal-ventral axis; however, there is no fine topographical organization within each zone (Ressler et al., 1993; Vassar et al., 1993). Individual monomolecular odorants therefore recruit broad, randomly distributed activity in the

MOE, corresponding to the activation of multiple OSN populations.

An obvious transformation in the organization of olfactory information occurs between the MOE and the OB. As mentioned in the previous section, the axons of the broadly distributed cells expressing the same OR converge onto a small number of glomerular foci within the MOB, which range in size from ~50-120 μm in diameter (Royet et al., 1988). In general, each population of OR-expressing cells targets two mirror-symmetric glomeruli. The position of each glomerulus is genetically defined – specified in part by the OR itself – and the position of a glomerulus corresponding to a specific OR is consistent across the two OBs of a given mouse and largely stereotyped across animals (Imai and Sakano, 2007; Wang et al., 1998). Therefore, the odor-specific patterns of glomerular activation are stereotyped across mice (although with some local variations (Soucy et al., 2009)) forming a reliable "map" of odor-driven activity (Bozza et al., 2002; Mombaerts, 2006). These reproducible, odor-specific glomerular activity maps provide an anatomical basis for odor discrimination by downstream brain regions (Giessel and Datta, 2014; Uchida et al., 2014).

The rules by which glomeruli are organized within the OB are still poorly understood, though there is evidence that glomeruli of the main olfactory system may be organized according to chemical properties of the odorants that activate those glomeruli (a chemotopic map) and/or according to OR tuning properties (a tunotopic map) (Ma et al., 2012; Mori et al., 2006). One study suggested that the MOB might be broadly divided into functionally distinct dorsal and ventral domains that mediate innate versus learned behaviors, respectively (Kobayakawa et al., 2007); however, a subsequent

study demonstrated that the ventral MOB is required for innate social and defensive behaviors (Matsuo et al., 2015). On a finer spatial scale, the proper targeting of OSN axons to their normal glomerular locations within a given OB domain also appears to be required for normal behavioral responses (Cho et al., 2011).

The main olfactory system is the primary means by which the animal detects small volatile molecules in the environment. Two primary roles of the main olfactory system are to facilitate odor discrimination and olfactory learning for the vast number of general chemical stimuli encountered by the animal (Giessel and Datta, 2014). In addition, behaviorally relevant stimuli – including the volatile pheromones α-farnesene, 2-heptanone, and (methylthio)methanethiol (MTMT); the predator odorant 2,4,5-trimethyl-3-thiazoline (TMT); and the spoiled food odorants pentanal and 2-methyl butyric (2MB) acid – also activate cells within the main olfactory system (Kobayakawa et al., 2007; Lin et al., 2004; Nara et al., 2011).

Experiments in which populations of OSNs innervating particular domains of the mouse OB were genetically ablated demonstrated that glomeruli within the dorsomedial MOB are both necessary and sufficient to mediate innate aversion of pentanal and 2MB acid, and the dorsal MOB is required for innate, but not learned, avoidance of TMT (Kobayakawa et al., 2007). *Cnga2-/-* mice – in which odor-evoked signaling is ablated in the majority of cells in the MOE, including OR-expressing cells – also exhibit deficits in mating behaviors and aggression (Mandiyan et al., 2005). Thus, the main olfactory system is both essential for general odor detection and required to mediate innate behavioral responses to a subset of ethologically important odorants.

Specialized Cells within the MOE

The MOE houses a number of molecularly distinct, non-OR-expressing populations of OSNs that also respond to ethologically important stimuli. For example, one population of cells expresses members of the TAAR family of GPCRs as their olfactory receptors. Of the fifteen *Taar* genes in the mouse, fourteen are expressed in the MOE (Liberles and Buck, 2006). Like ORs, TAARs are monoallelically expressed in a one receptor per neuron fashion (Johnson et al., 2012). Cells expressing the same TAAR are broadly distributed within the MOE and their axons converge onto a small number of stereotyped glomeruli within a restricted dorsomedial domain of the MOB (Liberles and Buck, 2006; Pacifico et al., 2012).

The TAAR subsystem mediates both innate attraction and innate aversion in response to specific ethologically relevant ligands. TAAR4-expressing cells respond to the innately aversive predator odorant 2-phenylethylamine (PEA), and TAAR4 itself is required to mediate innate aversion to that cue (Dewan et al., 2013; Ferrero et al., 2011). Similarly, TAAR5 detects an innately attractive pheromone, trimethylamine, and attraction to this odorant is lost in *Taar5-/-* mice (Li et al., 2013). Interestingly, the TAAR4 and TAAR5 glomeruli are adjacent to each other within the OB. This suggests that while the MOB may contain broad, spatially defined functional domains (such as those corresponding to innate versus learned aversion (Kobayakawa et al., 2007)), glomeruli within the MOB are not spatially segregated into domains defined by the behavioral valence of their ligands.

In contrast to TAAR-expressing OSNs – which employ different olfactory

receptors but the same cAMP-dependent signaling pathways as OR-expressing cells – a second population of specialized OSNs within the MOE is characterized by the expression of membrane-bound GC-D and use cGMP-dependent signaling pathways (Juilfs et al., 1997; Meyer et al., 2000). This GC-D subsystem exhibits other pronounced differences with regards to its distribution of cells within the MOE and its glomerular organization within the OB, and is described in much more detail later in this section.

Finally, populations of cells that express members of the TRP channel family have also been identified within the MOE. TRPM5-expressing cells comprise a large population of cells that is activated by volatile urinary pheromones (López et al., 2014) and that project axons to a large number of glomeruli (~500,(Lin et al., 2007)) located primarily within the ventral MOB, a region previously shown by electrophysiology to respond to volatile pheromones (Lin et al., 2006; 2005). TRPC2-expressing cells are also present within the MOE (TRPC2 is a required component of signaling in the VNO), though ligands that activate these cells have not yet been identified. These cells project to a small number of glomeruli (perhaps the usual two) within the posteroventral MOB. Of note, TRPC2 itself marks a heterogeneous population of OSNs comprised of “type A” cells that express adenylate cyclase 3 (and presumably use a cAMP-dependent signaling pathway for odor transduction), and “type B” cells that instead express guanylate cyclase 1b, suggesting that they may employ cGMP-dependent signaling pathways similar to GC-D cells (Omura and Mombaerts, 2015).

The Vomeronasal Olfactory Subsystem

OSNs of the vomeronasal olfactory subsystem are located within the VNO, a fluid-filled, tube-shaped cavity that is located anterior to the MOE and connected to the nasal cavity via a small duct. Olfactory stimuli are actively pumped into the lumen of the VNO, where they are detected by two different classes of GPCRs that are expressed by vomeronasal sensory neurons (VSNs). The sensory epithelium of the VNO is stratified into molecularly and anatomically distinct apical and basal layers. VSNs within the apical VNO express members of the vomeronasal type I (V1R) receptor family, couple to the $G_{\alpha i2}$ G protein, and project axons to the anterior portion of the AOB. Basal VSNs express members of the vomeronasal type II (V2R) receptor family, couple to $G_{\alpha o}$, and project axons to the posterior portion of the AOB. In the mouse the V1R family is comprised of ~200 members, while the V2R family is comprised of ~70 members (Liberles, 2014). Receptor expression in the VNO also generally abides by the "one receptor-one neuron" rule. V1R-expressing cells express only a single allele of a single receptor gene; V2R-expressing cells monoallelically express a unique receptor in addition to a member of the atypical V2RC clade, the members of which have been proposed to function as co-receptors (Ishii and Mombaerts, 2011).

Glomerular organization of the vomeronasal system is quite distinct from the main olfactory system, reflecting specializations that likely facilitate the detection of ethologically relevant odorants. Within the AOB, VSNs that express the same receptor coalesce into glomeruli; however, the average number of glomeruli corresponding to a given receptor ranges from 4-30 for V1R glomeruli in the anterior AOB (Belluscio et al.,

1999; Rodriguez et al., 1999; Wagner et al., 2006), and from 3-10 for V2R glomeruli within the posterior AOB (Del Punta et al., 2002; Haga et al., 2010). While the coarse pattern of glomeruli corresponding to a given receptor is similar across animals, the AOB lacks a stereotypic glomerular map like that present in the MOB (Belluscio et al., 1999; Rodriguez et al., 1999) due to both differences in the positions and the number of glomeruli per VR across animals, as well as structural differences between the AOB and MOB. For example, the EPL and MCL are not clearly separated within the AOB and – likely due to size constraints within the AOB relative to the MOB – glomeruli within the AOB are vertically stacked on top of each other instead of horizontally arranged within a thin layer (Ennis and Holy, 2015).

AOB glomeruli tend to be smaller and more diffuse than MOB glomeruli, with many glomeruli as small as 10 μm in diameter. Individual AOB glomeruli are not as clearly delineated by cell bodies within the glomerular layer relative to MOB glomeruli (Ennis and Holy, 2015; Meisami and Bhatnagar, 1998), and some appear to exist as interconnected, ganglion-like chains (Rodriguez et al., 1999). Furthermore, in contrast to M/T cells of the MOB – each of which innervates only a single glomerulus – AOB M/T cells extend apical dendrites into multiple glomeruli, effectively sampling information across glomeruli (Larriva-Sahd, 2008). In general, a given M/T cell innervates multiple glomeruli expressing the same VR (Del Punta et al., 2002), though additional pooling from glomeruli corresponding to closely related VR species has also been observed (Belluscio et al., 1999; Wagner et al., 2006).

Thus, within the AOB, olfactory information conveyed by a given receptor first

diverges across multiple glomeruli, and subsequently converges by means of M/T cells that also sample glomeruli corresponding to other VRs. This unique glomerular organization – specifically, the use of many glomeruli per receptor – may increase the signal-to-noise of olfactory signals due to recruitment of additional lateral inhibition, and may thus facilitate the recognition of behaviorally important odorants (Del Punta et al., 2002; Kay and Sherman, 2007). Lateral inhibition within the AOB has also been shown to shape the selectivity of AOB cells in response to sex-specific cues (Hendrickson et al., 2008). Similarly, the integration of information from different receptors by M/T cells has been proposed to enable the detection of pheromone mixtures comprised of specific ratios of different molecules (Del Punta et al., 2002; Luo and Katz, 2004).

The vomeronasal subsystem is specialized to detect and mediate innate behaviors to ethologically important stimuli including sex-specific pheromones like the sulfated steroids found in female urine (Nodari et al., 2008) and the male-specific exocrine gland-secreting peptide 1 (ESP1) (Haga et al., 2010), as well as predator-derived odorants like the major urinary proteins (MUPs) (Papes et al., 2010). V1Rs primarily respond to small volatile molecules, while non-volatile chemical cues like peptides and proteins are detected by V2Rs. Within the VR repertoire, many receptors are specifically tuned to particular ethological classes of stimuli: some are selectively activated by sex-specific cues, some by predator odorants, and some by mouse-specific odorants (Haga et al., 2010; Isogai et al., 2011). Of note, the VNO also houses a small population of cells that expresses members of a different family of GPCRs – the formyl peptide receptors (FPRs) – which may be involved in the detection of pathogenic and

inflammation-related compounds (Boillat et al., 2015; Liberles et al., 2009).

Surgical or genetic manipulations that result in loss-of-function of the VNO demonstrate the vomeronasal subsystem's crucial role in eliciting odor-evoked innate behaviors. For example, surgical removal of the VNO impairs aggression, mating behaviors, and ultrasonic vocalizations (Wysocki and Lepri, 1991), while mice null for *Trpc2* – a cation channel required for signal transduction in the VNO – display deficits in aggression, reproductive behaviors and predator avoidance (Ferrero et al., 2013; Isogai et al., 2011; Kimchi et al., 2007; Leypold et al., 2002; Papes et al., 2010). In contrast, *Trpc2-/-* mice (as well as mice lacking $G_{\alpha o}$) exhibit normal behavioral responses to the main olfactory system-activating predator odorant TMT (Papes et al., 2010; Pérez-Gómez et al., 2015), underscoring the fact that the main and vomeronasal subsystems mediate similar behavioral responses – such as defensive behaviors – in response to specific olfactory cues. In addition to its clearly established role in detecting behaviorally important stimuli, the vomeronasal subsystem is also activated by volatile "general odorants" (Trinh and Storm, 2003); thus, like the main olfactory system, the accessory olfactory system serves many functions.

The GC-D "Necklace" Olfactory Subsystem

The GC-D "necklace" olfactory subsystem is comprised of OSNs within the MOE that express membrane-bound GC-D. GC-D cells do not express ORs, nor do they express proteins involved in canonical, cAMP-mediated olfactory signal transduction like adenylate cyclase 3 (AC3), phosphodiesterase 4A (PDE4A) or the cyclic nucleotide-

gated channel alpha 2 subunit (CNGA2). Instead, GC-D cells express the proteins carbonic anhydrase 2 (CAR2), the phosphodiesterase PDE2A, and a different CNG alpha subunit, CNGA3 (Greer et al., 2016).

With the exception of GC-D, which has been shown to act as a receptor in these cells, no other olfactory receptor proteins had been identified in these cells until recently, when our laboratory discovered that GC-D cells express members of the membrane-spanning, 4-pass A (*Ms4a*) gene family, and that these proteins act as chemosensors (Greer et al., 2016). Notably, the MS4As are the first known family of mammalian olfactory receptors that are not GPCRs. Furthermore, of the twelve family members found to be expressed in olfactory tissue (of seventeen annotated *Ms4a* genes in the mouse genome), multiple MS4A proteins are co-expressed in each GC-D cell. This violation of the "one receptor-one neuron" rule of olfactory receptor expression obeyed by other mammalian olfactory systems suggests that the GC-D system employs a unique strategy to detect and convey olfactory signals.

Beyond its molecular oddities, the peripheral anatomical organization of the GC-D subsystem also suggests an atypical sensory coding strategy. Within the MOE, GC-D cells are concentrated within isolated pockets of the caudal epithelium called cul-de-sacs. In the OB, the axons of GC-D cells project to a seemingly interconnected ring of 25-40 glomeruli that encircles the caudal end of MOB (Walz et al., 2007). The "beads-on-a-string" appearance of the GC-D glomeruli is the reason this olfactory subsystem has been termed the GC-D "necklace". The function of this necklace-like glomerular organization is completely unknown, though the discovery of the MS4A receptors and

their ligands will facilitate future functional dissection of this subsystem.

GC-D glomeruli are located just anterior to the AOB, in a region termed the olfactory limbus (OL). Structurally, the OL is a transition region between the MOB and AOB that is characterized, for example, by a progressive collapse of the glomerular, external plexiform and mitral cell layers (Larriva-Sahd, 2012). In many ways the GC-D glomeruli are more similar to AOB glomeruli than to MOB glomeruli, including the number of glomeruli, the lack of stereotypy in their positions and numbers both between the two OBs and across animals, and the existence of diffuse, ganglion-like glomeruli within the necklace (Walz et al., 2007). Thus, the distribution of sensory information across necklace glomeruli may serve similar functions as those proposed for glomeruli within the AOB. However, the necklace glomeruli are not completely analogous to AOB glomeruli due to the expression of multiple olfactory receptors in all GC-D cells (and therefore all glomeruli). Furthermore, it is unknown how information from individual GC-D glomeruli is conveyed to downstream M/T cells. One study reported that M/T cells innervating GC-D glomeruli exhibit the typical, uniglomerular morphology of MOB M/T cells; however, no images of M/T cells were included in the paper (Cockerham et al., 2009). Thus, whether M/T cells within the necklace integrate information from across multiple glomeruli remains an open question.

Thus far, all of the compounds shown to activate GC-D cells carry ethological significance to the mouse, though their biological sources and meanings vary. GC-D itself has been shown to detect CO_2 – an innately aversive odorant – and avoidance to CO_2 is lost in mice lacking a functional CAR2 enzyme (Hu et al., 2007). GC-D also acts

as the receptor for two peptides found in urine and feces, guanylin and uroguanylin. These peptides and carbon disulfide (CS_2, a component of rodent breath that activates GC-D cells via an unknown mechanism) mediate a form of appetitive olfactory learning called socially transmitted food preference (STFP), for which GC-D is required (Arakawa et al., 2013; Munger et al., 2010). STFP is a phenomenon in which scented food that is paired with either uroguanylin or CS_2 is subsequently preferred by a mouse even in the absence of the GC-D ligand. It is "socially transmitted" because CS_2 and uroguanylin are normally encountered during interactions with another mouse, via its breath or its feces, respectively.

Individual MS4A receptors respond to a distinct set of behaviorally important odors like the aversive mouse pheromone 2,5-dimethylpyrazine (DMP) (Zhang et al., 2007), appetitive sulfated steroids found in female urine (Nodari et al., 2008), and appetitive polyunsaturated fatty acids found in food sources of mice in the wild (Sabir et al., 2012). Putative GC-D cells have also been shown to respond to still other attractive pheromones like 2-heptanone and α-farnesene, whose specific receptors have yet to be identified (Gao et al., 2010; Lin et al., 2004). Thus, the GC-D subsystem detects a wide range of ethologically meaningful stimuli that induce a variety of innate behaviors, but the subsystem is also required for a specific form of olfactory learning. How exactly the GC-D necklace subsystem enables innate behaviors or mediates STFP – especially in light of the subsystem's atypical molecular and peripheral anatomical organization – is unknown. A better understanding of the rules by which the GC-D subsystem processes olfactory information will no doubt provide valuable insight into the mechanisms by

which the mammalian brain mediates adaptive responses to ethologically salient stimuli in the environment.

Other “Necklace” Subsystems

The GC-D subsystem is not the only olfactory subsystem that employs a “necklace” of glomeruli. In fact, multiple distinct necklaces have been identified within the same posterior region of the MOB. Cells of the Grueneberg ganglion (GG) – a small patch of epithelial tissue located at the tip of the mouse’s nose – comprise yet another olfactory subsystem that mediates innate responses to the mouse alarm pheromone 2-*sec*-butyl-4,5-dihydrothiazole (SBT) and structurally related predator odorants like TMT and 2-propylthietane (2-PT) (Brechbuhl et al., 2008; Brechbühl et al., 2013; Pérez-Gómez et al., 2015). These cells project axons to a necklace of ~10 glomeruli that resides slightly rostral to the GC-D necklace (Matsuo et al., 2012).

GG cells are, in fact, molecularly similar to GC-D cells, as they also express PDE2A, CNGA3, and a different guanylate cyclase, guanylate cyclase G (GC-G) (Hanke et al., 2013). Somewhat paradoxically, GG OSNs do not have direct access to the nasal cavity, as they are covered by a layer of keratin (Brechbuhl et al., 2008). Thus, the precise mechanism by which odorants reach the OSNs is unknown. Due to the uncharacteristically early development of the GG, and its atrophy in the adult mouse, the GG has been proposed to function primarily in neonatal mice, when odor diffusion to the OSNs might be more easily achieved (Brechbuhl et al., 2008; Fleischer et al., 2007; Fuss et al., 2005).

A third glomerular necklace in the posterior OB was recognized prior to the discovery of the GC-D and GG subsystems and is defined by its dense innervation of centrifugal cholinergic fibers from the basal forebrain. These heavily cholinergic glomeruli have traditionally simply been called the “atypical glomeruli” (Ojima et al., 1988; Zheng et al., 1987). To date, almost nothing is known about these glomeruli, including the identity of the OSNs innervating them. The atypical glomeruli are distinct from the GC-D and GG necklaces (based on lack of PDE2A expression), but they are often located adjacent to PDE2A glomeruli (Juilfs et al., 1997; Salcedo et al., 2011).

Finally, various other early-discovered glomerular necklaces were identified based on strong labeling by antibodies against human placental antigen X-P2 (hPAX – P2) (Shinoda et al., 1993; 1989), as well as by two antibodies (2C6 and MAb 213) whose antigens are unknown (Ring et al., 1997). These markers appear to describe partially overlapping glomerular populations; however no systematic characterization of the relationships among the various necklaces has been conducted. Thus, while we still have much to learn about the identities and functions of the various glomerular necklaces, the existence of multiple, adjacent necklaces within the posterior MOB suggests that the necklaces together may comprise a functionally defined olfactory subsystem that may play a unique role in olfactory perception.

DOWNSTREAM OLFACTORY REGIONS

As described in the previous section, multiple olfactory subsystems including the main, TAAR, TRPM5, vomeronasal, GC-D, and GG subsystems have been shown to detect various types of ethologically meaningful olfactory cues. To understand how innate behaviors are ultimately generated in response to specific olfactory stimuli, one must consider the downstream circuitry of each olfactory subsystem, beginning with the direct targets of the M/T cells. With the exception of one study involving the TRPM5 subsystem (Thompson et al., 2012), only the downstream targets for the canonical main and vomeronasal subsystems have been identified. The extensive body of anatomical literature characterizing the projections from these two subsystem forms the basis of our current understanding of higher-order mammalian olfactory processing in its entirety, including as it relates to the generation of innate behaviors.

The simplest odor-evoked behaviors are attraction and aversion, and these approach or avoidance behaviors each comprise one facet of much more complex behavioral displays such as mating behaviors in response to pheromones or defensive behaviors in response to predator odors, respectively. The known downstream anatomy of the main and vomeronasal olfactory subsystems – as well as our current understanding of the anatomical and functional basis of the general categories of olfactory-mediated innate behaviors mentioned above – is summarized below.

The earliest characterizations of the distribution of OB efferents were made by lesioning the MOB or AOB and assessing regions of axon terminal degeneration. These experiments revealed that the two portions of the OB project to distinct downstream

brain regions. The MOB targets the piriform cortex (PCtx), olfactory tubercle (OT), entorhinal cortex (Ent), and the anterior and posterolateral portions of the cortical amygdala (aCoA and plCoA, respectively); while the AOB projects to the medial amygdala (MeA), the posteromedial portion of the cortical amygdala (pmCoA), the bed nucleus of the accessory olfactory tract (BAOT) and the bed nucleus of the stria terminalis (BNST)(Devor, 1976; Scalia and Winans, 1975). These results have since been confirmed by various anatomical tracing approaches that employ horseradish peroxidase (HRP), diffusible fluorescent dyes, or viruses to label M/T axons and/or cell bodies, and the list of brain regions innervated by the MOB has been expanded to include the tenia tecta (TT), anterior olfactory nucleus (AON), and the nucleus of the lateral olfactory tract (nLOT) (Haberly and Price, 1977; Halpern, 1987; Hintiryan et al., 2012; Igarashi et al., 2012; Lo and Anderson, 2011; Miyamichi et al., 2011; Nagayama et al., 2010; Sosulski et al., 2011; Walz et al., 2006).

These early anatomical characterizations formed the basis of the “dual olfactory hypothesis,” which postulated the existence of two parallel, anatomically segregated olfactory systems that serve unique functions (Halpern, 1987; Scalia and Winans, 1975). The dual olfactory hypothesis remained prominent following the discovery of the OR and VR receptor families in the 1990s, as the detection of general volatile odorants versus pheromones was thought to be exclusively mediated by the main and vomeronasal subsystems, respectively (Buck and Axel, 1991; Dulac and Axel, 1995; Herrada and Dulac, 1997). However, we now know that proposed division to be an oversimplification, as the main olfactory system is required for some pheromone-

mediated (Mandiyan et al., 2005) and predator odor-induced (Kobayakawa et al., 2007; Papes et al., 2010) innate behaviors, and the vomeronasal system also detects general volatile odorants (Trinh and Storm, 2003).

Recent studies have provided (at least in part) an anatomical basis for the mixed abilities of the main and vomeronasal subsystems, as they have demonstrated that the MOB projects to two classically vomeronasal targets – the MeA and the BAOT – and the AOB projects to the aCoA and the nLOT, two targets of the main olfactory system (Kang et al., 2009; 2011; Martínez-Marcos, 2009; Pro-Sistiaga et al., 2007; 2008; Tirindelli et al., 2009). In addition, most brain regions innervated by the MOB are heavily and reciprocally interconnected with two major AOB targets, the MeA and the pmCoA (Cádiz-Moretti et al., 2014; Gutierrez-Castellanos et al., 2014; Martínez-Marcos, 2009; Pro-Sistiaga et al., 2008). Thus, while the main and vomeronasal systems each exhibit clear anatomical and functional specializations, there also exist multiple conduits to pass sensory information between the two processing streams, indicating some common ability by both systems to mediate similar odor-evoked behaviors **(Fig. 1.3)**.

The basic architecture of the neural circuits mediating odor-evoked innate defensive and reproductive behaviors has been delineated, and in particular the MeA has been identified from amongst the secondary olfactory targets as a key node of those circuits (Choi et al., 2005; Hashikawa et al., 2016; Martinez et al., 2011; Sokolowski and Corbin, 2012; Takahashi, 2014; Wu et al., 2009). Briefly, the posterior medial amygdala is anatomically and functionally divided into dorsal (pdMeA) and ventral (pvMeA) regions that mediate reproductive and defensive behaviors,

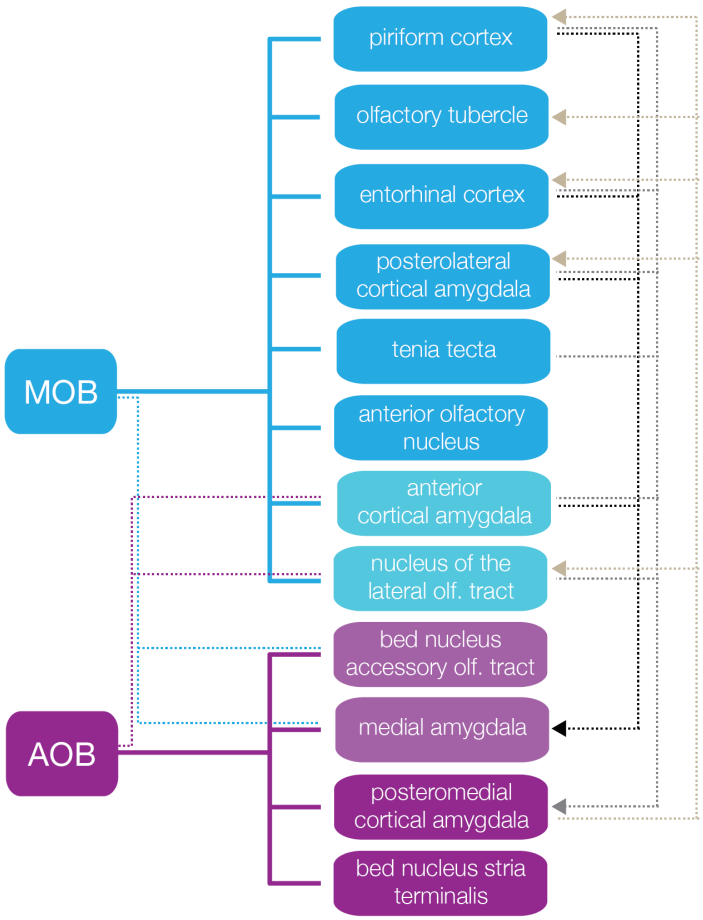

Figure 1.3. Projections of the Main and Vomeronasal Olfactory Systems

Summary of the mitral/tufted cell projections from the main olfactory system (blue) and the vomeronasal system (purple). The blue and purple dotted lines indicate minor projections from one subsystem to brain regions classically targeted by the other subsystem. The primary source of innervation is indicated by the color of the brain region. Dotted lines on the right side of the image depict some of the tertiary connections between main and vomeronasal targets to give a sense of the high degree of crosstalk. Connections shown are not comprehensive. Refer to text for references.

respectively (Bergan et al., 2014; Choi et al., 2005; Meredith and Westberry, 2004).

This anatomical and functional segregation is preserved in downstream hypothalamic and midbrain components of the circuits. Innate defensive behaviors in response to predator cues are mediated by projections from the pvMeA to three highly interconnected hypothalamic nuclei collectively referred to as the “medial hypothalamic defense circuit” (Canteras, 2002): the dorsomedial portion of the ventromedial hypothalamic nucleus (dmVMH), the anterior hypothalamic nucleus (AHN), and the dorsal premammilary nucleus (dPMN). The dPMN in turn projects to a motor control region in the midbrain, the dorsolateral periaqueductal gray (dlPAG), which projects to motor circuitry in the spinal cord (Canteras et al., 1997; Choi et al., 2005; Dielenberg et al., 2001; Gross and Canteras, 2012; McGregor et al., 2004; Pérez-Gómez et al., 2015; Sokolowski and Corbin, 2012; Sukikara et al., 2010).

The expression of sex-specific mating behaviors engages parallel circuitry involving projections from the pdMeA to the ventrolateral VMH (vlVMH), the medial preoptic nucleus (MPN) and the ventral premammilary nucleus (vPMN), the last of which provides the hypothalamic output to midbrain regions like the dorsomedial PAG (dmPAG). (Choi et al., 2005; Lin et al., 2011; Lonstein and Stern, 1998; Sokolowski and Corbin, 2012; Wu et al., 2009). Intriguingly, the vlVMH is also critical for the expression of male-male aggression, though the subsets of cells within this brain region that mediate mating versus aggression are largely non-overlapping, despite being intermingled within the nucleus (Lin et al., 2011). Thus, these two parallel amygdalar-

hypothalamic-midbrain circuits are functionally organized to mediate behaviors in response to predators versus conspecifics, respectively.

The importance of the MeA in generating both defensive and reproductive behaviors underscores the vomeronasal system's specialized role in the detection of predator-derived odorants and pheromones (owing to the major AOB projection to the MeA), and the revelation that the main olfactory system also has direct access to the MeA via direct projections from the MOB (Kang et al., 2009; Pro-Sistiaga et al., 2007) seemingly provides a parsimonious explanation as to how the main olfactory system itself mediates innate behaviors – namely, by directing accessing the vomeronasal amygdalar circuitry. In support of this, experiments coupling immediate early gene (IEG) mapping with anatomical tracing have shown that in female mice, the MeA-projecting M/T cells within the MOB are activated in response to urinary volatiles from male, but not female, mice (Kang et al., 2009). These cells likely correspond in part to the population of TRPM5+ cells, which have been shown to project to the MeA (Thompson et al., 2012).

However, while the MOB-MeA projection may convey pheromone signals detected by the main olfactory system, there is evidence that at least some defensive behaviors mediated by main olfactory system – such as those in response to the fox-derived odorant, TMT – recruit distinct downstream circuits (Rosen et al., 2015). Despite one report that silencing the MeA in rats via muscimol infusion results in a complete loss of freezing behavior in response to TMT (Müller and Fendt, 2006), a number of recent studies in mice fail to observe evidence of MeA activation in response to TMT exposure

(as assessed by expression of the immediate early gene c-Fos) (Fendt et al., 2005; Li and Liberles, 2015; Pérez-Gómez et al., 2015). Furthermore, lesion experiments have demonstrated that innate defensive behaviors induced by TMT do not require the medial hypothalamic defense circuit that is recruited by vomeronasal pathways (Pagani and Rosen, 2009; Takahashi, 2014).

Alternate pathways to the PAG in the midbrain that bypass the hypothalamus have therefore been proposed based on other brain regions known to be required for TMT-evoked defensive behaviors. One such region is the BNST (Fendt et al., 2003; Müller and Fendt, 2006; Rosen et al., 2015), which receives afferents from the MeA and which projects directly to the vlPAG. However, the proposed flow of information (MOB → MeA (either directly or via the plCoA) → BNST → vlPAG) assumes a role for the MeA, despite evidence to the contrary. An alternative entry point to the PAG is the lateral septum (LSr), which is also required for TMT-induced freezing behavior (Endres and Fendt, 2008). The LSr is densely interconnected with the MeA and BNST, but it also receives direct input from the Ent. Therefore in theory a circuit comprised of MOB → Ent → LSr → PAG would bypass both the MeA and the hypothalamus. The Ent is required for some forms of fear conditioning (Ferry et al., 2006), though it has no known role in innate fear behaviors. Thus, the exact neural pathways mediating innate, TMT-induced defensive behaviors remain to be elucidated.

In comparison to the relatively minor projection to the MeA, the MOB sends much more robust projections to its other targets. Even MeA-projecting cells themselves send extensive axon collaterals into other brain regions innervated by the MOB, including the

PCtx, plCoA, and aCoA. Thus, many studies have sought to establish a role for any of the major targets of the main olfactory system in mediating innate, odor-driven behaviors, particularly with respect to odor valence (e.g. attraction versus aversion).

The plCoA is an attractive candidate to mediate innate behaviors due to its pattern of innervation by M/T axons (Miyamichi et al., 2011; Sosulski et al., 2011) and analogies to the anatomical and functional organization of olfaction in *Drosophila* (Jefferis et al., 2007; Wong et al., 2002). The projections of M/T cells innervating a given glomerulus are spatially confined to subdomains within the plCoA, and different glomeruli exhibit distinct, yet stereotyped, projection patterns within this brain region (Sosulski et al., 2011). This observation suggests that the subdomains of M/T innervation within the plCoA are genetically specified, and in theory these domains could differentially route information from specific subsets of glomerular channels – such as those activated by innately aversive versus innately attractive odorants – to distinct downstream behavioral circuits. A precedent for this exists in the lateral horn of *Drosophila*, wherein axon branches of projection neurons (analogous to mammalian M/T cells) are spatially segregated based upon the behavioral significance of the odorants that activate those cells (e.g. food cues versus pheromones (Jefferis et al., 2007), or appetitive versus aversive odors (Min et al., 2013)).

In contrast to the pattern observed in the plCoA, M/T cells corresponding to a single glomerulus provide broad, distributed innervation to the PCtx that lacks stereotypy either within or among different glomerular types (Sosulski et al., 2011); in addition, individual PCtx cells are innervated by M/T cells that are broadly distributed

across the MOB and which correspond to multiple glomerular channels (Miyamichi et al., 2011). Consistent with this anatomy, monomolecular odorants activate randomly distributed ensembles of cells within the PCtx, which enables the structure to mediate odor discrimination and learning (Choi et al., 2011; Illig and Haberly, 2003; Poo and Isaacson, 2009; Stettler and Axel, 2009).

A recent study in which the photosensitive ion channel channelrhodopsin was selectively expressed in plCoA neurons previously activated by either an innately aversive or attractive odorant provides direct functional evidence that activation of distinct populations of cells within the plCoA is sufficient to evoke innate, odor-evoked aversion or attraction, though the ensembles of cells activated by either aversive (e.g. TMT) or attractive (e.g. 2-phenylethanol) odorants do not exhibit clean spatial segregation within the structure. (There does, however, appear to be an enrichment of cells mediating innate attraction at the posterior end of the plCoA) (Root et al., 2014). This same study demonstrated that both indiscriminate silencing of cells within the plCoA or select silencing of just M/T cell axons innervating the plCoA via the photosensitive chloride channel halorhodopsin resulted in a profound loss of both innate attraction and aversion, along with a loss of TMT-evoked freezing behavior.

Together these experiments imply that the plCoA is both necessary and sufficient for innate attraction and aversion. This study further suggests that the plCoA may specifically function to decode the behavioral significance of odorants through the recruitment of unique ensembles of cells that route information to distinct downstream circuits to mediate specific behaviors. However, unpublished electrophysiology data

from our laboratory failed to reveal any valence-specific populations within the plCoA – despite recording from over 600 neurons throughout a large extent of the structure – suggesting that the exact role of the plCoA in mediating innate behaviors may be more nuanced (Iurilli and Datta, submitted).

One other MOB target that has been implicated in encoding behaviorally salient features of olfactory stimuli is the OT. The OT is an anatomically and cellularly complex structure that is contiguous with the ventral striatum, and is therefore commonly referred to as the "olfactory striatum." The OT is densely connected with many brain regions including other olfactory regions, the thalamus, hypothalamic targets, neuromodulatory and septal regions, and the striatum (Wesson and Wilson, 2011). The OT was recently reported to encode odor valence, as electrophysiological recordings from an awake mouse engaged in an odor discrimination task demonstrated that OT neurons increased their firing in response to rewarded odors. Reversal learning – in which a previously rewarded odor was no longer rewarded and a previously unrewarded odor was rewarded – demonstrated the increase in firing to be flexible, and confirmed that the neuronal response was dependent on the conditioned valence of the odorants as opposed to odor identify (Gadziola et al., 2015). Furthermore, stimulation of the OT induces activation of brain regions critical for motivated behaviors – such as the LSr and nucleus accumbens (NAc) – and is also capable of altering a mouse's odor preferences (FitzGerald et al., 2014).

As the OT is a very large and genetically heterogeneous structure, experiments to optogenetically implicate the structure as either necessary or sufficient for innate

behaviors are technically challenging. However, since the OT receives projections from the plCoA in addition to its direct projections from the MOB, one might hypothesize that the OT works in concert with the plCoA to interpret the behavioral valence of ethologically relevant odorants before forwarding the information to downstream hypothalamic circuits.

OPEN QUESTIONS

As has been demonstrated by the large body of work comparing the main versus accessory olfactory systems, a great deal of general insight into the organization and function of specific neural circuits can be obtained by studying the differences – e.g. molecular or anatomical – between olfactory subsystems. As such, dissection of the GC-D necklace subsystem – which exhibits unique molecular and peripheral anatomical organization compared to other olfactory subsystems – will no doubt advance our general understanding of mammalian olfaction and the circuits mediating innate behaviors.

As a first step towards the functional dissection of the GC-D necklace subsystem, we have set out to further elucidate the peripheral anatomical organization of the GC-D subsystem and to identify the downstream targets of M/T cells within this subsystem. Included in this dissertation is a description of new experimental approaches we developed to perform *in vivo* anatomical tracing from GC-D glomeruli (Chapter 2), a presentation of our data characterizing the anatomical connectivity of the GC-D necklace subsystem (Chapter 3), and a description of our future experimental plans to test specific hypotheses regarding the functional implications of the unique anatomy of the GC-D subsystem (Chapter 4).

REFERENCES

Adipietro, K.A., Mainland, J.D., and Matsunami, H. (2012). Functional evolution of mammalian odorant receptors. PLoS Genet. *8*, e1002821.

Arakawa, H., Kelliher, K.R., Zufall, F., and Munger, S.D. (2013). The Receptor Guanylyl Cyclase Type D (GC-D) Ligand Uroguanylin Promotes the Acquisition of Food Preferences in Mice. Chem Senses *38*, 391–397.

Belluscio, L., Koentges, G., Axel, R., and Dulac, C. (1999). A map of pheromone receptor activation in the mammalian brain. Cell *97*, 209–220.

Bergan, J.F., Ben-Shaul, Y., and Dulac, C. (2014). Sex-specific processing of social cues in the medial amygdala. Elife *3*, e02743.

Boillat, M., Challet, L., Rossier, D., Kan, C., Carleton, A., and Rodriguez, I. (2015). The vomeronasal system mediates sick conspecific avoidance. Curr Biol *25*, 251–255.

Bozza, T., Feinstein, P., Zheng, C., and Mombaerts, P. (2002). Odorant receptor expression defines functional units in the mouse olfactory system. Journal of Neuroscience *22*, 3033–3043.

Brechbuhl, J., Klaey, M., and Broillet, M.C. (2008). Grueneberg Ganglion Cells Mediate Alarm Pheromone Detection in Mice. Science *321*, 1092–1095.

Brechbühl, J., Moine, F., Klaey, M., Nenniger-Tosato, M., Hurni, N., Sporkert, F., Giroud, C., and Broillet, M.-C. (2013). Mouse alarm pheromone shares structural similarity with predator scents. Proc Natl Acad Sci USA *110*, 4762–4767.

Buck, L., and Axel, R. (1991). A novel multigene family may encode odorant receptors: A molecular basis for odor recognition. Cell *65*, 175–187.

Canteras, N.S., Chiavegatto, S., Ribeiro do Valle, L.E., and Swanson, L.W. (1997). Severe reduction of rat defensive behavior to a predator by discrete hypothalamic chemical lesions. Brain Res. Bull. *44*, 297–305.

Canteras, N.S. (2002). The medial hypothalamic defensive system: hodological organization and functional implications. Pharmacol. Biochem. Behav. *71*, 481–491.

Cádiz-Moretti, B., Otero-García, M., Martinez-Garcia, F., and Lanuza, E. (2014). Afferent projections to the different medial amygdala subdivisions: a retrograde tracing study in the mouse. Brain Struct Funct *221*, 1033–1065.

Chess, A., Simon, I., Cedar, H., and Axel, R. (1994). Allelic inactivation regulates olfactory receptor gene expression. Cell *78*, 823–834.

Cho, J.H., Prince, J.E.A., Cutforth, T., and Cloutier, J.F. (2011). The pattern of glomerular map formation defines responsiveness to aversive odorants in mice. Journal of Neuroscience *31*, 7920–7926.

Choi, G.B., Dong, H.-W., Murphy, A.J., Valenzuela, D.M., Yancopoulos, G.D., Swanson, L.W., and Anderson, D.J. (2005). Lhx6 delineates a pathway mediating innate reproductive behaviors from the amygdala to the hypothalamus. Neuron *46*, 647–660.

Choi, G.B., Stettler, D.D., Kallman, B.R., Bhaskar, S.T., Fleischmann, A., and Axel, R. (2011). Driving Opposing Behaviors with Ensembles of Piriform Neurons. Cell *146*, 1004–1015.

Cleland, T.A. (2014). Construction of odor representations by olfactory bulb microcircuits. Prog. Brain Res. *208*, 177–203.

Cockerham, R.E., Puche, A.C., and Munger, S.D. (2009). Heterogeneous sensory innervation and extensive intrabulbar connections of olfactory necklace glomeruli. PLoS ONE *4*, e4657.

Cury, K.M., and Uchida, N. (2010). Robust odor coding via inhalation-coupled transient activity in the mammalian olfactory bulb. Neuron *68*, 570–585.

D'Souza, R.D., and Vijayaraghavan, S. (2014). Paying attention to smell: cholinergic signaling in the olfactory bulb. Front Synaptic Neurosci *6*, 21.

Del Punta, K., Puche, A., Adams, N.C., Rodriguez, I., and Mombaerts, P. (2002). A divergent pattern of sensory axonal projections is rendered convergent by second-order neurons in the accessory olfactory bulb. Neuron *35*, 1057–1066.

Devor, M. (1976). Fiber trajectories of olfactory bulb efferents in the hamster. J Comp Neurol *166*, 31–47.

Dewan, A., Pacifico, R., Zhan, R., Rinberg, D., and Bozza, T. (2013). Non-redundant coding of aversive odours in the main olfactory pathway. Nature *497*, 486–489.

Dielenberg, R.A., Hunt, G.E., and McGregor, I.S. (2001). "When a rat smells a cat": the distribution of Fos immunoreactivity in rat brain following exposure to a predatory odor. Nsc *104*, 1085–1097.

Duchamp-Viret, P. (1999). Odor Response Properties of Rat Olfactory Receptor Neurons. Science *284*, 2171–2174.

Dulac, C., and Axel, R. (1995). A novel family of genes encoding putative pheromone receptors in mammals. Cell *83*, 195–206.

Endres, T., and Fendt, M. (2008). Inactivation of the lateral septum blocks fox odor-induced fear behavior. NeuroReport *19*, 667–670.

Ennis, M., and Holy, T.E. (2015). Anatomy and Neurobiology of the Main and Accessory Olfactory Bulbs. Doty/Handbook of Olfaction and Gustation 157–182.

Fendt, M., Endres, T., and Apfelbach, R. (2003). Temporary inactivation of the bed nucleus of the stria terminalis but not of the amygdala blocks freezing induced by trimethylthiazoline, a component of fox feces. Journal of Neuroscience *23*, 23–28.

Fendt, M., Endres, T., Lowry, C.A., Apfelbach, R., and McGregor, I.S. (2005). TMT-induced autonomic and behavioral changes and the neural basis of its processing. Neuroscience & Biobehavioral Reviews *29*, 1145–1156.

Ferrero, D.M., Lemon, J.K., Fluegge, D., Pashkovski, S.L., Korzan, W.J., Datta, S.R., Spehr, M., Fendt, M., and Liberles, S.D. (2011). Detection and avoidance of a carnivore odor by prey. Proc Natl Acad Sci USA *108*, 11235–11240.

Ferrero, D.M., Moeller, L.M., Osakada, T., Horio, N., Li, Q., Roy, D.S., Cichy, A., Spehr, M., Touhara, K., and Liberles, S.D. (2013). A juvenile mouse pheromone inhibits sexual behaviour through the vomeronasal system. Nature *502*, 368–371.

Ferry, B., Ferreira, G., Traissard, N., and Majchrzak, M. (2006). Selective involvement of the lateral entorhinal cortex in the control of the olfactory memory trace during conditioned odor aversion in the rat. Behavioral Neuroscience *120*, 1180–1186.

FitzGerald, B.J., Richardson, K., and Wesson, D.W. (2014). Olfactory tubercle stimulation alters odor preference behavior and recruits forebrain reward and motivational centers. Front Behav Neurosci *8*.

Fleischer, J., Schwarzenbacher, K., and Breer, H. (2007). Expression of Trace Amine-Associated Receptors in the Grueneberg Ganglion. Chem Senses *32*, 623–631.

Fuss, S.H., Omura, M., and Mombaerts, P. (2005). The Grueneberg ganglion of the mouse projects axons to glomeruli in the olfactory bulb. European Journal of Neuroscience *22*, 2649–2654.

Fülle, H.J., Vassar, R., Foster, D.C., Yang, R.B., Axel, R., and Garbers, D.L. (1995). A receptor guanylyl cyclase expressed specifically in olfactory sensory neurons. Proc Natl Acad Sci USA *92*, 3571–3575.

Gadziola, M.A., Tylicki, K.A., Christian, D.L., and Wesson, D.W. (2015). The olfactory tubercle encodes odor valence in behaving mice. Journal of Neuroscience *35*, 4515–4527.

Gao, L., Hu, J., Zhong, C., and Luo, M. (2010). Integration of CO2 and odorant signals in the mouse olfactory bulb. Nsc *170*, 881–892.

Giessel, A.J., and Datta, S.R. (2014). Olfactory maps, circuits and computations. Curr Opin Neurobiol *24*, 120–132.

Gire, D.H., and Schoppa, N.E. (2009). Control of on/off glomerular signaling by a local GABAergic microcircuit in the olfactory bulb. Journal of Neuroscience *29*, 13454–13464.

Godfrey, P.A., Malnic, B., and Buck, L. (2004). The mouse olfactory receptor gene family. Proc Natl Acad Sci USA *101*, 2156–2161.

Greer, P.L., Bear, D.M., Lassance, J.-M., Bloom, M.L., Tsukahara, T., Pashkovski, S.L., Masuda, F.K., Nowlan, A.C., Kirchner, R., Hoekstra, H.E., et al. (2016). A Family of non-GPCR Chemosensors Defines an Alternative Logic for Mammalian Olfaction. Cell *165*, 1734–1748.

Gross, C.T., and Canteras, N.S. (2012). The many paths to fear. Nat Rev Neurosci *13*, 651–658.

Gutierrez-Castellanos, N., Pardo-Bellver, C., Martinez-Garcia, F., and Lanuza, E. (2014). The vomeronasal cortex - afferent and efferent projections of the posteromedial cortical nucleus of the amygdala in mice. European Journal of Neuroscience *39*, 141–158.

Haberly, L.B., and Price, J.L. (1977). The axonal projection patterns of the mitral and tufted cells of the olfactory bulb in the rat. Brain Res *129*, 152–157.

Haga, S., Hattori, T., Sato, T., Sato, K., Matsuda, S., Kobayakawa, R., Sakano, H., Yoshihara, Y., Kikusui, T., and Touhara, K. (2010). The male mouse pheromone ESP1 enhances female sexual receptive behaviour through a specific vomeronasal receptor. Nature *466*, 118–122.

Halpern, M. (1987). The organization and function of the vomeronasal system. Annu Rev Neurosci *10*, 325–362.

Hanke, W., Mamasuew, K., Biel, M., Yang, R.-B., and Fleischer, J. (2013). Odorant-evoked electrical responses in Grueneberg ganglion neurons rely on cGMP-associated signaling proteins. Neuroscience Letters *539*, 38–42.

Hashikawa, K., Hashikawa, Y., Falkner, A., and Lin, D. (2016). ScienceDirect The neural circuits of mating and fighting in male mice. Curr Opin Neurobiol *38*, 27–37.

Hendrickson, R.C., Krauthamer, S., Essenberg, J.M., and Holy, T.E. (2008). Inhibition shapes sex selectivity in the mouse accessory olfactory bulb. Journal of Neuroscience *28*, 12523–12534.

Herrada, G., and Dulac, C. (1997). A novel family of putative pheromone receptors in mammals with a topographically organized and sexually dimorphic distribution. Cell *90*, 763–773.

Hintiryan, H., Gou, L., Zingg, B., Yamashita, S., Lyden, H.M., Song, M.Y., Grewal, A.K., Zhang, X., Toga, A.W., and Dong, H.-W. (2012). Comprehensive connectivity of the mouse main olfactory bulb: analysis and online digital atlas. Front Neuroanat *6*, 30.

Igarashi, K.M., Ieki, N., An, M., Yamaguchi, Y., Nagayama, S., Kobayakawa, K., Kobayakawa, R., Tanifuji, M., Sakano, H., Chen, W.R., et al. (2012). Parallel mitral and tufted cell pathways route distinct odor information to different targets in the olfactory cortex. Journal of Neuroscience *32*, 7970–7985.

Ihara, S., Yoshikawa, K., and Touhara, K. (2013). Chemosensory signals and their receptors in the olfactory neural system. Neuroscience *254*, 45–60.

Illig, K.R., and Haberly, L.B. (2003). Odor-evoked activity is spatially distributed in piriform cortex. J Comp Neurol *457*, 361–373.

Imai, T., and Sakano, H. (2007). Roles of odorant receptors in projecting axons in the mouse olfactory system. Curr Opin Neurobiol *17*, 507–515.

Ishii, T., and Mombaerts, P. (2011). Coordinated coexpression of two vomeronasal receptor V2R genes per neuron in the mouse. Mol. Cell. Neurosci. *46*, 397–408.

Isogai, Y., Si, S., Pont-Lezica, L., Tan, T., Kapoor, V., Murthy, V.N., and Dulac, C. (2011). Molecular organization of vomeronasal chemoreception. Nature *478*, 241–245.

Jefferis, G.S.X.E., Potter, C.J., Chan, A.M., Marin, E.C., Rohlfing, T., Maurer, C.R., and Luo, L. (2007). Comprehensive maps of Drosophila higher olfactory centers: spatially segregated fruit and pheromone representation. Cell *128*, 1187–1203.

Johnson, M.A., Tsai, L., Roy, D.S., Valenzuela, D.H., Mosley, C., Magklara, A., Lomvardas, S., Liberles, S.D., and Barnea, G. (2012). Neurons expressing trace amine-associated receptors project to discrete glomeruli and constitute an olfactory subsystem. Proc Natl Acad Sci USA *109*, 13410–13415.

Juilfs, D.M., Fülle, H.J., Zhao, A.Z., Houslay, M.D., Garbers, D.L., and Beavo, J.A. (1997). A subset of olfactory neurons that selectively express cGMP-stimulated phosphodiesterase (PDE2) and guanylyl cyclase-D define a unique olfactory signal transduction pathway. Proc Natl Acad Sci USA *94*, 3388–3395.

Kang, N., Baum, M.J., and Cherry, J.A. (2009). A direct main olfactory bulb projection to the “vomeronasal” amygdala in female mice selectively responds to volatile pheromones from males. European Journal of Neuroscience *29*, 624–634.

Kang, N., Baum, M.J., and Cherry, J.A. (2011). Different profiles of main and accessory olfactory bulb mitral/tufted cell projections revealed in mice using an anterograde tracer and a whole-mount, flattened cortex preparation. Chem Senses *36*, 251–260.

Kay, L.M., and Sherman, S.M. (2007). An argument for an olfactory thalamus. Trends Neurosci *30*, 47–53.

Kimchi, T., Xu, J., and Dulac, C. (2007). A functional circuit underlying male sexual behaviour in the female mouse brain. Nature *448*, 1009–1014.

Kobayakawa, K., Kobayakawa, R., Matsumoto, H., Oka, Y., Imai, T., Ikawa, M., Okabe, M., Ikeda, T., Itohara, S., Kikusui, T., et al. (2007). Innate versus learned odour processing in the mouse olfactory bulb. Nature *450*, 503–508.

Larriva-Sahd, J. (2008). The accessory olfactory bulb in the adult rat: a cytological study of its cell types, neuropil, neuronal modules, and interactions with the main olfactory system. J Comp Neurol *510*, 309–350.

Larriva-Sahd, J. (2012). Cytological organization of the alpha component of the anterior olfactory nucleus and olfactory limbus. Front Neuroanat *6*, 23.

Leypold, B.G., Yu, C.R., Leinders-Zufall, T., Kim, M.M., Zufall, F., and Axel, R. (2002). Altered sexual and social behaviors in trp2 mutant mice. Proc Natl Acad Sci USA *99*, 6376–6381.

Li, Q., and Liberles, S.D. (2015). Aversion and attraction through olfaction. Curr Biol *25*, R120–R129.

Li, Q., Korzan, W.J., Ferrero, D.M., Chang, R.B., Roy, D.S., Buchi, M., Lemon, J.K., Kaur, A.W., Stowers, L., Fendt, M., et al. (2013). Synchronous evolution of an odor biosynthesis pathway and behavioral response. Curr Biol *23*, 11–20.

Liberles, S.D. (2014). Mammalian pheromones. Annu. Rev. Physiol. *76*, 151–175.

Liberles, S.D., and Buck, L. (2006). A second class of chemosensory receptors in the olfactory epithelium. Nature *442*, 645–650.

Liberles, S.D., Horowitz, L.F., Kuang, D., Contos, J.J., Wilson, K.L., Siltberg-Liberles, J., Liberles, D.A., and Buck, L. (2009). Formyl peptide receptors are candidate chemosensory receptors in the vomeronasal organ. Proc Natl Acad Sci USA *106*, 9842–9847.

Lin, D.Y., Shea, S.D., and Katz, L.C. (2006). Representation of Natural Stimuli in the Rodent Main Olfactory Bulb. Neuron *50*, 937–949.

Lin, D.Y., Zhang, S.-Z., Block, E., and Katz, L.C. (2005). Encoding social signals in the mouse main olfactory bulb. Nature *434*, 470–477.

Lin, D., Boyle, M.P., Dollar, P., Lee, H., Lein, E.S., Perona, P., and Anderson, D.J. (2011). Functional identification of an aggression locus in the mouse hypothalamus. Nature *470*, 221–226.

Lin, W., Margolskee, R., Donnert, G., Hell, S.W., and Restrepo, D. (2007). Olfactory neurons expressing transient receptor potential channel M5 (TRPM5) are involved in sensing semiochemicals. Proc Natl Acad Sci USA *104*, 2471–2476.

Lin, W., Arellano, J., Slotnick, B., and Restrepo, D. (2004). Odors detected by mice deficient in cyclic nucleotide-gated channel subunit A2 stimulate the main olfactory system. Journal of Neuroscience *24*, 3703–3710.

Lo, L., and Anderson, D.J. (2011). A Cre-Dependent, Anterograde Transsynaptic Viral Tracer for Mapping Output Pathways of Genetically Marked Neurons. Neuron *72*, 938–950.

Lonstein, J.S., and Stern, J.M. (1998). Site and behavioral specificity of periaqueductal gray lesions on postpartum sexual, maternal, and aggressive behaviors in rats. Brain Res *804*, 21–35.

López, F., Delgado, R., López, R., Bacigalupo, J., and Restrepo, D. (2014). Transduction for pheromones in the main olfactory epithelium is mediated by the Ca2+ -activated channel TRPM5. Journal of Neuroscience *34*, 3268–3278.

Luo, M., and Katz, L.C. (2004). Encoding pheromonal signals in the mammalian vomeronasal system. Curr Opin Neurobiol *14*, 428–434.

Ma, L., Qiu, Q., Gradwohl, S., Scott, A., Yu, E.Q., Alexander, R., Wiegraebe, W., and Yu, C.R. (2012). Distributed representation of chemical features and tunotopic organization of glomeruli in the mouse olfactory bulb. Proc Natl Acad Sci USA *109*, 5481–5486.

Malnic, B., Hirono, J., Sato, T., and Buck, L. (1999). Combinatorial Receptor Codes for Odors. Cell *96*, 713–723.

Mandiyan, V.S., Coats, J.K., and Shah, N.M. (2005). Deficits in sexual and aggressive behaviors in Cnga2 mutant mice. Nat Neurosci *8*, 1660–1662.

Martinez, R.C., Carvalho-Netto, E.F., Ribeiro-Barbosa, E.R., Baldo, M.V.C., and Canteras, N.S. (2011). Amygdalar roles during exposure to a live predator and to a predator-associated context. Neuroscience *172*, 314–328.

Martínez-Marcos, A. (2009). On the organization of olfactory and vomeronasal cortices. Prog Neurobiol *87*, 21–30.

Matsuo, T., Hattori, T., Asaba, A., Inoue, N., Kanomata, N., Kikusui, T., Kobayakawa, R., and Kobayakawa, K. (2015). Genetic dissection of pheromone processing reveals main olfactory system-mediated social behaviors in mice. Proc Natl Acad Sci USA *112*, E311–E320.

Matsuo, T., Rossier, D.A., Kan, C., and Rodriguez, I. (2012). The wiring of Grueneberg ganglion axons is dependent on neuropilin 1. Development *139*, 2783–2791.

McGregor, I.S., Hargreaves, G.A., Apfelbach, R., and Hunt, G.E. (2004). Neural correlates of cat odor-induced anxiety in rats: region-specific effects of the benzodiazepine midazolam. Journal of Neuroscience *24*, 4134–4144.

Meisami, E., and Bhatnagar, K.P. (1998). Structure and diversity in mammalian accessory olfactory bulb. Microsc. Res. Tech. *43*, 476–499.

Meredith, M., and Westberry, J.M. (2004). Distinctive responses in the medial amygdala to same-species and different-species pheromones. Journal of Neuroscience *24*, 5719–5725.

Meyer, M.R., Angele, A., Kremmer, E., Kaupp, U.B., and Muller, F. (2000). A cGMP-signaling pathway in a subset of olfactory sensory neurons. Proc Natl Acad Sci USA *97*, 10595–10600.

Min, S., Ai, M., Shin, S.A., and Suh, G.S.B. (2013). Dedicated olfactory neurons mediating attraction behavior to ammonia and amines in Drosophila. Proc Natl Acad Sci USA *110*, E1321–E1329.

Miyamichi, K., Amat, F., Moussavi, F., Wang, C., Wickersham, I., Wall, N.R., Taniguchi, H., Tasic, B., Huang, Z.J., He, Z., et al. (2011). Cortical representations of olfactory input by trans-synaptic tracing. Nature *472*, 191–196.

Mombaerts, P. (2006). Axonal wiring in the mouse olfactory system. Annu. Rev. Cell Dev. Biol. *22*, 713–737.

Mombaerts, P., Wang, F., Dulac, C., Chao, S.K., Nemes, A., Mendelsohn, M., Edmondson, J., and Axel, R. (1996). Visualizing an Olfactory Sensory Map. Cell *87*, 675–686.

Mori, K., Nagao, H., and Yoshihara, Y. (1999). The olfactory bulb: coding and processing of odor molecule information. Science *286*, 711.

Mori, K., Takahashi, Y.K., Igarashi, K.M., and Yamaguchi, M. (2006). Maps of odorant molecular features in the Mammalian olfactory bulb. Physiological Reviews *86*, 409–433.

Munger, S.D., Leinders-Zufall, T., McDougall, L.M., Cockerham, R.E., Schmid, A., Wandernoth, P., Wennemuth, G., Biel, M., Zufall, F., and Kelliher, K.R. (2010). An olfactory subsystem that detects carbon disulfide and mediates food-related social learning. Curr Biol *20*, 1438–1444.

Müller, M., and Fendt, M. (2006). Temporary inactivation of the medial and basolateral amygdala differentially affects TMT-induced fear behavior in rats. Behavioural Brain Research *167*, 57–62.

Nagayama, S., Enerva, A., Fletcher, M.L., Masurkar, A.V., Igarashi, K.M., Mori, K., and Chen, W.R. (2010). Differential axonal projection of mitral and tufted cells in the mouse main olfactory system. Frontiers in Neural Circuits *4*.

Nagayama, S., Homma, R., and Imamura, F. (2014). Neuronal organization of olfactory bulb circuits. Frontiers in Neural Circuits *8*, 98.

Nara, K., Saraiva, L.R., Ye, X., and Buck, L. (2011). A large-scale analysis of odor coding in the olfactory epithelium. Journal of Neuroscience *31*, 9179–9191.

Nodari, F., Hsu, F.-F., Fu, X., Holekamp, T.F., Kao, L.-F., Turk, J., and Holy, T.E. (2008). Sulfated Steroids as Natural Ligands of Mouse Pheromone-Sensing Neurons. Journal of Neuroscience *28*, 6407–6418.

Ojima, H., Yamasaki, T., Kojima, H., and Akashi, A. (1988). Cholinergic innervation of the main and the accessory olfactory bulbs of the rat as revealed by a monoclonal antibody against choline acetyltransferase. Anat Embryol *178*, 481–488.

Omura, M., and Mombaerts, P. (2014). Trpc2-expressing sensory neurons in the main olfactory epithelium of the mouse. Cell Rep *8*, 583–595.

Omura, M., and Mombaerts, P. (2015). Trpc2-expressing sensory neurons in the mouse main olfactory epithelium of type B express the soluble guanylate cyclase Gucy1b2. Mol. Cell. Neurosci. *65*, 114–124.

Pacifico, R., Dewan, A., Cawley, D., Guo, C., and Bozza, T. (2012). An olfactory subsystem that mediates high-sensitivity detection of volatile amines. Cell Reports *2*, 76–88.

Pagani, J.H., and Rosen, J.B. (2009). The medial hypothalamic defensive circuit and 2,5-dihydro-2,4,5-trimethylthiazoline (TMT) induced fear: Comparison of electrolytic and neurotoxic lesions. Brain Res *1286*, 133–146.

Papes, F., Logan, D.W., and Stowers, L. (2010). The Vomeronasal Organ Mediates Interspecies Defensive Behaviors through Detection of Protein Pheromone Homologs. Cell *141*, 692–703.

Pérez-Gómez, A., Bleymehl, K., Stein, B., Pyrski, M., Birnbaumer, L., Munger, S.D., Leinders-Zufall, T., Zufall, F., and Chamero, P. (2015). Innate Predator Odor Aversion Driven by Parallel Olfactory Subsystems that Converge in the Ventromedial Hypothalamus. Curr Biol 1–8.

Poo, C., and Isaacson, J.S. (2009). Odor Representations in Olfactory Cortex: “Sparse” Coding, Global Inhibition, and Oscillations. Neuron *62*, 850–861.

Pro-Sistiaga, P., Mohedano-Moriano, A., Ubeda-Bañon, I., Del Mar Arroyo-Jimenez, M., Marcos, P., Artacho-Pérula, E., Crespo, C., Insausti, R., and Martínez-Marcos, A. (2007). Convergence of olfactory and vomeronasal projections in the rat basal telencephalon. J Comp Neurol *504*, 346–362.

Pro-Sistiaga, P., Mohedano-Moriano, A., Ubeda-Bañon, I., la Rosa-Prieto, de, C., Saiz-Sanchez, D., and Martínez-Marcos, A. (2008). Projections of olfactory bulbs to the olfactory and vomeronasal cortices. NeuroReport *19*, 1541–1544.

Ressler, K.J., Sullivan, S.L., and Buck, L. (1993). A zonal organization of odorant receptor gene expression in the olfactory epithelium. Cell *73*, 597–609.

Ressler, K.J., Sullivan, S.L., and Buck, L. (1994). Information coding in the olfactory system: evidence for a stereotyped and highly organized epitope map in the olfactory bulb. Cell *79*, 1245–1255.

Ring, G., Mezza, R.C., and Schwob, J.E. (1997). Immunohistochemical identification of discrete subsets of rat olfactory neurons and the glomeruli that they innervate. J Comp Neurol *388*, 415–434.

Rivière, S., Challet, L., Fluegge, D., Spehr, M., and Rodriguez, I. (2009). Formyl peptide receptor-like proteins are a novel family of vomeronasal chemosensors. Nature *459*, 574–577.

Rodriguez, I., Feinstein, P., and Mombaerts, P. (1999). Variable patterns of axonal projections of sensory neurons in the mouse vomeronasal system. Cell *97*, 199–208.

Root, C.M., Denny, C.A., Hen, R., and Axel, R. (2014). The participation of cortical amygdala in innate, odour-driven behaviour. Nature *515*, 269–273.

Rosen, J.B., Asok, A., and Chakraborty, T. (2015). The smell of fear: innate threat of 2,5-dihydro-2,4,5-trimethylthiazoline, a single molecule component of a predator odor. Front. Neurosci. *9*, 85–12.

Royet, J.P., Souchier, C., Jourdan, F., and Ploye, H. (1988). Morphometric study of the glomerular population in the mouse olfactory bulb: numerical density and size distribution along the rostrocaudal axis. J Comp Neurol *270*, 559–568.

Rubin, B.D., and Katz, L.C. (1999). Optical imaging of odorant representations in the mammalian olfactory bulb. Neuron *23*, 499–511.

Sabir, A., Unver, A., and Kara, Z. (2012). The fatty acid and tocopherol constituents of the seed oil extracted from 21 grape varieties (Vitis spp.). J. Sci. Food Agric. *92*, 1982–1987.

Salcedo, E., Tran, T., Ly, X., Lopez, R., Barbica, C., Restrepo, D., and Vijayaraghavan, S. (2011). Activity-Dependent Changes in Cholinergic Innervation of the Mouse Olfactory Bulb. PLoS ONE *6*, e25441.

Scalia, F., and Winans, S.S. (1975). The differential projections of the olfactory bulb and accessory olfactory bulb in mammals. J Comp Neurol *161*, 31–55.

Shao, Z., Puche, A.C., and Shipley, M.T. (2013). Intraglomerular inhibition maintains mitral cell response contrast across input frequencies. J Neurophysiol *110*, 2185–2191.

Shinoda, K., Ohtsuki, T., Nagano, M., and Okumura, T. (1993). A possible functional necklace formed by placental antigen X-P2-immunoreactive and intensely acetylcholinesterase-reactive (PAX/IAE) glomerular complexes in the rat olfactory bulb. Brain Res *618*, 160–166.

Shinoda, K., Shiotani, Y., and Osawa, Y. (1989). “Necklace olfactory glomeruli” form unique components of the rat primary olfactory system. J Comp Neurol *284*, 362–373.

Shusterman, R., Smear, M.C., Koulakov, A.A., and Rinberg, D. (2011). Precise olfactory responses tile the sniff cycle. Nat Neurosci *14*, 1039–1044.

Sokolowski, K., and Corbin, J.G. (2012). Wired for behaviors: from development to function of innate limbic system circuitry. Frontiers in Molecular Neuroscience *5*, 55.

Sosulski, D.L., Bloom, M.L., Cutforth, T., Axel, R., and Datta, S.R. (2011). Distinct representations of olfactory information in different cortical centres. Nature *472*, 213–216.

Soucy, E.R., Albeanu, D.F., Fantana, A.L., Murthy, V.N., and Meister, M. (2009). Precision and diversity in an odor map on the olfactory bulb. Nat Neurosci *12*, 210–220.

Stettler, D.D., and Axel, R. (2009). Representations of odor in the piriform cortex. Neuron *63*, 854–864.

Sukikara, M.H., Mota-Ortiz, S.R., Baldo, M.V., Felicio, L.F., and Canteras, N.S. (2010). The periaqueductal gray and its potential role in maternal behavior inhibition in response to predatory threats. Behavioural Brain Research *209*, 226–233.

Takahashi, L.K. (2014). Olfactory systems and neural circuits that modulate predator odor fear. Front Behav Neurosci *8*, 72.

Thompson, J.A., Salcedo, E., Restrepo, D., and Finger, T.E. (2012). Second-order input to the medial amygdala from olfactory sensory neurons expressing the transduction channel TRPM5. J Comp Neurol *520*, 1819–1830.

Tirindelli, R., Dibattista, M., Pifferi, S., and Menini, A. (2009). From Pheromones to Behavior. Physiological Reviews *89*, 921–956.

Trinh, K., and Storm, D.R. (2003). Vomeronasal organ detects odorants in absence of signaling through main olfactory epithelium. Nat Neurosci *6*, 519–525.

Uchida, N., Poo, C., and Haddad, R. (2014). Coding and transformations in the olfactory system. Annu Rev Neurosci *37*, 363–385.

Vassar, R., Chao, S.K., Sitcheran, R., Nun, J.M., and Vosshall, L.B. (1994). Topographic organization of sensory projections to the olfactory bulb. Cell *79*, 981–991.

Vassar, R., Ngai, J., and Axel, R. (1993). Spatial segregation of odorant receptor expression in the mammalian olfactory epithelium. Cell *74*, 309–318.

Wagner, S., Gresser, A.L., Torello, A.T., and Dulac, C. (2006). A multireceptor genetic approach uncovers an ordered integration of VNO sensory inputs in the accessory olfactory bulb. Neuron *50*, 697–709.

Walz, A., Feinstein, P., Khan, M., and Mombaerts, P. (2007). Axonal wiring of guanylate cyclase-D-expressing olfactory neurons is dependent on neuropilin 2 and semaphorin 3F. Development *134*, 4063–4072.

Walz, A., Omura, M., and Mombaerts, P. (2006). Development and topography of the lateral olfactory tract in the mouse: Imaging by genetically encoded and injected

fluorescent markers. J Neurobiol *66*, 835–846.

Wang, F., Nemes, A., Mendelsohn, M., and Axel, R. (1998). Odorant receptors govern the formation of a precise topographic map. Cell *93*, 47-60.

Wesson, D.W., and Wilson, D.A. (2011). Sniffing out the contributions of the olfactory tubercle to the sense of smell: Hedonics, sensory integration, and more? Neuroscience & Biobehavioral Reviews *35*, 655–668.

Wilson, R.I., and Mainen, Z. (2006). Early events in olfactory processing. Annu Rev Neurosci *29*, 163–201.

Wong, A.M., Wang, J.W., and Axel, R. (2002). Spatial representation of the glomerular map in the Drosophila protocerebrum. Cell *109*, 229–241.

Wu, M.V., Manoli, D.S., Fraser, E.J., Coats, J.K., Tollkuhn, J., Honda, S.-I., Harada, N., and Shah, N.M. (2009). Estrogen masculinizes neural pathways and sex-specific behaviors. Cell *139*, 61–72.

Wysocki, C.J., and Lepri, J.J. (1991). Consequences of removing the vomeronasal organ. J. Steroid Biochem. Mol. Biol. *39*, 661–669.

Zhang, J.-X., Sun, L., and Novotny, M.V. (2007). Mice Respond Differently to Urine and Its Major Volatile Constituents from Male and Female Ferrets. J Chem Ecol *33*, 603–612.

Zheng, L.M., Ravel, N., and Jourdan, F. (1987). Topography of centrifugal acetylcholinesterase-positive fibres in the olfactory bulb of the rat: evidence for original projections in atypical glomeruli. Neuroscience *23*, 1083–1093.

CHAPTER 2

Novel Methods to Interrogate the Anatomy of the Mouse GC-D Necklace Olfactory Subsystem *In Vivo*

Taralyn M. Tan and Sandeep R. Datta

INTRODUCTION

General background

Mice use multiple olfactory subsystems to detect environmental stimuli. While the body of knowledge on the various subsystems continues to grow, our current understanding of the basic principles that govern odor detection and the peripheral processing of olfactory information in mammals is largely the result of investigations of the "canonical" main olfactory system. In this subsystem, olfactory sensory neurons (OSNs) are located within the main olfactory epithelium (MOE) of the nose and individual OSNs express only a single receptor protein belonging to the large family of G protein-coupled receptors (GPCRs) called the olfactory receptor (OR) family (Buck and Axel, 1991; Chess et al., 1994). The OSNs projects axons to the main olfactory bulb (MOB) of the brain, where the axons of cells that express the same OR converge onto two mirror-symmetric structures called glomeruli (Vassar et al., 1994).

The wealth of knowledge we have gained on odor coding from studying the main olfactory system is due in no small part to the ease with which the dorsal aspect of the MOB can be surgically exposed via a craniotomy or the partial thinning of the overlying skull to grant *in vivo* optical access. This accessibility has facilitated both functional experiments – in which the neural activity of olfactory glomeruli is assayed using hemodynamics (Meister and Bonhoeffer, 2001; Rubin and Katz, 1999; Uchida et al., 2000) or genetically encoded indicators of neural activity (Bozza et al., 2004; Wachowiak et al., 2013) – as well as experiments to define the anatomical and molecular organization of the main olfactory system. For example, researchers have

targeted and dye-labeled individual glomeruli *in vivo* as a strategy to identify the ORs that detect specific odorants – by retrogradely labeling the cell bodies of OSNs innervating an odor-responsive glomerulus (Oka et al., 2006; Shirasu et al., 2014) – and our laboratory developed an anterograde anatomical tracing approach to compare the axonal patterns of the projection neurons (mitral/tufted (M/T) cells) innervating different, genetically identified glomeruli (Sosulski et al., 2011).

Thus, it is clear that optical access to the glomeruli of a given olfactory subsystem *in vivo* confers the ability to better understand the functional, molecular, and anatomical aspects of that subsystem. The guanylate cyclase D (GC-D) "necklace" subsystem is a smaller and less well-understood olfactory subsystem than the canonical main olfactory system that to date has been optically inaccessible *in vivo*. The GC-D subsystem is comprised of a population of OSNs that largely resides within caudal portions of the MOE called cul-de-sacs. These OSNs are molecularly distinct from canonical OSNs, as they do not express ORs or the relevant downstream signaling molecules (Juilfs et al., 1997; Meyer et al., 2000). Rather, these cells express membrane-bound GC-D and members of the membrane-spanning, four-pass A (MS4A) family, a family of non-GPCR chemosensors recently identified by our laboratory (Fülle et al., 1995; Greer et al., 2016). The axons of GC-D cells innervate a string of seemingly interconnected glomeruli that encircles the back of the MOB and that bears resemblance to a necklace (Walz et al., 2007).

The GC-D subsystem detects a variety of odorants that carry innate ethological significance to mice and mediates a form of social olfactory learning (Arakawa et al.,

2013; Munger et al., 2010). However, almost nothing is known about the specific role of this subsystem in generating olfactory-driven behaviors. The limited knowledge of the function of this subsystem reflects an even more fundamental lack of knowledge about the anatomy of the subsystem. For example, the significance of having a “necklace” of glomeruli is completely unknown, nor is it known how OSNs within different cul-de-sacs of the MOE map onto different necklace glomeruli. Furthermore, the downstream brain targets of this subsystem have yet to be identified. To address these large gaps in knowledge, we have developed a method to expose glomeruli of the GC-D necklace *in vivo* and have optimized our previously published electroporation cell-labeling technique to perform anatomical tracing from individual GC-D glomeruli. Here we provide a detailed protocol for these novel experimental approaches. Beyond its utility to characterize the anatomy of this subsystem (as described here), our surgical preparation can also be used with mice that express genetically encoded calcium indicators or light-activated ion channels to interrogate the functional properties of this subsystem in either the OB or at OSN cell bodies within the cul-de-sacs of the MOE.

Surgical Preparation to Expose GC-D Glomeruli *In Vivo*

The glomeruli of the GC-D necklace are located at the caudal-most extent of the MOB, just anterior to the portion of the OB (the accessory olfactory bulb (AOB)) innervated by sensory neurons of the vomeronasal olfactory subsystem **(Fig. 2.1A)**. The AOB is inaccessible via a dorsal craniotomy, as it resides beneath a thin layer of overlying cortical tissue. Using a mouse line in which the necklace OSNs

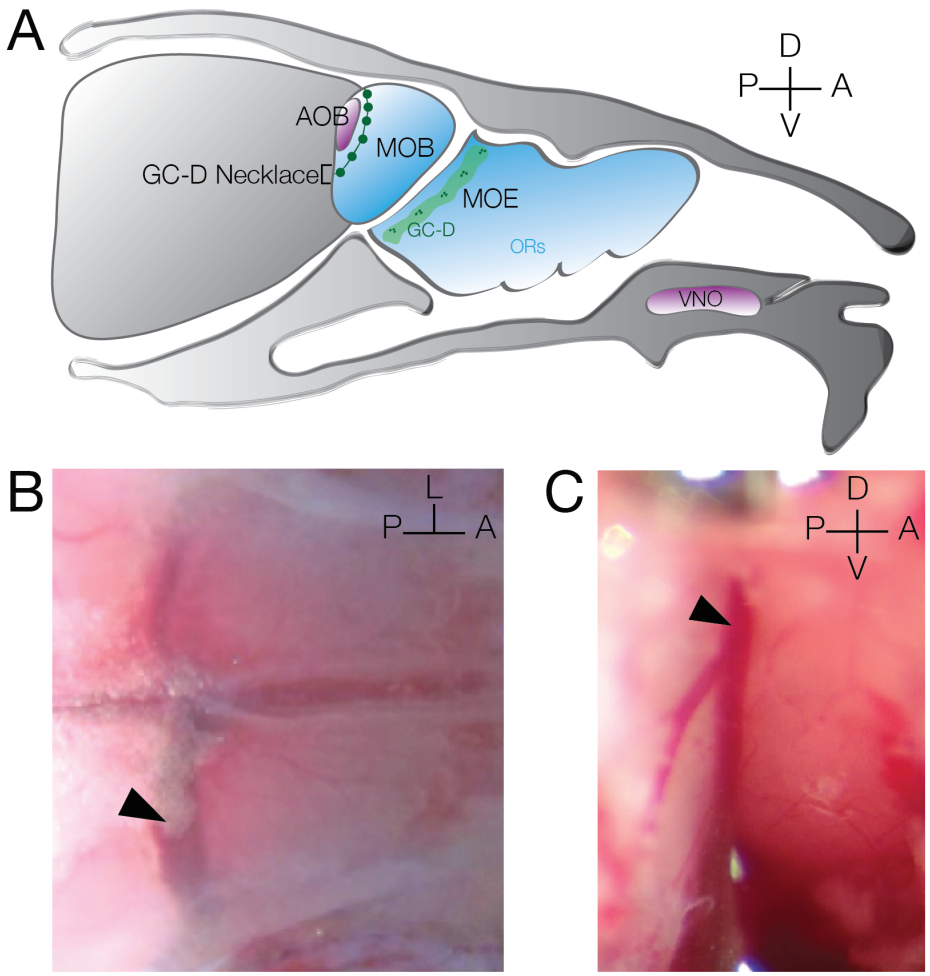

Figure 2.1. Inaccessibility of GC-D Necklace Due to Vasculature

(A) Schematic illustrating the approximate location of GC-D cells within the MOE and the position of the GC-D necklace glomeruli relative to the MOB and the AOB.

(B) Image of the dorsal surface of the skull showing the rostral rhinal vein (arrowhead) that obstructs access to the caudal MOB.

(C) Dorsolateral view of the caudal OB following cauterization and removal of the rostral rhinal vein, in which the inferior cerebral vein (arrowhead) located within the brain continues to obstruct access to the necklace glomeruli that reside inferior to the blood vessel.

express tau-GFP from the *Gucy2d* locus via an internal ribosomal entry site (referred to here as GCD-IRES-GFP, (Greer et al., 2016)), we made initial efforts to expose GC-D glomeruli via a modified dorsal craniotomy that required obstructing the blood flow from the rostral rhinal vein via a coagulating gelfoam or vessel cauterization in order to expose the caudal-most extent of the dorsal MOB **(Fig. 2.1B)**. However, these experiments revealed that, with a few exceptions, dorsal GC-D glomeruli (like glomeruli within the AOB) are inaccessible. In most cases, GC-D axons could be observed coursing caudally along the surface of the OB, but they disappeared beneath the inferior cerebral vein (shown in **Fig. 2.1C**). In only a few instances were glomeruli visible for targeting.

To reliably expose GC-D glomeruli *in vivo* we therefore developed a bulbar preparation in which part of the ventrolateral aspect of the OB, lateral olfactory tract (LOT), and the anterior basal forebrain are exposed **(Fig. 2.2A)**. In addition to requiring cauterization of the rostral rhinal vein as it exits the skull, this preparation requires the removal of the mouse's eye to gain access to the ventrolateral surface of the OB. GC-D axons enter the OB ventrally, coalescing into glomeruli as they course caudally and dorsally (Walz et al., 2007). Thus, ventrolateral GC-D glomeruli are located slightly more anterior than the dorsal GC-D glomeruli and are not obscured by vasculature. Our ventrolateral bulbar preparation allows us to visualize approximately one to five GC-D glomeruli per mouse via two-photon microscopy **(Fig. 2.2B)**. The positions of most GC-D glomeruli are not stereotyped from mouse to mouse, though a large ventral glomerular "complex" can be reliably identified between animals (Walz et al., 2007). This

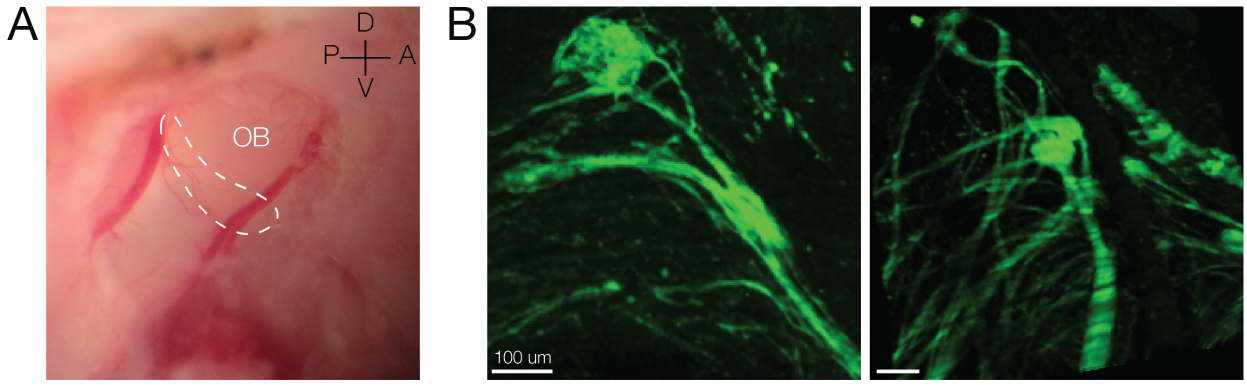

Figure 2.2. Exposure of GC-D Necklace Glomeruli *In Vivo*

(A) Photo of the surgical preparation, with a portion of the ventrolateral OB and basal forebrain exposed. The approximate region occupied by the GC-D glomeruli is delineated by the dotted line.

(B) Exposed GC-D glomeruli in two preparations, illustrating variability observed between mice.

stochasticity of glomerular position accounts for much of the variability in the number of glomeruli exposed per surgical preparation, with the remainder of the variability due to differences in the exact position and size of the craniotomy.

Labeling Individual GC-D Glomeruli via a Dye Electroporation Technique

Our laboratory previously developed a method to selectively label glomeruli innervated by OR-expressing OSNs *in vivo* using a dye electroporation technique (Sosulski et al., 2011). Briefly, this entails targeting a glass pipette filled with the red fluorescent dye tetramethylrhodamine (TMR)-dextran to the center of a glomerulus under two-photon guidance and applying electrical pulses to eject dye from the pipette and promote uptake of the dye by processes of cells associated with that glomerulus. We have demonstrated that this method selectively labels only cells associated with the target glomerulus, which is likely due to the fact that the glomerulus – a dense neuropil structure comprised of axonal and dendritic processes – is an electrically insulated structure. Under appropriate stimulation conditions, the extent of the electric field generated by the electrical pulses can be restricted to a single glomerulus. Electric pulses facilitate the uptake of small molecules by inducing transient pores in cell membranes as a result of abrupt changes in the transmembrane potential (Martinez and Hollenbeck, 2003).

This method can in theory be employed using single-photon, epifluorescence illumination. However, we find that the additional axial resolution afforded by multiphoton microscopy is essential to ensure precise targeting of the pipette to the

center of the glomerulus (thereby maximizing the specificity of labeling to a single glomerulus). Additionally, the processes of cells associated with a given glomerulus are not uniformly distributed within the glomerulus, but rather exhibit compartmentalization. In particular, OSN axon terminals preferentially occupy the dorsal portion of the glomerulus, while the dendritic tufts of M/T cells are enriched within the ventral portion of the glomerulus (Kasowski et al., 1999). In our experience, we can bias the labeling of OSN axons or M/T cells through slight shifts in pipette position along the dorsal-ventral axis within a glomerulus, but such precise adjustments can only be made under two-photon guidance. Such fine targeting allows us to optimize labeling for specific experiments, such as the anterograde tracing of M/T axons to higher brain regions versus the retrograde labeling of OSN cell bodies within the MOE.

To achieve specific and robust labeling of GC-D glomeruli *in vivo*, several modifications were made to the protocol published by Sosulski *et. al.*, necessitated by the difference in size and character of GC-D glomeruli as compared to canonical glomeruli. As a population, GC-D glomeruli exhibit a trimodal distribution of three distinct sizes (Walz et al., 2007), with approximately half of the necklace glomeruli corresponding to the smallest size (average diameter 66.6 ± 10.9 μm) (Walz et al., 2007). This is on the small end of OR-expressing glomeruli, which largely range from 50-120 μm in diameter (Royet et al., 1988). Furthermore, while conventional glomeruli are characteristically very dense structures, the OSN inputs to many GC-D glomeruli appear much less dense, or more “wispy” (Walz et al., 2007). For these seemingly less-dense (and likely less electrically insulated) GC-D glomeruli, we observed a tendency

for non-specific labeling when using the previously published stimulation conditions.

Other experimental considerations further necessitated an optimization of our electroporation protocol. First, we modified the stimulation parameters and recovery times so as to optimize cell health and labeling for the anterograde tracing of M/T cell axons or the retrograde labeling of OSN cell bodies, respectively. Second, we took extra precautions to maximize tissue health since this surgical exposure – which includes the removal and cauterization of tissue and blood vessels, a duratomy of highly vascularized ventral dura, and the exposure of forebrain tissue – is more severe than traditional dorsal OB craniotomies. Overall, the major modifications to the published protocol involved establishing strict requirements for the shape and electrical resistance of the glass pipette used to deliver the dye and minimizing the deleterious effects of electrical stimulation on cell health by reducing the duration and intensity of the electroporation protocol.

With this protocol we can selectively label individual GC-D glomeruli, including the innervating OSN axons and associated M/T cells **(Fig. 2.3A)**. After the appropriate amount of recovery time to allow for dye transport, we are able to recover labeled OSN cell bodies in the MOE **(Fig. 2.3B)** and labeled M/T cell axons in many downstream brain regions **(Fig. 2.3C)**. We have not yet optimized this technique to trace fibers from GC-D glomeruli to the most posterior regions of the brain; however, we are confident that we could further optimize experimental parameters to better approximate the degree of labeling achieved in Sosulski *et. al.*. (For more comments on this, see the Notes on Technical Limitations and Troubleshooting section.)

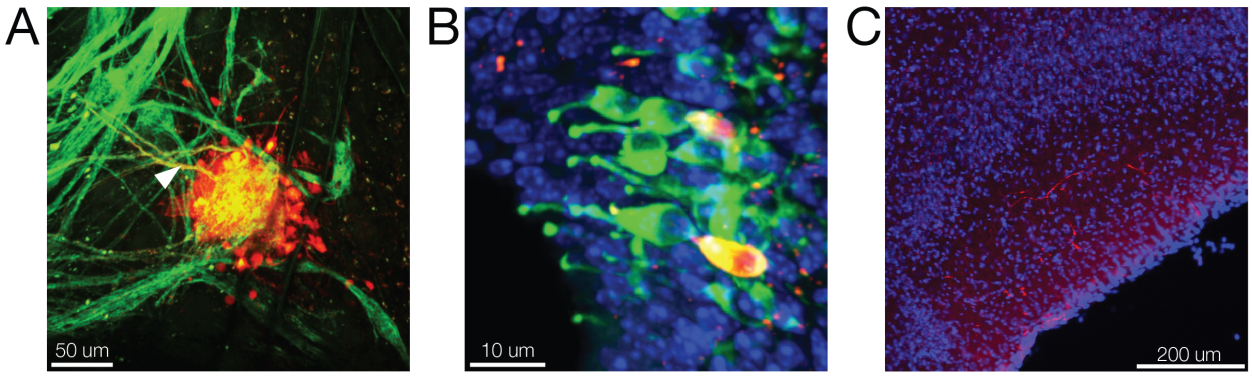

Figure 2.3. Individual GC-D Glomeruli and their Connections Labeled by Electroporation

(A) GC-D glomerulus labeled by electroporation. Axons of OSNs innervating the glomerulus (arrowhead) and cell bodies associated with the glomerulus are labeled.

(B) Following recovery of the mouse, labeled GC-D OSNs (yellow) are visible in the cul-de-sacs of the epithelium.

(C) TMR-labeled axons of M/T cells are also visible in the brain.

Modifications to Surgical Preparation to Expose GC-D OSN Cell Bodies in the MOE

Notably, this surgical preparation can also be used to expose OSN cell bodies within the caudal portions of the MOE by extending the craniotomy in the anterior direction. In a GCD-IRES-GFP mouse the cul-de-sac regions are easily identified by their GFP fluorescence **(Fig. 2.4A,B)**. Thus, in conjunction with a genetically encoded calcium indicator, this preparation could be used to image the odor responses of GC-D cell bodies in the MOE and even to compare them to the odor-evoked responses within individual GC-D glomeruli within the same animal. To date, no such comparisons between OSN responses at the cell body (which solely reflect receptor activation) and those exhibited by glomeruli (which reflect the summed responses of OSN activation and local inhibitory inputs onto OSN axons) have been feasible for the GC-D or any other mammalian olfactory subsystem. This preparation therefore has wide-reaching applications that promise to provide new insights into the general principles governing mammalian olfaction.

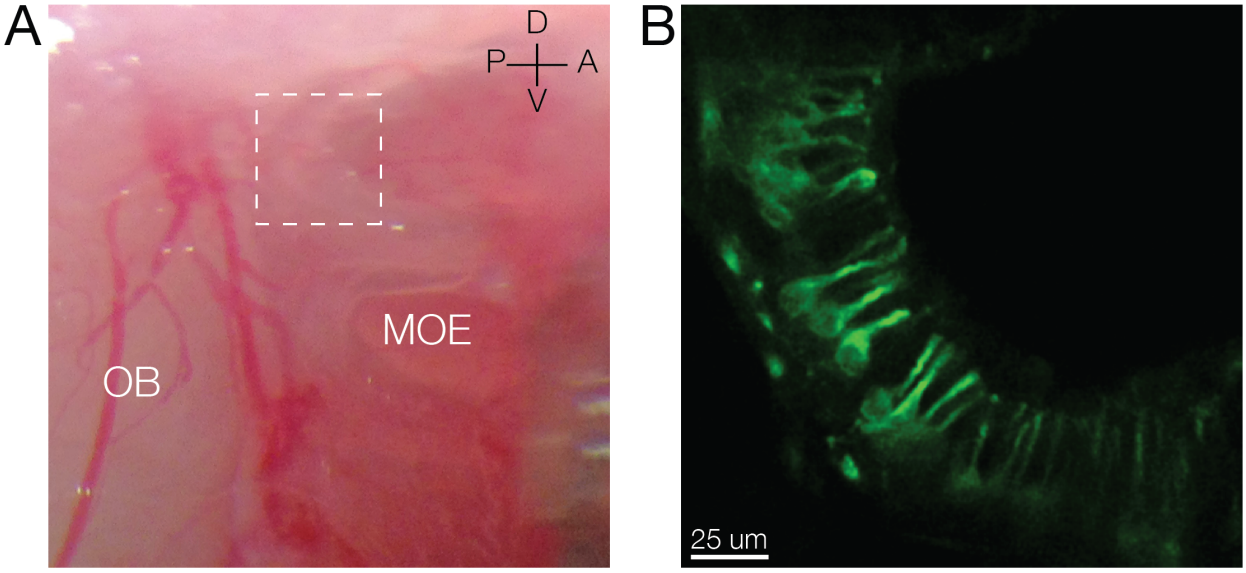

Figure 2.4. A Modified Surgical Exposure to Visualize GC-D OSNs *In Vivo*

(A) Photo of the modified ventrolateral surgical preparation exposing the cul-de-sacs (e.g. the outlined region) and posterior portion of the MOE.

(B) GC-D cells within a cul-de-sac of the MOE are visible under a multiphoton microscope. The field of view is similar to the outlined region in **A**.

MATERIALS

Surgical Exposure

Reagents

*Mice, e.g. GCD-IRES-GFP (The Jackson Laboratory, strain #006704)

- Note: All procedures must be done in accordance with institutional IACUC guidelines

*Bleach, 10% (disinfectant, diluted in double-distilled H_2O)

*Ethanol, 70% (disinfectant, diluted in double-distilled H_2O from 200-proof stock)

*Betadine, 7.5% (disinfectant)

*Air canister

*Sterile lactated Ringer's solution (saline wash)

*Petroleum jelly (eye lubricant)

*Kwik-Sil (fast-setting silicone used to make imaging well)

*Kwik-Cast (silicone sealant to cover exposure during recovery)

*ESPE RelyX luting cement

*Gelfoam

*Anesthetics

- Induction via ketamine/xylazine/acepromazine cocktail diluted in sterile lactated Ringer's solution, dose at 100mg/kg K; 10mg/kg X; 3mg/kg A. *Note: ketamine is a controlled substance and should be handled according to institutional rules.*

- Maintenance with ketamine diluted in sterile lactated Ringer's solution (dose at 30mg/kg)

*Analgesics

- Bupivacaine, apply as intradermal nerve block prior to incision, dose at 1 mg/kg, at a volume < 0.2 mL.

- Lidocaine jelly, 2%, apply topically to tissue prior to eye/tissue removal and to skull before drilling

- Buprenorphine diluted in lactated Ringer's solution, dose at 0.05 mg/kg (i.p. injection, at least 4 doses given every 12 hours) for post-operative pain relief. *Note: buprenorphine is a controlled substance and should be handled according to institutional rules.*

*Anti-inflammatories

- Dexamethasone/Carprofen, apply subcutaneously as a cocktail diluted in sterile lactated Ringer's solution, dose at 0.2 mg/kg dex; 5 mg/kg carp.

*Low-melt agarose, 2% w/v in lactated Ringer's solution

Equipment

*Personal protective equipment (as per required by institutional guidelines, e.g. sterile gloves, lab coat, hair net, face masks)

*Laboratory scale

*Electric clippers

*Hand-held air drill

*Cautery

*Temperature-controlled circulating water pad

*Breadboard (e.g. ThorLabs), fitted with posts to attach to head post

*Steel head post

*Surgical tools (e.g. Fine Science Tools, including surgical scissors, multiple pairs of #55 forceps (blunted for bone removal, sharp for duratomy), #7 fine forceps)

*Dissecting microscope (e.g. Leica MZ75) and light source (e.g. Leica KL1500 LCD)

*Sterile cotton swabs with wooden dowels

*Eye spears (BVI visitec)

*Plastic transfer pipettes

*Bench pads

*Microwaveable heating pads

*Recovery cage (e.g. disposable plastic cage with clean bedding, Kimwipes, plastic water bottle, food pellets, cap of a 50mL conical tube filled with water and placed on floor of cage)

Electroporation

Reagents

*Dextran, tetramethylrhodamine 3000 MW, anionic, lysine-fixable (Thermofisher D3308), 12.5 mg/mL in sterile lactated Ringer's solution

*Sterile lactated Ringer's solution

*Electrode cream (e.g. signa crème)

Equipment

*0.1um microcentrifuge filters

*1.0 mm O.D. x 0.78 mm I.D. thin-walled borosilicate glass w/filament (Sutter)

*Micropipette puller (we use the Sutter P-2000)

*Light microscope with eyepiece reticule (to measure pipette diameters)

*Impedance meter (e.g. as supplied with microelectrode bevelers like the Sutter BV-10, to measure pipette resistance)

*Small electric heating pad

*Epifluorescence light box with filters for FITC and TRITC

*Bright-field lamp

*Two-photon microscope (e.g. Prairie microscope with a Coherent Discovery laser, imaging performed at 860-880 nm)

*Micromanipulator (e.g. Sutter MP-285)

*Electrode holder (World Precision Instruments, MEH7W-1.0 O.D.)

*Micro-Fil tips (World Precision Instruments, MF34G-5") and 1 mL syringes

*Grass Technologies SD 9 stimulator, with insulated wires to connect from the cathode to the electrode holder, and from the anode to the mouse's rear paw (via a metal alligator clip)

Tissue Processing

Reagents

*Anesthesia for perfusion (overdose of K/X/A or isoflurane)

*Phosphate-buffered saline

*Paraformaldehyde, 4% in 1x phosphate-buffered saline (PBS)

*Sucrose, 20% w/v in 1x PBS (for processing brain tissue)

*Tissue freezing medium (VWR)

*0.45M EDTA, pH 8.0 (diluted in 10x PBS from 0.5M stock, for processing MOE)

*Vectashield mounting medium, with DAPI (for mounting MOE sections)

*Clear nail polish (to seal slides)

*For IHC of TMR axonal signal in brain slices:

- Rabbit-anti-TMR antibody (Abcam ab191343, 1:500 in block solution)

- Donkey-anti-rabbit-AlexaFluor555 (ThermoFisher A-31572, use at 1:250 dilution in block solution)

- Block solution (1x PBS + 2% TX-100 + 0.5% BSA + 0.02% NaN_3)

- Wash solution (1xPBS + 0.1% TX-100)

- NeuroTrace 435/455 (Nissl stain, 1:100 in block solution)

- Vectashield mounting medium

Equipment

*Tools for animal perfusion (e.g. syringes, butterfly needle, dissection tools including large scissors, bone scissors, blunt forceps, fine #55 forceps)

*Plastic cryomolds

*Cryostat, with slide warmer

*Superfrost Plus microscope slides and #1 coverglass

*Incubation chambers for IHC

PROTOCOL

Surgical Exposure (Timing: ~1.5-2 hrs for exposure, ~15 min for post-imaging recovery)

1) Prepare the surgical area. Wipe down the area and dissection scope with 70% ethanol and 10% bleach, and lay out a fresh bench pad. Make sure proper PPE is worn.
2) Weigh the mouse on the scale and calculate the appropriate volume of the induction anesthesia to give a dose of 100mg/kg K; 10mg/kg X; 3 mg/kg A. Inject the anesthesia intraperitoneally using a 1mL syringe. Briefly withdraw the plunger of the syringe prior to injection to ensure there is no blood. (Note: during the extent of the surgery and electroporation procedure, monitor the mouse's level of anesthesia and supplement with 30mg/kg ketamine when needed. *Do not give the mouse additional xylazine!*)
3) As soon as the mouse is immobile (~2 minutes), place the animal on the circulating water heating pad and wait until the mouse reaches surgical-level anesthesia (lack of response to nociceptive stimuli) before proceeding. This normally takes 10-15 minutes. During this time, inject the dexamethasone/carprofen solution subcutaneously into the scruff of the mouse's neck at a dose of 1.2 mg/kg dex; 5 mg/kg carp.
4) Shave the fur on the skull and as much around the right eye as possible. Clean skin with 70% ethanol followed by betadine, repeated 3x.
5) Intradermally inject the bupivacaine (1 mg/kg) in a patch of skin posterior to the whisker patch and wait ~ 5 minutes before removing the skin. Remove a large

swath of skin overlying the dorsal skull by grasping the skin with forceps and cutting the skin off of the skull with scissors, starting approximately at the caudal end of the whisker patch and cutting in the caudal direction until just past the skull. (The extent of the skull should be exposed, in addition to a small amount of tissue just posterior to the skull.)

6) Place petroleum jelly over the left eye to keep it moist throughout the procedure.
7) Dry the skull with the air canister and apply freshly mixed luting cement to the back of the skull. Affix the head post (rest the mouse's head on the bulb of a plastic transfer pipette that is cut in half to raise the head slightly off of the ground) and let the cement cure for 10-15 minutes.
8) Using blunted forceps, carefully tease away the tissue above the eye socket that is connected to the skull. With the cautery, cauterize the rostral rhinal vein as it exits the skull and any other small vessels anchoring the eye to the socket. Roll small squares of dry gelfoam between the fingers to make compact rolls and gently position into the base of the eye socket of the skull using forceps. Stuff enough gelfoam into the socket so that it compresses the eyestalk. This will result in less bleeding when the eye is removed.
9) Apply lidocaine jelly to the eye and wait 2-5 minutes before using the scissors to remove the eye and connective tissue. Use additional gelfoam, eyespears, and/or cauterization to stop any bleeding.
10) Gently cauterize the tissue immediately ventral to the zygomatic bone along the bone's length in preparation for bone removal. Drill through the zygomatic bone

at its anterior and posterior ends to release a bone segment. Remove the segment with blunt forceps.

11) At this point, cauterize any tissue that will interfere with drilling the craniotomy or accessing the brain under the two-photon microscope. Stuff dry gelfoam into the tissue pocket/cavity behind the lacrimal bone (against the frontal bone, at the anterior end of the exposure), as this tends to bleed during the craniotomy. Rinse with saline (lactated Ringer's solution) and place a large square of gelfoam soaked in lactated Ringer's solution over the skull and exposed tissue while the imaging well is made.

12) Break a small piece of the wooden dowel from a cotton swab (approximately the length from the head post to the tip of the nose). To construct the imaging well, use a mixer tip to mix and apply a ring of Kwik-Sil at the skin's edge completely surrounding the exposure (i.e. against the base of the head post, ventral to the orbital socket, anterior to the whisker pad, and back in the posterior direction along the skin on the dorsal surface of the contralateral hemisphere). Before the Kwik-Sil sets (~ 1 minute), place the wooden dowel in the Kwik-Sil on the contralateral (left) dorsal surface of the skull. One must "build up" this side of the well in order for the well to hold liquid, as the mouse's head will be tilted under the microscope (right side facing up). Add another layer of Kwik-Sil along the extent of the well, applying it over the wooden dowel. (Note: do not add an excessive height of Kwik-Sil ventral to the orbital bone, as the pipette for electroporation will need to access the prep from that angle.) Use a wooden

dowel that has been snapped in half to yield a pointed end to finely adjust the Kwik-Sil well before it solidifies. To test the well, remove the moistened gelfoam, tilt the mouse's head, and apply lactated Ringer's solution to the well using a plastic transfer pipette. Ensure that the liquid is held in the imaging well.

13) Flush the well once more with lactated Ringer's solution. Remove the solution and, with the mouse's head at an angle, drill the craniotomy by lightly drilling the outline of the exposure and repeatedly passing over the outline with the drill to thin the skull. Continue to flush the bone with lactated Ringer's solution The craniotomy should extend to a small portion of the forebrain in the posterior direction and just posterior to the nasal epithelium in the anterior direction, following along the contour of the cribriform plate. (Refer to **Fig. 2.2A** for an example exposure.) (Note: for the modified MOE exposure, shift the entire extent of the craniotomy in the anterior direction. Remove the bone overlying the caudal end of the dorsal-most nasal turbinates in the anterior direction, and end the exposure just before the forebrain in the posterior direction, see **Fig. 2.3A**.) When the skull is thinned (or even cracked at the edges of the exposure) use the #7 forceps to gently break into the bone at the center of the exposure, where the OB meets the forebrain. The bone is thickest here. Carefully bring the tips of the forceps together to break the remaining bone anchoring the bone fragment to the rest of the skull and pull outward. The bone overlying the craniotomy should "peel" open from the dorsal surface down, like the opening of an oven door. (A

critical note: make sure you do not lose hold of the bone, as it has a tendency to fall *into* the side of the brain, destroying the preparation.)

14) Flush the preparation with lactated Ringer's solution, and keep the exposed brain submerged with liquid as the duratomy is performed. To remove the dura gently drag *very sharp* #55 forceps along the dura until it snags. Slowly peel the dura away, taking care to not pull on it. (Note: duratomizing the brain is essential for the electroporation procedure. While pipette tips that can puncture dura can be crafted from harder glass like quartz, the dye remains trapped beneath the dura during the period of recovery and this yields non-specific labeling.) The mouse is now ready to image.

Proceed with in vivo *imaging and/or electroporation (See electroporation protocol below.) Upon completion of imaging, recover the mouse as follows:*

15) Place a fresh square of gelfoam – moistened in lactated Ringer's solution – over the entire exposed brain.
16) Over the gelfoam, fill the well with a warm 2% low-melt agarose solution. (Note: do not apply this solution while hot. We fill a plastic transfer pipette with the hot agarose solution and run it under cold water until it cools to the point that we can place the pipette comfortably against the skin above the upper lip of the skin of the medial wrist.)

17) Once the agarose has solidified, cover the entire exposed area with freshly mixed Kwik-Cast and allow it to cure (~5 minutes). Once cured, carefully remove the head post and luting cement from the skull (using scissors if necessary) and cover the exposed skull and tissue with additional Kwik-Cast.
18) Administer the first post-operative dose of buprenorphine (0.05mg/kg) intraperitoneally. Leave the mouse on the circulating water heating pad until he shows signs of waking. Transfer the mouse to a clean cage containing food pellets on the ground, a water-filled 50mL conical tube cap placed on the ground (in addition to the hanging water bottle), and a few Kimwipes overlaid onto the bedding. Place the mouse onto the Kimwipes. Microwave a heating pad for 3 minutes and place beneath cage. Monitor the mouse until it wakes up.

<u>Electroporation (Timing: ~1-3 hrs, including set-up and imaging, depends on time allowed for dye diffusion away from injection site)</u>

0) Before beginning the surgery, pull pipettes of the correct size and resistance. *Critical: pipettes must be pulled to an inner diameter of ~5 µm. Optimal pipette resistance is ~2 MΩ. (Lower resistance can still be used, though the dye will spontaneous flow from tip and must be halted prior to the electroporation by applying a train of pulses with the opposite polarity. Higher resistance, in decreasing the current delivered to the tissue, results in less successful labeling under the normal stimulation conditions.)* In general, it is difficult to pull glass pipettes to large diameters without breaking the tips to achieve the desired size.

However, Sutter Instruments provides upon request a discussion of strategies to achieve large tips on the P-2000 laser pipette puller. While the exact program must constantly be adjusted due to environmental factors and the pipette puller itself, a good starting program is shown below. (Note that this is for 1.0 mm O.D. x 0.78 mm I.D. borosilicate glass.) Even the "optimized" program introduces a degree of variability; as such, researchers must visually inspect and measure the diameter of each tip using a light microscope fitted with a reticule in the eyepiece. The resistance of the pipettes can be measured using an impedance meter such as those supplied with microelectrode bevelers. Back-fill the pipette with, and submerge the tip in, lactated Ringer's solution when measuring the resistance.

Line	Heat	Filament	Velocity	Delay	Pull
1	320	5	80	200	0
2	320	4	60	200	0
3	290	4	30	200	0
4	290	4	30	200	0

1) Pass a small amount of the 12.5 mg/mL TMR-dextran solution through a 0.1 um filter in a tabletop centrifuge at maximum speed for 2-3 minutes. (Note: TMR-dextran solution that is leftover from the day's injections can be stored at 4°C and re-filtered for use on another day.)
2) Back-fill the pipette with the TMR-dextran solution using a Micro-Fil tip fitted onto a 1 mL syringe. Place the pipette onto an electrode holder that is mounted on a

microcontroller connected to the two-photon microscope stage. Connect the stimulator cathode (-) to the electrode holder.

3) Place the mouse under the two-photon microscope, on top of an electric heating pad. Place a Kimwipe beneath the mouse's rear right foot and apply electrode cream to the paw. Clamp the alligator clip of the wire connected to the stimulator anode (+) to the rear paw.
4) Use the epifluorescence box to find a GC-D glomerulus and bring it to the center of the field of view. Change the filter cube and slowly bring the pipette under the objective and use the fluorescence of the dye to find the tip. Briefly turn on the stimulator to test that pulses of dye emerge from the tip. Switch to the bright-field lamp and lower the pipette to just above the surface of the brain.
5) Switch to two-photon illumination and slowly guide the tip of the pipette into the center of the target glomerulus. (Note: For large, dense glomeruli, position the pipette in the lower half of the glomerulus for anterograde tracing of M/T cell axons, and in the upper half of the glomerulus for retrograde labeling of OSN cell bodies.)
6) (Optional) Collect a Z-stack showing the position of the pipette within the glomerulus before the electroporation. We use the PrairieView software by Bruker Fluorescence Microscopy for multiphoton image acquisition.
7) Turn on the stimulator briefly to deliver ~5 "test pulses", then turn off and wait ~ 5 min to allow for diffusion of the dye away from the site of injection. Use the following stimulation settings for the electroporation:

Voltage: 20 V

Pulses Per Second (PPS): 2-3

Pulse Duration: 20-30 msec

Monophasic pulses, reverse polarity, continuous pulses

8) At this point clear labeling of a single glomerulus (including cell bodies) should be evident. If not, the pipette is not correctly positioned. Re-position the pipette if necessary. Otherwise, continue with the actual electroporation protocol. Using the same stimulation conditions, electroporate the glomerulus for **30-60 sec**, repeated **2-5 times** (depending on the size of the glomerulus and the completeness of labeling). Allow sufficient time between stimulation bouts for dye diffusion away from the injection site. Immediately after one stimulation bout, thoroughly flush the imaging well with lactated Ringer's solution and **wait 5-30 minutes** before the next round of stimulation. For particularly large glomeruli, one may wish to slightly shift the position of the pipette between stimulation bouts if labeling appears restricted to sub-compartments within the glomerulus. (Note: One can also install a perfusion system to constantly drip fresh lactated Ringer's solution onto the prep during stimulation, though the motion artifacts introduced by such as system prevent quality imaging. Therefore, turn off the perfusion system during image acquisition.)
9) After the final round of electroporation, collect a Z-stack of the electroporated glomerulus. (Note: Depending on the time elapsed following the final stimulation period, one may be able to visualize intrabulbar labeled fibers innervating other

GC-D glomeruli within the field of view.) Recover the mouse as per *Step 15* of the **Surgical Exposure** protocol above. For retrograde labeling of OSNs, the mouse should be recovered for 1-3 days; for anterograde tracing of M/T axons, the mouse should be recovered for 2-7 days, depending on the brain region of interest. (Longer recovery times result in greater dye transport but also deteriorated tissue health.)

Tissue Processing

We follow standard protocols to process and stain the tissue. Briefly:

1) Following recovery (1-3 days for labeling OSNs, 2-7 days for labeling M/T cells), sacrifice the mouse by transcardial perfusion. Perfuse 10 mL of 1x phosphate-buffered saline (PBS) followed by 15 mL of 4% paraformaldehyde (PFA).
2) Dissect out the brain (with OB attached) and drop-fix in 4% PFA overnight at 4ºC. To dissect the MOE, remove the septal bones from the snout and remove the palate and any other remaining tissue on the ventral side of the snout. Drop-fix the nose in 4% PFA overnight at 4ºC.
3) Cryoprotect the brain by transferring it to 20% sucrose solution overnight at 4ºC. De-calcify the nose by transferring it to 0.45M EDTA solution overnight at 4ºC.
4) Prepare the tissues for cryosectioning. First rinse each with 1x PBS and place each in a plastic cryomold filled with tissue-freezing medium (TFM). Equilibrate at room temperature for at least 30 minutes. Freeze the blocks on dry ice and place blocks in cryostat. Equilibrate for at least one hour before sectioning.

5) Cryosection the tissue. We typically collect 50 µm coronal sections of the brain and 20-50 µm sections of the OB (including the necklace region). We typically collect 30 µm coronal sections of the MOE.
6) For MOE sections, wash the slides 2x in wash solution (see recipe in *Reagents* section) to remove TFM and mount in Vectashield+DAPI. Seal slides with nail polish and image. For brain sections, wash slides 2x in wash solution and proceed with immunohistochemistry (IHC) procedure to amplify TMR-dextran signal, as described below.
7) *IHC protocol for TMR stain (adapted from* (Sosulski et al., 2011)*):* After rinsing the slides in wash solution, incubate with rb-anti-TMR (1:500) and NeuroTrace 435/455 (1:100), diluted in block solution (see recipe in *Reagents* section) overnight at room temperature. Rinse 3x5 minutes in wash solution and incubate with dk-anti-rb-AF555 (1:250, diluted in block solution) for 1-2 hours at room temperature. (Note: Centrifuge the secondary antibody at maximum speed in a tabletop centrifuge at 4ºC for 5 minutes before using.) Wash 3x5 minutes in wash solution and mount in Vectashield mounting medium. Seal slides with nail polish and image.

NOTES ON TECHNICAL LIMITATIONS AND TROUBLESHOOTING

The most critical factor for successful labeling is the health of the brain tissue during the extent of the surgical exposure, electroporation procedure, and recovery period. Pre-surgical administration of dexamethasone and carprofen has proven essential to minimize brain inflammation. Extra care must also be taken during the bone drilling and duratomy steps of the surgical procedure to maximize tissue health. When drilling to make the craniotomy, only light pressure should be applied to the bone and the well must be frequently flushed with saline to prevent thermal damage of the tissue. When removing the dura, take care to avoid pulling on the dura or accidentally rupturing small blood vessels that span the dura and the brain, which results in small foci of hemorrhaging on the brain. Keep the brain moist at all times. Minimize blood loss during the surgical procedure. During recovery, ensure that there are no active sources of bleeding before placing the gelfoam and agarose over the brain. Make sure that the agarose is not too hot when applied to the exposure, as this often induces thermal damage and bleeding in the adjacent tissue. In the best-case scenario, the brain should have no evidence of hemorrhaging upon dissection (i.e. the brain should look identical to a normally dissected brain from a non-surgical mouse). Significant hemorrhaging on either the OB or forebrain indicates a sub-optimal surgical exposure or recovery.

A second feature that appears to correlate with tissue health is the degree to which an immune response is induced in the OB and forebrain, as indicated by the presence of fluorescently labeled microglia/macrophage-like cells within the tissue. (Presumably these cells represent activated immune cells that internalized either TMR-

dextran associated with damaged/dying processes or free-floating extracellular TMR-dextran within the tissue.) In particular, the glial limitans is prominently labeled in most mice following this ventral surgical exposure. The glial limitans is a thin barrier comprised of astrocytic endfeet and basal lamina that resides just beneath the pia mater. It is also found at blood vessels within the brain and comprises part of the blood-brain barrier (McGavern and Kang, 2011). Some degree of labeling of the glial limitans following this ventral surgical exposure is unavoidable, though it is almost always absent from the traditional dorsal OB exposure. This likely, therefore, reflects the increased severity of the ventral surgical preparation. Strong labeling of the glial limitans can make it difficult to identify labeled M/T fibers (which have comparably weaker fluorescence) in ventrally located olfactory brain regions that lie immediately adjacent to the edge of the brain.

In optimizing the stimulation parameters of the electroporation protocol, one must sacrifice some degree of cell labeling to maintain specificity and cell health. Using the conditions described here, cell viability is maintained for days after the electroporation (we have not tested time periods beyond 7 days) and labeled M/T cell axons can be found at distances up to 5 mm from the OB. However, the fibers become fainter as they progress caudally in the brain and we rarely observe fibers in the posterior-most reaches of olfactory targets like the entorhinal cortex, even in “control” electroporations of ventral OR-expressing glomeruli known to project to this region. As such, we recognize that with the current experimental conditions our electroporation technique can be used to identify *some* targets of GC-D glomeruli M/T axons, though the tracing

results do not necessarily reflect a comprehensive catalog of the downstream brain targets. With further modification of the electroporation protocol and surgical preparation to increase cell viability, we are confident that we could further optimize the extent of labeling. In the interim, we advocate for the use of a second, target-based tracing strategy, such as one of the virally mediated anatomical approaches (Callaway and Luo, 2015; Wachowiak et al., 2013), to probe and validate posterior targets.

REFERENCES

Arakawa, H., Kelliher, K.R., Zufall, F., and Munger, S.D. (2013). The Receptor Guanylyl Cyclase Type D (GC-D) Ligand Uroguanylin Promotes the Acquisition of Food Preferences in Mice. Chem Senses *38*, 391–397.

Bozza, T., McGann, J.P., Mombaerts, P., and Wachowiak, M. (2004). In Vivo Imaging of Neuronal Activity by Targeted Expression of a Genetically Encoded Probe in the Mouse. Neuron *42*, 9–21.

Buck, L., and Axel, R. (1991). A novel multigene family may encode odorant receptors: A molecular basis for odor recognition. Cell *65*, 175–187.

Callaway, E.M., and Luo, L. (2015). Monosynaptic Circuit Tracing with Glycoprotein-Deleted Rabies Viruses. Journal of Neuroscience *35*, 8979–8985.

Chess, A., Simon, I., Cedar, H., and Axel, R. (1994). Allelic inactivation regulates olfactory receptor gene expression. Cell *78*, 823–834.

Fülle, H.J., Vassar, R., Foster, D.C., Yang, R.B., Axel, R., and Garbers, D.L. (1995). A receptor guanylyl cyclase expressed specifically in olfactory sensory neurons. Proc Natl Acad Sci USA *92*, 3571–3575.

Greer, P.L., Bear, D.M., Lassance, J.-M., Bloom, M.L., Tsukahara, T., Pashkovski, S.L., Masuda, F.K., Nowlan, A.C., Kirchner, R., Hoekstra, H.E., et al. (2016). A Family of non-GPCR Chemosensors Defines an Alternative Logic for Mammalian Olfaction. Cell *165*, 1734–1748.

Juilfs, D.M., Fülle, H.J., Zhao, A.Z., Houslay, M.D., Garbers, D.L., and Beavo, J.A. (1997). A subset of olfactory neurons that selectively express cGMP-stimulated phosphodiesterase (PDE2) and guanylyl cyclase-D define a unique olfactory signal transduction pathway. Proc Natl Acad Sci USA *94*, 3388–3395.

Kasowski, H.J., Kim, H., and Greer, C.A. (1999). Compartmental organization of the olfactory bulb glomerulus. J Comp Neurol *407*, 261–274.

Martinez, C., and Hollenbeck, P. (2003). Methods in Cell Biology (Elsevier).

McGavern, D.B., and Kang, S.S. (2011). Illuminating viral infections in the nervous system. Nature Publishing Group *11*, 318–329.

Meister, M., and Bonhoeffer, T. (2001). Tuning and topography in an odor map on the rat olfactory bulb. Journal of Neuroscience *21*, 1351–1360.

Meyer, M.R., Angele, A., Kremmer, E., Kaupp, U.B., and Muller, F. (2000). A cGMP-signaling pathway in a subset of olfactory sensory neurons. Proc Natl Acad Sci USA *97*, 10595–10600.

Munger, S.D., Leinders-Zufall, T., McDougall, L.M., Cockerham, R.E., Schmid, A., Wandernoth, P., Wennemuth, G., Biel, M., Zufall, F., and Kelliher, K.R. (2010). An olfactory subsystem that detects carbon disulfide and mediates food-related social learning. Curr Biol *20*, 1438–1444.

Oka, Y., Katada, S., Omura, M., Suwa, M., Yoshihara, Y., and Touhara, K. (2006). Odorant receptor map in the mouse olfactory bulb: in vivo sensitivity and specificity of receptor-defined glomeruli. Neuron *52*, 857–869.

Royet, J.P., Souchier, C., Jourdan, F., and Ploye, H. (1988). Morphometric study of the glomerular population in the mouse olfactory bulb: numerical density and size distribution along the rostrocaudal axis. J Comp Neurol *270*, 559–568.

Rubin, B.D., and Katz, L.C. (1999). Optical imaging of odorant representations in the mammalian olfactory bulb. Neuron *23*, 499–511.

Shirasu, M., Yoshikawa, K., Takai, Y., Nakashima, A., Takeuchi, H., Sakano, H., and Touhara, K. (2014). Olfactory receptor and neural pathway responsible for highly selective sensing of musk odors. Neuron *81*, 165–178.

Sosulski, D.L., Bloom, M.L., Cutforth, T., Axel, R., and Datta, S.R. (2011). Distinct representations of olfactory information in different cortical centres. Nature *472*, 213–216.

Uchida, N., Takahashi, Y.K., Tanifuji, M., and Mori, K. (2000). Odor maps in the mammalian olfactory bulb: domain organization and odorant structural features. Nat Neurosci *3*, 1035–1043.

Vassar, R., Chao, S.K., Sitcheran, R., Nun, J.M., and Vosshall, L.B. (1994). Topographic organization of sensory projections to the olfactory bulb. Cell *79*, 981–991.

Wachowiak, M., Economo, M.N., Díaz-Quesada, M., Brunert, D., Wesson, D.W., White, J.A., and Rothermel, M. (2013). Optical dissection of odor information processing in vivo using GCaMPs expressed in specified cell types of the olfactory bulb. Journal of Neuroscience *33*, 5285–5300.

Walz, A., Feinstein, P., Khan, M., and Mombaerts, P. (2007). Axonal wiring of guanylate cyclase-D-expressing olfactory neurons is dependent on neuropilin 2 and semaphorin 3F. Development *134*, 4063–4072.

CHAPTER 3

Unique Architecture of the GC-D Necklace Olfactory Subsystem Suggests Novel Functions

Taralyn M. Tan, Kristen L. Drummey, Neha D. Bhagat,

Jesse M. Katon, and Sandeep R. Datta

Author Contributions:

TMT and SRD designed the study. TMT performed the experiments with the following contributions from others: KLD performed stereotactic viral injections and assisted with tissue processing, imaging, and data analysis (rabies experiment quantification, **Fig. 3.8**); NDB assisted with tissue processing, imaging, and data analysis (MOE quantification, **Fig. 3.2**); JMK assisted with tissue processing. TMT made the figures and wrote the text with input from SRD and other members of the lab.

INTRODUCTION

Mice have evolved a number of anatomically and molecularly distinct olfactory subsystems to detect and process the vast range of olfactory stimuli in their environment. These subsystems work in concert to mediate innate, learned, and context-dependent behaviors in response to specific chemical cues. However, the exact mechanisms by which this cooperation occurs – and the specific roles for each subsystem in olfactory perception – remain poorly understood.

The largest and best-characterized subsystems are the main olfactory system and the accessory (or vomeronasal) olfactory system, whose olfactory sensory neurons (OSNs) are located within the main olfactory epithelium (MOE) or the vomeronasal organ (VNO), respectively. There also exist a number of smaller, less understood subsystems defined by the physical locations of their OSNs – such as the Grueneberg ganglion and the septal organ – or by their atypical molecular signatures, such as the guanylate cyclase D (GC-D) subsystem and the trace amine-associated receptor (TAAR) subsystem that are each comprised of specialized populations of OSNs within the MOE (Ihara et al., 2013; Liberles, 2014; Stowers and Logan, 2010).

In mammals, olfaction is initiated by the binding of odorant molecules to molecular receptors expressed by OSNs in the nose, which project axons to segregated structures of neuropil within the olfactory bulb (OB) of the brain called glomeruli. Within the glomeruli, OSN axons synapse onto second-order projection neurons called mitral and tufted (M/T) cells, which route olfactory information to a large number of downstream brain regions. Within this general framework of mammalian olfaction, the

rules by which olfactory information is encoded in the periphery and decoded by downstream behavioral circuits are contingent upon the specific anatomy of a given olfactory subsystem. Thus, elucidating the anatomical organization of a given olfactory subsystem is a critical first step to understand its function.

The main and accessory olfactory subsystems serve overlapping functions, though they are particularly specialized for odor discrimination/olfactory learning and pheromone-mediated innate behaviors, respectively (Su et al., 2009). Accordingly, each subsystem is endowed with molecular and anatomical features that support its specific functions. OSNs within the main olfactory system express members of the large olfactory receptor (OR) family of G protein-coupled receptors (GPCRs) (Buck and Axel, 1991) in a strict one receptor per neuron fashion (Chess et al., 1994). The OSNs that express a given OR are broadly distributed within a specific zone of the MOE, but their axons converge onto a small number of stereotyped glomeruli within the main olfactory bulb (MOB) (Vassar et al., 1994; 1993). Each M/T cell of the MOB innervates only a single glomerulus; thus, individual glomeruli within the MOB (which correspond to different OR species) constitute segregated and homogenous information channels that provide a suitable substrate for odor discrimination (Tirindelli et al., 2009). M/T cells of the MOB project to brain regions consistent with the subsystem's involvement in odor discrimination and olfactory learning – cortical areas like the piriform cortex (PCtx), anterior olfactory nucleus (AON), and entorhinal cortex (Ent) – in addition to regions like the posterolateral division of the cortical amygdala (plCoA) and olfactory tubercle (OT)

that may facilitate the subset of innate and motivated behaviors mediated by the main olfactory system (Haberly and Price, 1977; Nagayama, 2010; Sosulski et al., 2011).

In contrast, the anatomy of the vomeronasal system appears uniquely specialized to mediate innate behaviors in response to chemical stimuli emitted by conspecifics, potential mates, and predators. Vomeronasal sensory neurons also each express only a single olfactory receptor (or two, including a common co-receptor (Dalton and Lomvardas, 2015)) from different families of GPCRs (the V1R and V2R vomeronasal receptor families) (Dulac and Axel, 1995; Herrada and Dulac, 1997). The axons of sensory neurons expressing the same VR project to an average of 4-30 glomeruli within the accessory olfactory bulb (AOB) that tend to be less well-defined and smaller than MOB glomeruli, and often appear in ganglion-like chains (Belluscio et al., 1999; Del Punta et al., 2002; Haga et al., 2010; Rodriguez et al., 1999; Wagner et al., 2006). The M/T cells of the AOB each innervate multiple glomeruli corresponding to OSNs expressing the same or closely related VR (Belluscio et al., 1999; Del Punta et al., 2002). Thus, the AOB is organized to first distribute inputs from a specific OSN population across multiple glomeruli and then to integrate information from across glomeruli corresponding to different VRs. Both of these features of the glomerular organization are likely to improve pheromone detection by increasing the signal-to-noise of sensory signals through the recruitment of additional lateral inhibition and facilitating the coincident detection of closely related odorants that constitute pheromone blends (Del Punta et al., 2002; Kay and Sherman, 2007; Luo and Katz, 2004). Centrally, M/T cells of the vomeronasal system project to a distinct set of brain regions than those

innervated by the main olfactory system that are known to play integral roles in the generation of innate, odor-driven behaviors. These include amygdalar and “extended amygdalar” regions like the medial amygdala (MeA), posteromedial division of the cortical amygdala (pmCoA), and the bed nucleus of the stria terminalis (BNST) (Devor, 1976; Scalia and Winans, 1975).

Much less is known about the functional organization of the GC-D “necklace” subsystem, though atypical molecular and anatomical features suggest that this subsystem may employ yet a third set of rules distinct from either the main or vomeronasal systems to process olfactory information. Functionally, the GC-D subsystem mediates diverse olfactory-driven behaviors, including innate avoidance of carbon dioxide (Hu et al., 2007) and a form of olfactory learning – socially transmitted food preference (STFP) – in which mice will learn to prefer a particularly scented food after that food has been paired with odorants from mouse breath or feces (Arakawa et al., 2013; Munger et al., 2010). In addition, the GC-D subsystem is activated by a range of ethologically important odorants including pheromones, predator-derived odorants, and food-derived odors (Gao et al., 2010; Greer et al., 2016), which underscores the importance of this subsystem to the animal.

GC-D cells are concentrated within isolated, caudal portions of the MOE called cul-de-sacs. GC-D OSNs do not express members of the OR (or any other GPCR) family as olfactory receptors; rather, odor detection is mediated by the membrane-bound GC-D, as well as by members of the membrane-spanning, 4-pass A (Ms4a) gene family (Greer et al., 2016). Each GC-D cell co-expresses several MS4A receptors,

which stands in stark contradiction to the “one receptor-one neuron” rule governing receptor expression in all other characterized mammalian OSNs.

GC-D cells project axons to a seemingly interconnected ring of approximately 25-40 glomeruli (Juilfs et al., 1997; Shinoda et al., 1989; Walz et al., 2007) that encircles the caudal end of the MOB, giving the appearance of a “necklace.” Necklace glomeruli share many features of AOB glomeruli – including a lack of stereotypy in their number or precise locations, and their wispy, ganglion-like appearance – though the co-expression of multiple receptors in GC-D cells distinguishes the organizational logic of the necklace from that of the vomeronasal system. While the function of the necklace-like glomerular organization is completely unknown, its existence suggests that this anatomical feature may serve a unique purpose in odor processing, especially since multiple “necklaces” corresponding to distinct OSN populations exist in this same region of the MOB (Matsuo et al., 2012; Ring et al., 1997; Shinoda et al., 1993; 1989; Zheng et al., 1987).

Beyond the obvious necklace-like organization of the GC-D glomeruli little is known about the anatomical logic of this subsystem, including how OSNs in the MOE are “mapped” to individual GC-D glomeruli, how GC-D glomeruli relate to one another, or the downstream targets of this subsystem in the brain. Here we define the anatomical architecture of the GC-D necklace subsystem using novel experimental approaches to trace the anatomical connections of individual GC-D glomeruli *in vivo*. We find that single GC-D glomeruli broadly sample sensory information from across the MOE, as opposed to receiving topographically organized inputs from particular cul-de-sacs. In the OB, GC-D glomeruli are heavily interconnected with themselves, though we find no

evidence that this occurs via bifurcated OSN axons; rather, the connecting fibers are postsynaptic to OSN input and appear to be mediated in part by multiglomerular M/T cells. M/T cells of the GC-D system project axons to targets of the main, but not accessory, olfactory system, and in addition we identify unique projections of the GC-D subsystem to two regions of the basal forebrain not known to receive direct input from the OB, the lateral septum and the nucleus of the diagonal band. Together, these results suggest a model in which the GC-D necklace subsystem processes olfactory information using fundamentally distinct logic from the main and accessory olfactory systems and may serve a specialized function in the general detection of ethologically salient odorants.

RESULTS

Experiments to study the anatomy of the GC-D necklace olfactory subsystem have been hindered by an inability to specifically target GC-D glomeruli *in vivo* for anatomical tracing. To overcome this limitation, we developed a surgical preparation that exposes the ventrolateral portion of the GC-D necklace **(Fig. 3.1A)**. Using mice that express tau-GFP from the *Gucy2d* locus (GCD-IRES-GFP mice, (Greer et al., 2016)), we can visualize (via epifluorescent illumination or multiphoton excitation) one-to-five GC-D glomeruli per animal with this surgical exposure. This surgical preparation was combined with a modified version of an anatomical tracing technique previously published by our laboratory (Sosulski et al., 2011) that we optimized for GC-D glomeruli. Briefly, under multiphoton guidance an individual GC-D glomerulus is selectively targeted and labeled with a tetramethylrhodamine (TMR) dextran-conjugated dye (TMR-dextran) that is introduced to cells via electroporation **(Fig. 3.1B-D)**. With this approach we can retrogradely label the cell bodies of OSNs that innervate individual GC-D glomeruli, locally label neurons within the olfactory bulb that are associated with a specific glomerulus, and anterogradely trace the axons of second-order M/T cells innervating a given GC-D glomerulus to higher brain regions.

GC-D OSNs project to approximately 25-40 glomeruli per OB (Walz et al., 2007), but the organization underlying the mapping of GC-D OSNs – which largely reside within multiple cul-de-sacs of the MOE – onto necklace glomeruli is completely unknown. To assay the distribution of OSNs that innervate an individual GC-D necklace glomerulus, we labeled a single GC-D glomerulus *in vivo* via our electroporation protocol, recovered

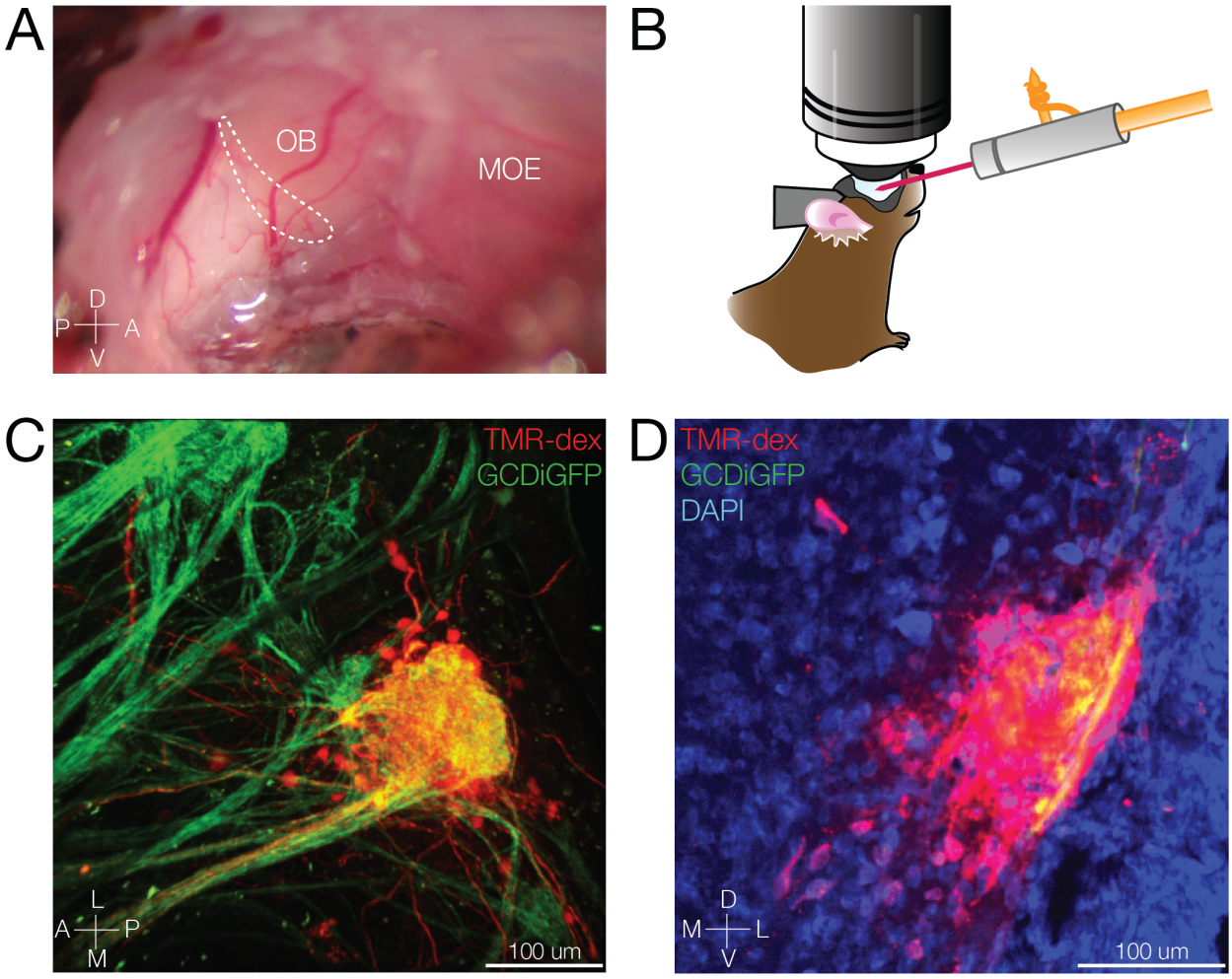

Figure 3.1. Experimental Approach to Label the GC-D Necklace *In Vivo*

(A) A novel surgical preparation exposes the ventrolateral portion of the OB, including part of the GC-D necklace (region delineated by dotted line).

(B) Schematic showing the position of the dye-filled pipette and mouse beneath a multi-photon microscope for the electroporation technique.

(C) Electroporation specifically labels the OSN axons and bulbar cells associated with a single GC-D glomerulus.

(D) The specificity of labeling can be assessed in coronal sections of the OB following the post-electroporation recovery period.

the mouse for 1-3 days to allow for retrograde transport of the dye, and analyzed the MOE for the presence of labeled OSN cell bodies. Following this protocol a number of cells robustly labeled by TMR-dextran were evident within the MOE. As these cells also express GFP, they appear yellow **(Fig. 3.2A)**. We found that the OSNs innervating an individual GC-D glomerulus were not spatially restricted to particular cul-de-sac regions; instead, the labeled cells were broadly distributed across the range of GC-D cells within the MOE **(Fig. 3.2A)**. Though we are only able to trace from ventrally located glomeruli in our preparation, the distribution of labeled cells within the MOE suggests that each glomerulus within the necklace samples sensory information from across the entire epithelial sheet. Therefore we hypothesize that the OSNs innervating dorsally located necklace glomeruli exhibit a similar distribution within the MOE, and that each glomerulus may thus exist as an identical, parallel processing unit.

TMR-dextran-labeled cells within the MOE that were not GFP+ were occasionally observed **(Fig. 3.2.B)**. Quantification of the cells within the MOE that were co-labeled by TMR-dextran and GFP (i.e. GC-D cells) revealed that 94.4% (± 5.1, n=5 mice) of the cells labeled by electroporation were GC-D cells. A comparable degree of co-labeling (90.6% ± 3.5, n=5 mice) was observed when an OR-expressing glomerulus (the 174-9 glomerulus, visualized in the 174-9-IRES-GFP mouse (Sosulski et al., 2011)) was electroporated under stimulation conditions optimized for the larger, more densely innervated glomeruli of the main olfactory system (see Experimental Methods section) **(Fig. 3.2C)**. The 174-9 glomerulus is innervated exclusively by cells that express the 174-9 receptor; as such, the fact that we recover a small percentage of cells labeled by

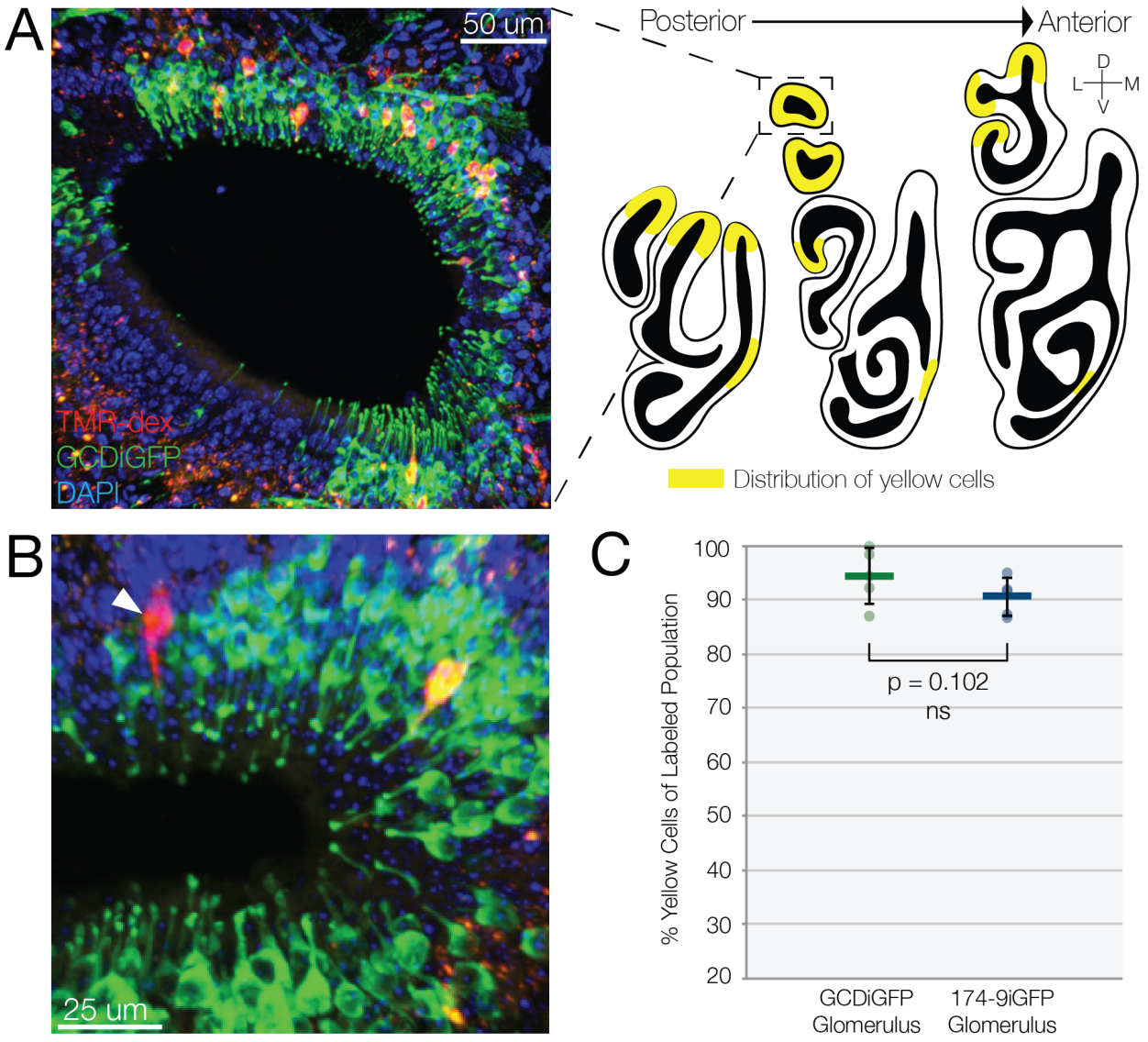

Figure 3.2. Individual Necklace Glomeruli Pool Information from GC-D Cells Throughout the Epithelium

(A) (Left) GC-D cells labeled by TMR-dextran are shown in a cul-de-sac of the MOE. (Right) Schematic depicting the approximate distribution of TMR-labeled cells (yellow-shaded regions) at three different positions along the anterior-posterior axis of the MOE, illustrating the wide distribution of GC-D cells innervating a single GC-D glomerulus. (B) A TMR-dextran-labeled cell that is not GFP+ (arrowhead).

Figure 3.2 (Continued). Individual Necklace Glomeruli Pool Information from GC-D Cells Throughout the Epithelium

(C) Quantification of the percentage of TMR-dex/GFP-labeled cells following electroporation of a GC-D versus the 174-9 glomerulus. The average percentage of TMR-labeled cells that were also GFP+ was 94.4% (± 5.1) and 90.6% (± 3.5) for GC-D glomeruli and 174-9 glomeruli, respectively. As there is no statistically significant difference between the degrees of co-labeling between the two glomerular types ($p=0.102$, one-tailed unpaired t-test), this suggests that GC-D glomeruli – like 174-9 glomeruli – are homogeneously innervated by a single OSN population.

TMR-dextran but not GFP reflects a small degree of non-specific retrograde labeling intrinsic to the electroporation technique. The percentage of yellow cells recovered from the GC-D electroporations was not statistically significantly different from that of the 174-9 electroporations ($p=0.102$, one-tailed unpaired t-test), suggesting that GC-D glomeruli – like 174-9 glomeruli – are homogeneously innervated by a single population of OSNs. These data contradict an earlier study that concluded – based upon patterns of genetically-encoded or antibody-labeled protein expression – that GC-D glomeruli are heterogeneously innervated by GC-D cells and a population of OR-expressing cells (Cockerham et al., 2009). Our experimental approach is not subject to caveats of immunohistochemical analyses, such as incomplete antibody penetration into tissue, that may have been factors in the previous study.

Having defined the general organization by which sensory space within the MOE is mapped onto individual necklace glomeruli, we next sought to better characterize the relationships among different GC-D glomeruli within the OB. The GC-D "necklace" is so named because it is comprised of a ring of seemingly interconnected glomeruli; however, it is unknown whether individual GC-D OSN axons actually bifurcate and innervate multiple glomeruli – which would distinguish these cells from canonical OSNs that exhibit unbranched axons (Mombaerts, 2006) – or whether the "beads-on-a-string" appearance is simply due to the crisscrossing of GC-D OSN axons that each only innervate a single necklace glomerulus. Connectivity among GC-D glomeruli downstream of the primary OSNs is also poorly understood.

To explore the relationship among GC-D glomeruli we conducted a series of

GC-D glomerulus electroporations in which we recovered the mice for a shorter period of time (on the order of hours instead of days) to maximize tissue health, and analyzed the OB for labeled fibers innervating GC-D glomeruli other than the glomerulus that was electroporated. GC-D+ axons innervating glomeruli other than the glomerulus that was electroporated were never observed (data not shown), which argues against the notion that individual GC-D OSNs innervate multiple glomeruli via bifurcating axons.

In contrast, we observed that – postsynaptically of the OSNs – the GC-D glomeruli are heavily interconnected with each other **(Fig. 3.3)**, consistent with a previous study in which GC-D glomeruli were labeled in fixed tissue *ex vivo* with the lipophilic tracer, DiI (Cockerham et al., 2009). However, in contrast to that earlier study – which stated that mitral cells innervating GC-D glomeruli exhibited typical uniglomerular morphology – labeled neurons that clearly project into multiple GC-D glomeruli and exhibit large diameters (>20 μm) and morphologies consistent with necklace mitral cells (Larriva-Sahd, 2012; Nagayama et al., 2014) were often observed. Thus, our data suggest that at least some of the connections observed between GC-D glomeruli are mediated by multiglomerular M/T cells, drawing an additional parallel between the GC-D necklace and glomeruli of the vomeronasal olfactory system.

In addition to dense connections among GC-D glomeruli, TMR-dextran-labeled fibers within glomeruli of the posterior OB that were not GC-D+ but were in many cases adjacent to or nearby GC-D glomeruli were also observed. As cells of the Grueneberg ganglion (GG) also project axons to a “necklace” of glomeruli within the OB, immunohistochemistry (IHC) with an antibody against the GG marker

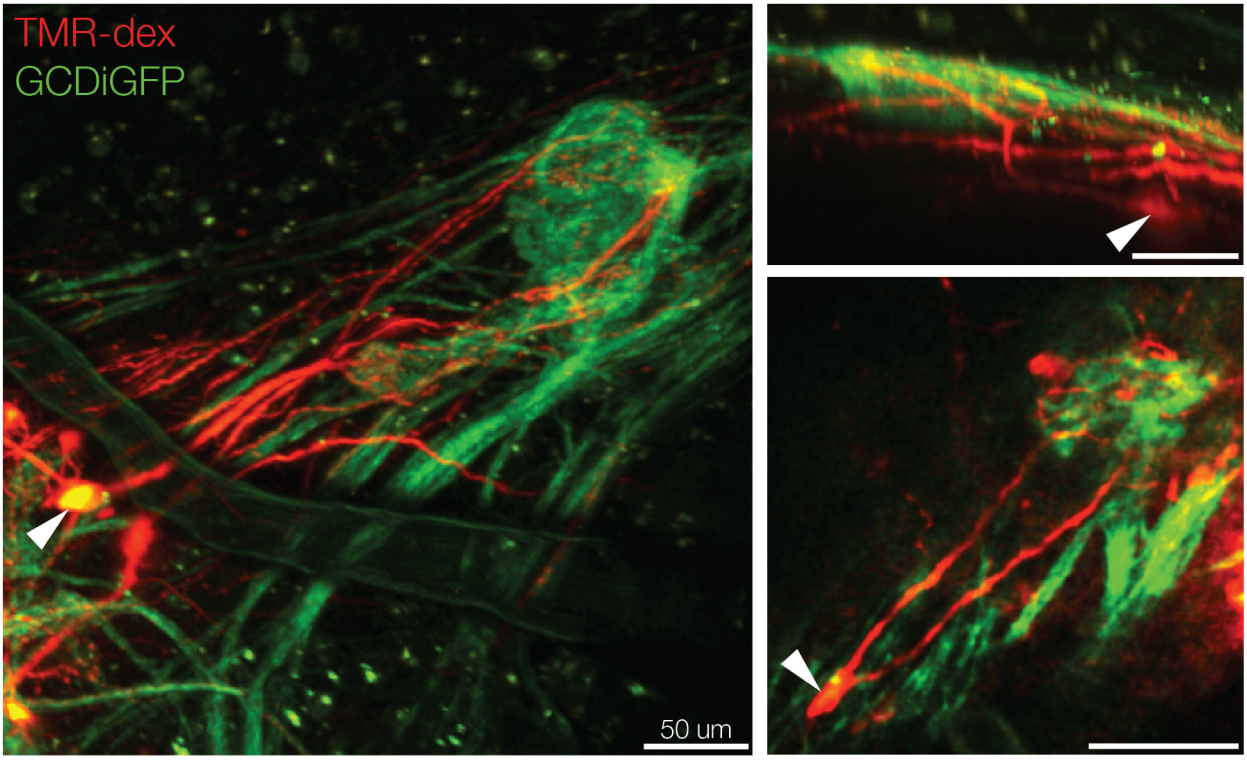

Figure 3.3. GC-D Glomeruli are Interconnected by Putative Multiglomerular Mitral Cells

Three examples of large (≥ 20 um diameter) cells (arrowheads) labeled by electroporation that extend processes into additional, non-electroporated GC-D glomeruli. Cell size and morphology are consistent with necklace mitral cells. (Electroporated glomerulus not shown, all scale bars = 50 μm.)

phosphodiesterase 2A (PDE2A) was performed to determine whether the innervated glomeruli corresponded to the GG necklace. Both GG and GC-D cells express PDE2A; however, in conjunction with GFP (expressed only in GC-D cells) the GC-D and GG necklaces can be differentiated. The PDE2A staining revealed that glomeruli within the GG necklace were, in fact, innervated by TMR-dextran-labeled fibers **(Fig. 3.4A)**, demonstrating that the GC-D and GG olfactory subsystems interact with each other within the OB downstream of the primary sensory neurons. Notably, this is the first report of crosstalk between anatomically segregated olfactory subsystems within the OB, and suggests a greater degree of coordination among the parallel olfactory subsystems than previously appreciated.

When electroporated mice were recovered for longer timescales (e.g. days), we consistently observed a string of GC-D-negative glomeruli within the posterior OB that received strikingly dense innervation by TMR-dextran-labeled fibers. These glomeruli were most apparent dorsal to the AOB **(Fig. 3.4B)**, though they were also found along the lateral surface of the OB. To our surprise, these necklace-like glomeruli were negative for PDE2A (data not shown). We next hypothesized that the labeled glomeruli may correspond to the so-called “atypical glomeruli,” a third necklace of glomeruli in the posterior OB that are identifiable by their strong expression of choline acetyltransferase (ChAT) and acetylcholinesterase (AChE), owing to dense innervation by centrifugal cholinergic inputs from the basal forebrain (Salcedo et al., 2011; Zheng et al., 1987). IHC using an antibody against ChAT was performed on the electroporated samples and confirmed that the densely labeled glomeruli correspond to the highly cholinergic

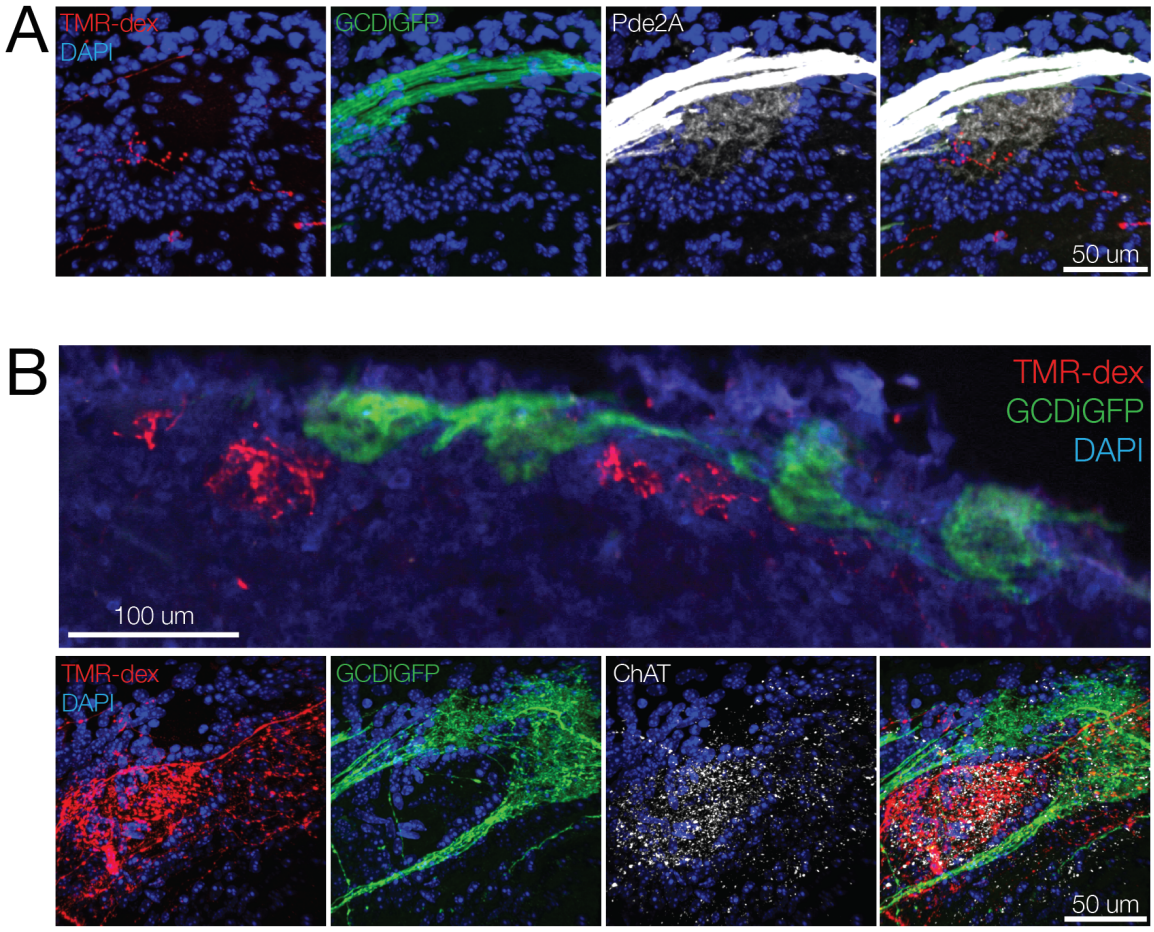

Figure 3.4. GC-D Glomeruli Integrate Information from Other Olfactory "Necklaces"

(A) TMR-dextran+ fibers labeled by electroporation of a GC-D glomerulus innervate glomeruli of the GG necklace, identifiable as PDE2A+/GFP-. Individual channels shown in first three panels, overlay shown in right-most image.

(B) (Top) Multiple, non-GC-D glomeruli that are strongly innervated by TMR-dextran-labeled fibers are consistently observed in the dorsal OB, just above the AOB (not shown). (Bottom) The heavily TMR-dextran+ glomeruli correspond to the highly ChAT+ glomeruli of the "atypical necklace." Individual channels shown in the first three panels, overlay shown in right-most image.

atypical glomeruli (hereafter referred to as ChAT glomeruli) **(Fig. 3.4B)**. The TMR-dextran-labeled fibers themselves were not ChAT+, arguing that the fibers labeled by electroporation truly reflect intrabulbar connections between the GC-D and ChAT necklaces as opposed to artifactual labeling of centrifugal cholinergic fibers. Taken together, our analyses of the intrabulbar anatomy of the GC-D necklace reveal that not only are individual GC-D glomeruli strongly interconnected amongst themselves, but the GC-D subsystem also integrates information from two other "necklace" subsystems in the posterior OB – the GG necklace and the ChAT glomeruli – through dense connections spanning distances as long as the entire dorsal-ventral axis of the OB.

Beyond the OB, the downstream targets of the GC-D necklace subsystem are unknown. The GC-D glomeruli technically reside within the MOB; as such, one prediction is that GC-D glomeruli project to characteristic targets of the main olfactory system. However, as the GC-D glomeruli reside at the boundary of the MOB and AOB and exhibit many features of AOB glomeruli, an alternate hypothesis is that the GC-D necklace projects to regions innervated by the vomeronasal system. To identify the downstream targets of the GC-D subsystem, we performed GC-D electroporations in which the pipette was positioned within the glomerulus to preferentially label the associated M/T cells. The mice were recovered for 2-7 days to allow for anterograde transport of the dye throughout M/T cell axons, and coronal brain sections were analyzed for the presence of labeled fibers. TMR signal in M/T cell axons was amplified via IHC using a primary antibody against TMR. From these experiments we observed labeled fibers within regions targeted by the main olfactory system – including the PCtx,

OT, tenia tecta (TT), anterior olfactory nucleus (AON), anterior cortical amygdalar area (aCoA) and the nucleus of the lateral olfactory tract (nLOT) – but we failed to see labeled fibers within targets of the vomeronasal system **(Fig. 3.5A** and data not shown**)**.

Robust labeling of fibers in posterior regions of the brain was not achieved with the current experimental conditions. For example, labeled fibers were rarely observed within the plCoA or Ent, two additional targets of the main olfactory system. This limitation could likely be overcome with further optimization of the stimulation and surgical conditions. At present, though, our data offer an incomplete description of the downstream targets, and a lack of fibers within posterior brain regions doesn't preclude innervation of those structures. Accordingly, because many of the regions innervated by the vomeronasal system – such as the pmCoA and MeA – are located posterior relative to many MOB targets, our failure to observe fibers in those structures may have simply been due to our experimental approach.

To verify that the GC-D subsystem projects to targets of the main, but not vomeronasal, olfactory system we therefore used a complementary viral tracing strategy. Adeno-associated viruses (AAVs) that express the fluorescent reporter GCaMP only in the presence of Cre recombinase (rAAV2/1.hSyn.FLEX.GCa) were injected into specific brain regions of transgenic mice that selectively express Cre recombinase in M/T cells via the protocadherin 21 (Pcdh21) promoter (Pcdh21-Cre) **(Fig. 3.5B, left)**. These specific viruses had been previously shown to be capable of infecting the axons of M/T cells (Wachowiak et al., 2013). As this approach only labels axons and not cell bodies, the spread of the viral infection in these experiments could

Figure 3.5. The GC-D Necklace Projects to Targets of the Main, but not Accessory, Olfactory System

(A) (Left) Schematic of the anterograde electroporation tracing approach in GCD-IRES-GFP mice. A pipette filled with TMR-dextran dye is targeted to a GC-D glomerulus genetically labeled by GFP. (Right) TMR-labeled fibers in regions targeted by the main olfactory system: the PCtx, OT, and TT. Sections are counterstained with the Nissl stain NeuroTrace 435.

(B) (Left) Schematic of the retrograde AAV viral tracing approach in Pcdh21-Cre mice. Cre-dependent virus encoding GCaMP is injected into target brain regions to infect M/T axons in a Pcdh21-Cre mouse that expresses Cre recombinase in all M/T cells. GC-D glomeruli are subsequently identified by IHC using an antibody against CAR2. (Center) The center of each injection is identified via red fluorescent retrobeads that are co-injected with the virus. Shown here is an injection into PCtx. (Right) GC-D glomeruli (stained with anti-CAR2) are innervated by Pcdh21-Cre+ M/T cells in a Pcdh21-Cre mouse that expresses the Ai14 conditional tdT reporter.

(C) GC-D glomeruli (stained with CAR2) are innervated by M/T cells virally labeled by AAV injection into targets of the main olfactory system (PCtx and OT).

(D) Viral injection into targets of the accessory olfactory system (pmCoA and MeA) robustly labels M/T cells within the AOB, but not cells innervating GC-D glomeruli.

Figure 3.5 (Continued). The GC-D Necklace Projects to Targets of the Main, but not Accessory, Olfactory System

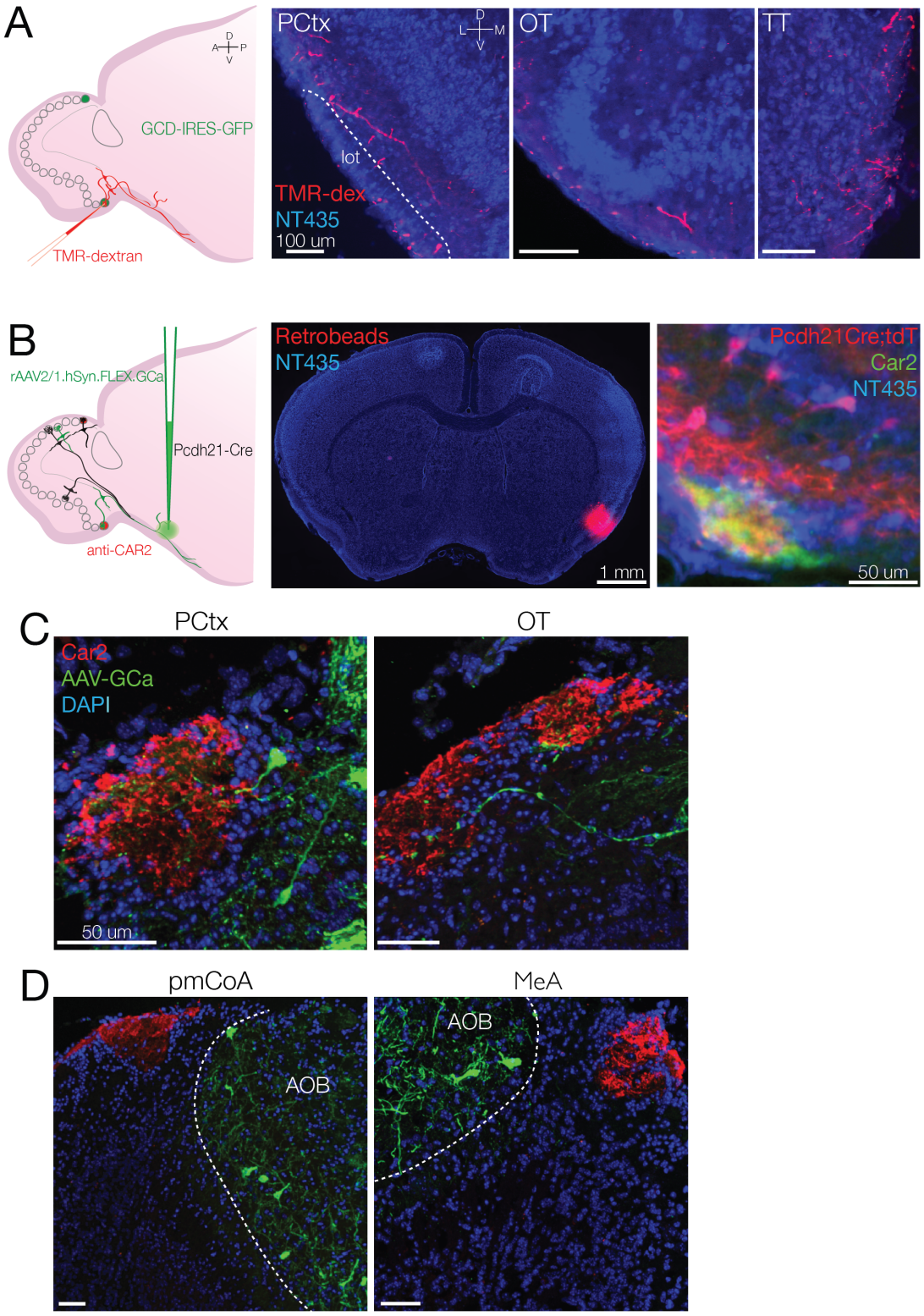

not be assessed; however, only samples for which the center of the injection was validated to be within the intended target – as identified by fluorescently labeled latex spheres (retrobeads) that were co-injected with the virus – were analyzed **(Fig. 3.5B, center)**. Pcdh21 is generally thought to be a marker of all M/T cells; however, its expression by M/T cells of the GC-D subsystem had not previously been verified. Thus, prior to beginning injections, we verified that GC-D glomeruli are innervated by M/T cells that express *Pcdh21*-Cre by staining the OBs of mice carrying the *Pcdh21-Cre* transgene and the *Ai14* conditional allele, which permits the expression of the fluorescent reporter tdTomato in the presence of Cre recombinase (Pcdh21-Cre;tdT) **(Fig. 3.5B, right)**.

To assess whether GC-D glomeruli project to the infected brain region, infected mice were recovered for 3-4 weeks to allow for strong expression of GCaMP in the infected cells, and then tissue sections of the OB were analyzed for the presence of GCaMP+ fibers within glomeruli stained with an antibody against the GC-D necklace-specific marker carbonic anhydrase 2 (CAR2) (Luo, 2008). Tissue sections were also stained with an antibody against GFP to amplify the basal GCaMP fluorescence. GCaMP-labeled fibers were observed within a subset of GC-D glomeruli following virus injection into the PCtx or OT but not after injections into the pmCoA or MeA **(Fig. 3.5C,D)**, confirming that the GC-D subsystem projects to targets of the main, but not vomeronasal, olfactory system. Notably, the MeA is known to receive a minor projection from glomeruli within the ventral MOB in addition to its innervation by the AOB (Kang et al., 2009), though we failed to observe any significant innervation of MOB glomeruli in

our MeA injections. This likely reflects the fact that we subsampled the inputs to the MeA as a result of a small injection volume, as AOB projections to the MeA outnumber MOB projections 100:1 (Bergan et al., 2014) and the two corresponding fiber tracts are spatially segregated within the MeA (Kang et al., 2009). However, given the concomitant lack of TMR-dextran-labeled fibers within the MeA, we believe it is unlikely that the GC-D subsystem sends significant direct projections to this region.

Surprisingly, our unbiased GC-D electroporation tracing experiments revealed that, in addition to projecting to known targets of the main olfactory system, the GC-D subsystem projects to two brain regions not previously reported to receive direct olfactory input from the OB, the lateral septum (LSr) and the medial septum (MS)/nucleus of the diagonal band (NDB) complex (hereafter just referred to as the NDB) **(Fig. 3.6A)**. To confirm the specificity of the GC-D projection to these brain regions, two sets of control electroporations were performed for comparison. In one set the dorsally located 174-9 glomerulus, as visualized in the 174-9-IRES-GFP mouse line, was electroporated. From these electroporations no labeled fibers were observed in either the LSr or the NDB (**Fig. 3.6A**), despite robust labeling of traditional main olfactory system targets (data not shown). In a second set of electroporations the ventral OB was exposed via the same surgical exposure used for GC-D electroporations and a canonical ventrally located glomerulus – as defined by expression of olfactory marker protein (OMP) – was electroporated. The OMP-GFP mouse line (Potter et al., 2001) was used to visualize all OMP+ glomeruli. In these samples occasional fibers along the midline adjacent to the anterior LSr were observed, which may reflect fibers of

Figure 3.6. The GC-D Subsystem Innervates Septal Targets

(A) TMR-labeled fibers labeled by electroporation of a GC-D glomerulus innervating the LSr (top) and the vNDB (bottom). Control electroporations of either a dorsally located OR-expressing glomerulus (the 174-9 glomerulus) or a random ventral, OR-expressing glomerulus visualized by its expression of OMP do not result in labeled fibers deep within the LSr, though some labeled fibers along the midline adjacent to the LSr are observed in the OMP control (top center). No labeled fibers are observed within the vNDB following electroporation of either a 174-9 or OMP glomerulus.

(B) Schematic summarizing the approximate areas of fiber innervation within the LSr and NDB at four anterior-posterior levels following electroporation of 174-9 glomeruli (yellow, n=3), ventral OMP glomeruli (purple, n=4), or GC-D glomeruli (green, n=10). Each semi-transparent box depicts one mouse; the approximate fiber pattern observed for each mouse is depicted within the enlarged brain regions, wherein darker colors indicate a higher incidence of innervation within a particular area over multiple animals. A key adjacent to each enlarged brain region depicts the darkness of each color that corresponds to different numbers of mice, from 0 (outlined boxes) to “n” (darkest boxes). The asterisks within the key indicate the number of mice in which any labeled fibers were observed at each specific coronal level shown.

Figure 3.6 (Continued). The GC-D Subsystem Innervates Septal Targets

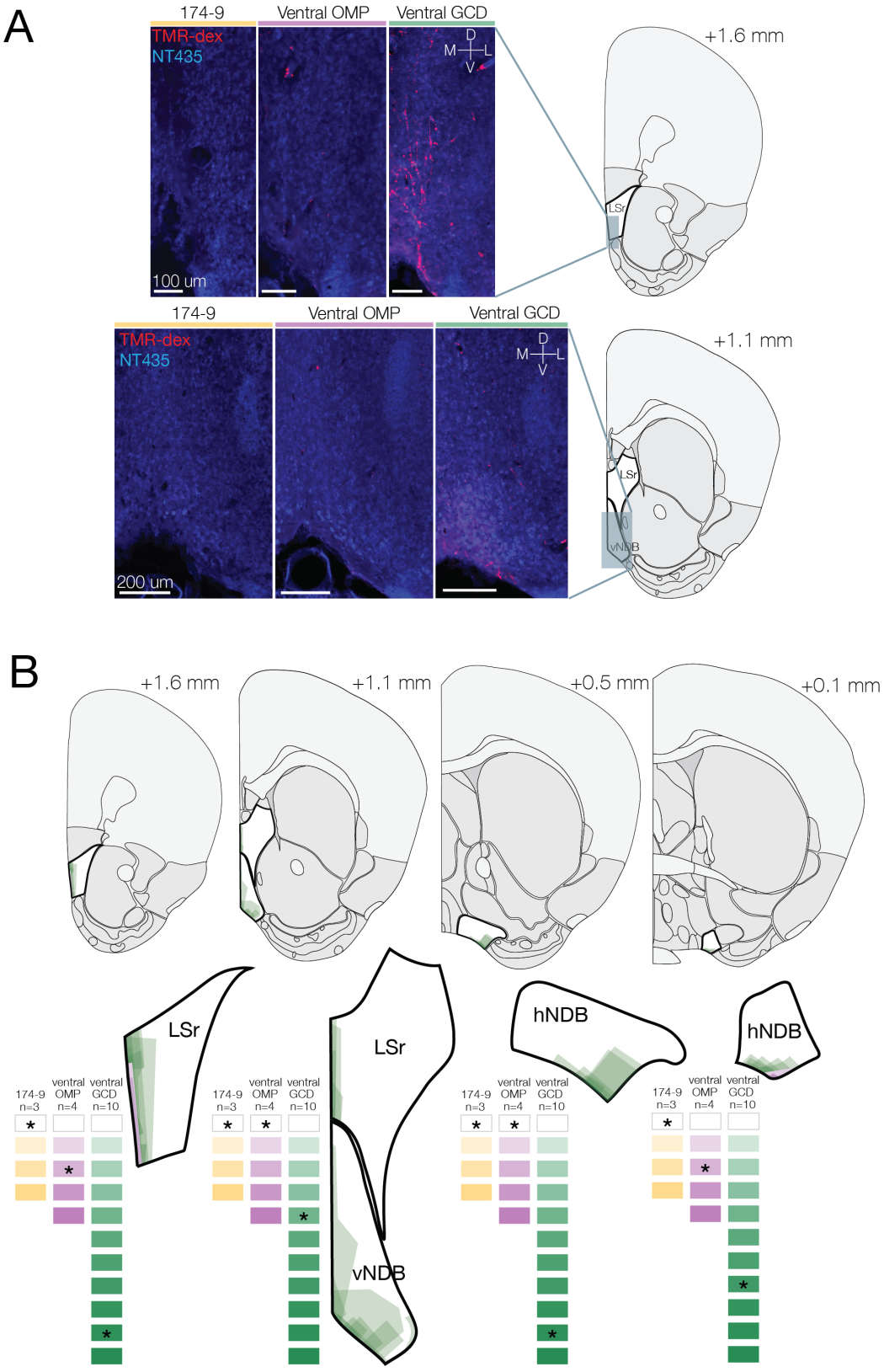

passage en route to the dorsally located TT. Labeled fibers were also observed at the lateral-most edge of the horizontal band of the NDB (hNDB), near the OT boundary; however, we never observed broad innervation of the LSr or NDB similar to that seen following electroporation of a GC-D glomerulus **(Fig. 3.6A,B**).

To further verify the specificity of the projection from the GC-D subsystem to the LSr and NDB, retrograde viral tracing was performed by injecting rAAV2/1.hSyn.FLEX.GCa into the anterior LSr and MS/vertical limb of the NDB (referred to here as LSr/NDB injections, as we cannot distinguish the areas). As with other AAV tracing experiments, fluorescent retrobeads were co-injected and only brains in which the center of the injection was confined within the intended target were analyzed **(Fig. 3.7A)**. From these experiments we observed strong innervation of GC-D glomeruli (as labeled by anti-CAR2) by GCaMP+ fibers **(Fig. 3.7A)**, and the labeled fibers selectively innervated GC-D glomeruli. The number of innervated glomeruli was quantified and the corresponding proportion of the specific glomerular population (either GC-D or non-GC-D glomeruli, see Experimental Methods for details) was calculated. Injection of virus into the LSr/NDB selectively labeled GC-D glomeruli (19.0% ± 15.8 GC-D versus 0.47% ± 0.3 non-GC-D, $p = 0.002$, paired t-test; n=10 injections). In contrast, the two populations of glomeruli were comparably labeled following viral injection into the OT (36.7% ± 17.5 GC-D versus 30.0% ± 11.4 non-GC-D, $p = 0.134$, paired t-test; n=6 injections). Intriguingly, the GC-D subsystem may be underrepresented in its projections to the PCtx compared to non-GC-D glomeruli (36.5% ± 22.1 GC-D versus 69.8% ± 19.0 non-GC-D, $p = 0.003$, paired t-test; n=5 injections) **(Fig. 3.7B)**.

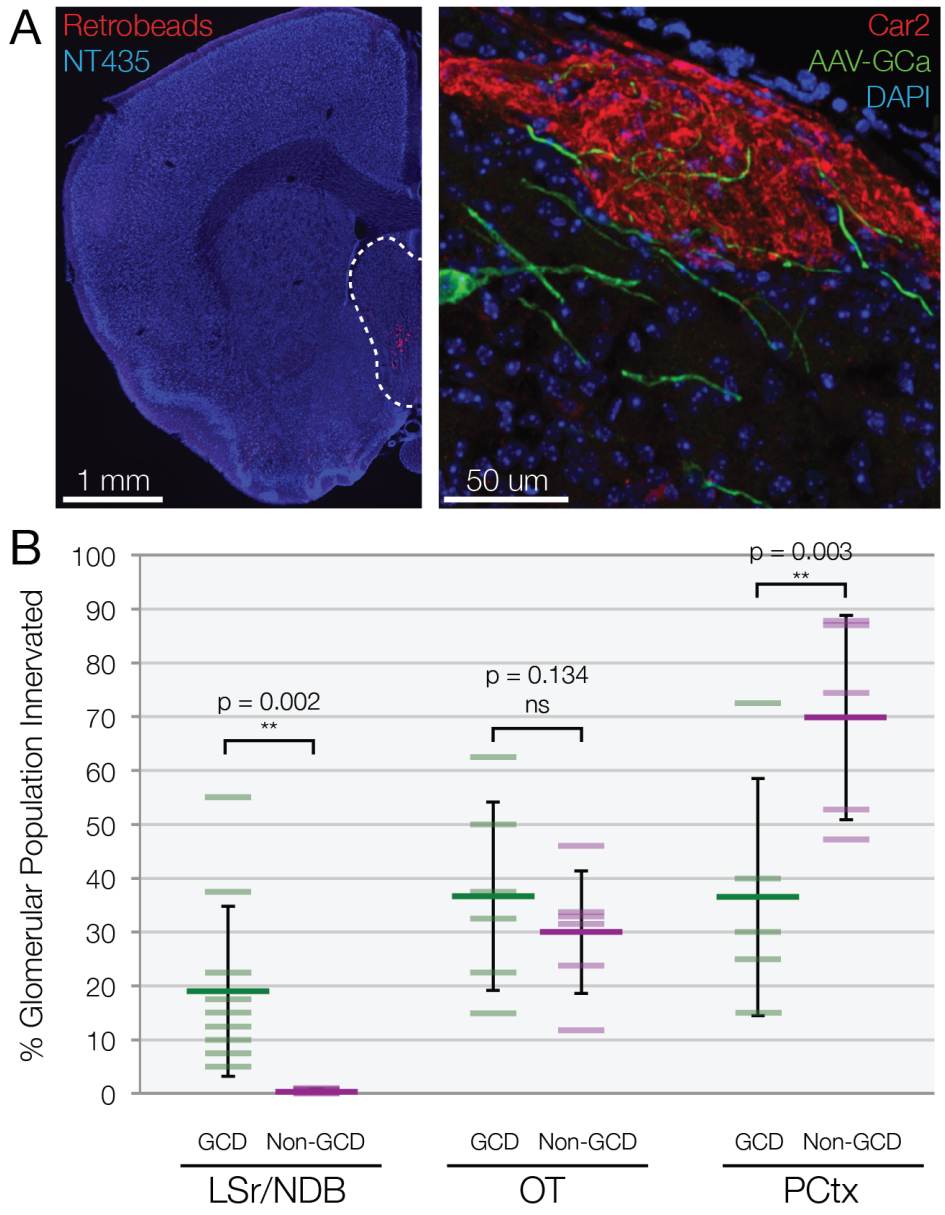

Figure 3.7. Septal Projections are Unique to GC-D Glomeruli

(A) (Left) Retrobeads within the septal region (outlined by the dashed line) depict the specific area targeted for retrograde viral injections. The region encompassed the LSr, the MS, and the vNDB. (Right) A GC-D glomerulus (stained with anti-CAR2) innervated by virally labeled M/T cells following virus injection into the LSr/NDB.

Figure 3.7 (Continued). Septal Projections are Unique to GC-D Glomeruli

(B) Quantification of the number of GC-D versus non-GC-D glomeruli innervated by virally infected fibers following infection of the LSr/NDB, OT, or PCtx, expressed as a percentage of the specific glomerular population (GC-D versus non-GC-D). Virus injections into the LSr/NDB specifically label GC-D glomeruli (19.0% ± 15.8 GC-D versus 0.47% ± 0.3 non-GC-D, $p = 0.002$, one-tailed paired t-test; $n = 10$ injections). GC-D and non-GC-D glomerular populations were equally innervated following virus injection into the OT (36.7% ± 17.5 GC-D versus 30.0% ± 11.4 non-GC-D, $p = 0.134$, one-tailed paired t-test; $n = 6$ injections); however, GC-D glomeruli were underrepresented relative to non-GC-D glomeruli following virus injection into the PCtx (36.5% ± 22.1 GC-D versus 69.8% ± 19.0 non-GC-D, $p = 0.003$, one-tailed paired t-test; $n = 5$ injections).

The septal nuclei are comprised of multiple cell types, and therefore the functional effects of the M/T projection from the GC-D subsystem to this region will depend upon the identities of the postsynaptic cells. One population of cells found within the septal regions targeted by the GC-D subsystem (in particular the MS/NDB complex) is cholinergic. Specifically, cholinergic cells within the hNDB provide centrifugal cholinergic innervation of glomeruli within the OB, including the dense innervation that defines the atypical ChAT glomeruli. Thus, an intriguing possibility is that M/T projections from the GC-D subsystem target cholinergic cells within the septal nuclei, and those cells may provide – either directly or via local, intraseptal circuits – neuromodulatory input to the OB, thereby defining a neuromodulatory circuit at the early stages of olfactory processing.

To test whether M/T cells of the GC-D subsystem synapse onto cholinergic neurons within the septal nuclei, retrograde trans-synaptic tracing was performed from ChAT+ cells using EnvA pseudotyped, G-deleted Rabies-EGFP virus (EnvA-RVdG-EGFP). Two helper AAVs encoding a Cre-dependent TVA-mCherry fusion protein (AAV2.9-CAG-DIO-TCB) and a Cre-dependent rabies glycoprotein (AAV2.9-CAG-DIO-RVG) were co-injected into the medial septal region encompassing the LSr/MS/vNDB of ChAT-IRES-Cre mice (Rothermel et al., 2014) and allowed to express for 2-4 weeks. EnvA-RVdG-EGFP was then injected at the same coordinates and allowed to express for 5-7 days before sacrificing the animals (Miyamichi et al., 2011). In these experiments, red cells at the injection site (i.e. those expressing TCB) represent the total possible population of cells (all ChAT+) that can be infected by the pseudotyped rabies

virus, as they express the TVA surface receptor. Cells that are initially infected by rabies will also express EGFP and therefore appear yellow. The subset of yellow cells that was also infected by the virus encoding RVG (which did not encode a fluorophore) constitutes the population of starter cells from which rabies can jump to the presynaptic partners. For our analyses, however, all yellow cells were defined as "starter cells." Presynaptic partners of the starter cells express EGFP from rabies but no TCB and therefore appear green **(Fig. 3.8.A)**.

For these trans-synaptic tracing experiments the number of starter (yellow) cells was quantified within each of three general anatomical regions: non-olfactory targets like the hypothalamus that do not receive monosynaptic input from the OB, septal targets (LSr/MS/NDB), and olfactory targets like the OT that are directly innervated by M/T cells. Only brains in which the number of starter cells within off-target olfactory regions was < 10% of the number of total starter cells in septal + olfactory targets were analyzed. (Starter cells in non-olfactory regions were excluded to establish a stricter inclusion criterion, and because those cells pose no risk of contaminating our results in the OB.) From the ensuing dataset (n=5 mice), 148 (± 56) starter cells were infected on average. Of the total population of starter cells across animals, 87.5% of starter cells were located within the septal nuclei, while only 2.5% of starter cells were found within off-target olfactory regions. The remaining 10.0% of off-target starter cells were located within non-olfactory regions **(Fig. 3.8B)**. Thus, the starter cell population generated in these experiments was fairly specific to the septal nuclei.

GC-D glomeruli were identified via anti-CAR2 IHC and the presence of EGFP+

Figure 3.8. Cholinergic Cells Within the Septal Nuclei are Postsynaptic to GC-D Necklace M/T Cells

(A) A coronal section through the septal nuclei illustrating the presence of AAV-infected, but not rabies-infected cells (red), AAV- and rabies-infected starter cells (yellow), and presynaptic partners of the starter cells, which are infected by rabies only (green).

(B) Quantification of starter cells by general anatomical regions, expressed as a percentage of the total population of starter cells. Across all mice (n=5), the majority of starter cells (87.5%) were confined to septal nuclei. Only 2.5% of starter cells were found in non-septal regions that receive direct OB input, while the remaining 10.0% of off-target cells resided in non-olfactory-recipient regions.

(C) Quantification of the number of GC-D versus non-GC-D glomeruli innervated by trans-synaptically labeled M/T cells following rabies infection of the septal region of ChAT-Cre mice, expressed as a percentage of the specific glomerular population (GC-D versus non-GC-D). The glomeruli innervated by rabies-infected fibers were almost exclusively GC-D+ (15.0% ± 5.1 GC-D versus 0.2% ± 0.1 non-GCD, $p = 0.001$, one-tailed paired t-test; $n = 5$ mice).

(D) A multiglomerular M/T cell that was labeled trans-synaptically by rabies virus (arrowhead). The nuclear DAPI stain delineates two GC-D (CAR2+) glomeruli, which are outlined by dotted lines for ease of viewing.

Figure 3.8 (Continued). Cholinergic Cells Within the Septal Nuclei are Postsynaptic to GC-D Necklace M/T Cells

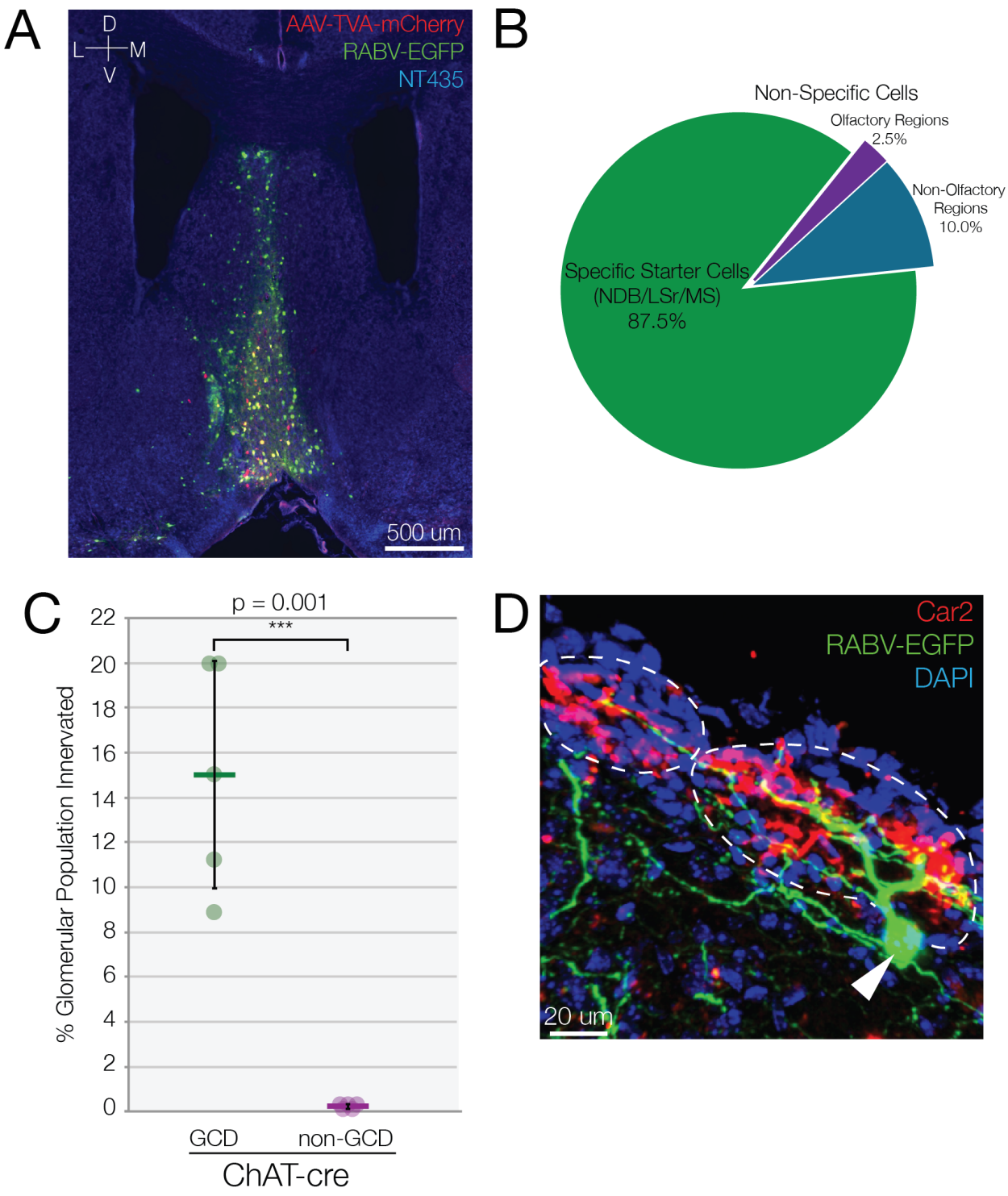

fibers within CAR2+ glomeruli was assessed. In a given mouse, 8.8-20.0% of the population of GC-D glomeruli was innervated by EGFP+ fibers, and innervated glomeruli within the OB were almost exclusively GC-D glomeruli (15.0% ± 5.1 GC-D population versus 0.2% ± 0.1 non-GCD population, $p = 0.001$, one-tailed paired t-test) **(Fig. 3.8C)**, further supporting the fact that the GC-D subsystem uniquely projects to the septal region of the brain.

As expected from trans-synaptic labeling of M/T cells, a small number of EGFP+ cell bodies were also observed within the OB. However, as the OB was visualized in coronal sections, many of the cell bodies were severed from their apical dendrites. Therefore all labeled fibers within the glomerular label were counted as presumptive M/T dendrites, as M/T cells are the only output neurons from the OB and therefore are the only bulbar cells that could have been infected as the presynaptic partners to starter cells within the septal nuclei.

False positives could potentially result from the innervation of glomeruli by EGFP+ axons of centrifugally projecting ChAT-Cre+ cells within the NDB; however, we believe this is not an issue for two reasons. First, cholinergic cells that provide centrifugal innervation of the OB are specifically located within the hNDB and the majority of starter cells within the septal region resided in the LSr/MS and the vertical limb of the NDB (vNDB). Second, hNDB cholinergic cells innervate all glomeruli within the OB, with no apparent enrichment of GC-D glomeruli (Juilfs et al., 1997; Salcedo et al., 2011). Therefore, if the observed glomerular EGFP signal were due to centrifugal

cholinergic axons, we would expect to see no enrichment of GC-D glomeruli as a population; instead we observe select innervation of GC-D glomeruli.

Finally, the sparse labeling and complete cell fills achieved by rabies tracing afford us the opportunity to analyze the morphologies of cells that can be unambiguously identified as M/T cells by virtue of the fact that M/T cells are the only bulbar cells that project beyond the OB. As mentioned above, many cells become severed from their apical dendrites – which extend along the anterior-posterior axis (Larriva-Sahd, 2012) – when the OB is sectioned; however, occasionally intact cells were recovered, a subset of which extended processes into multiple GC-D glomeruli **(Fig. 3.8D)**. These observations provide further evidence for the existence of atypical, multiglomerular M/T cells within the GC-D necklace subsystem.

DISCUSSION

The multiple olfactory subsystems of the mouse serve overlapping functions including mediating innate and learned odor-evoked behaviors; however, each subsystem is endowed with unique molecular and anatomical features that enable specific functional contributions to olfactory perception. An important first step towards ultimately understanding those specific contributions and how coordination among the various specialized subsystems enables olfactory-driven behavior is to define the molecular and anatomical framework within which each olfactory subsystem operates.

Recently our laboratory identified an atypical molecular logic employed by the cells of the GC-D necklace subsystem to detect odorants beyond those that directly activate GC-D itself. GC-D cells use a family of non-GPCR proteins (the MS4As) as chemoreceptors – the first example of non-GPCR-mediated odor detection in mammals (Greer et al., 2016). Furthermore, the MS4A proteins are expressed in a many-to-all (or possibly all-to-all) pattern within GC-D cells, thereby violating the “one receptor-one neuron” principle by which other mammalian olfactory subsystems abide. While the functional significance of this molecular organization of the GC-D subsystem is unknown, the discovery of the MS4As allows us to propose and test specific hypotheses to reveal its function.

Similarly, with this body of work we have elucidated the anatomical framework of the GC-D necklace subsystem, revealing unique anatomical substrates for olfactory perception within this subsystem **(Fig. 3.9)**. The atypical necklace-like organization of glomeruli within the GC-D subsystem has long been noted, though our data provide

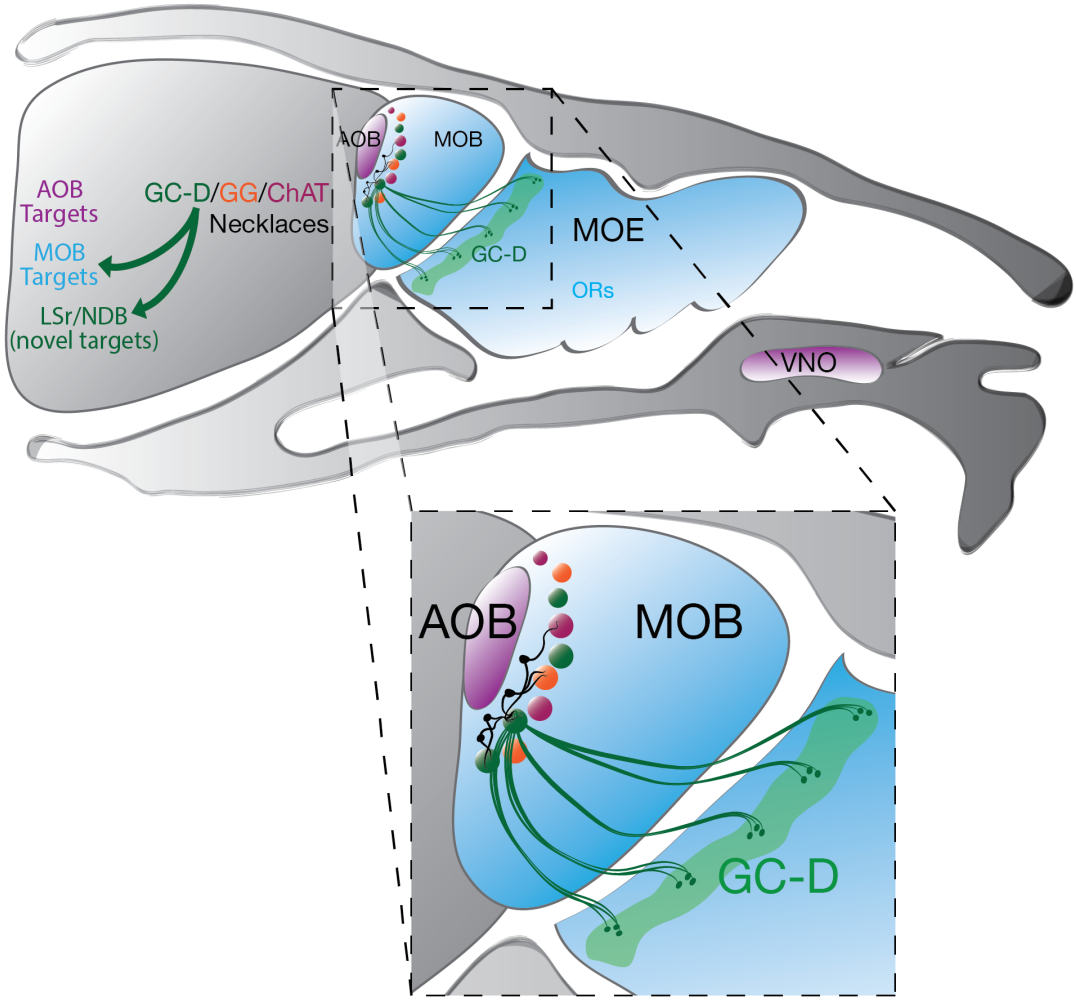

Figure 3.9. Newly Characterized Anatomy of the GC-D Necklace Subsystem

Schematic summarizing our major anatomical findings. A single GC-D glomerulus is homogeneously innervated by GC-D cells that are broadly distributed across the epithelium. GC-D necklace glomeruli are interconnected (by putative multiglomerular mitral cells) with glomeruli of the GG and atypical cholinergic (ChAT) necklaces. M/T cells of GC-D glomeruli project to targets of the main, but not the accessory, olfactory bulbs, and they also project to novel targets within the septal region, the LSr and NDB. (Inset) Zoomed-in view showing details of the MOE-to-OB and intrabulbar projections.

additional context for this glomerular system – such as the organization of MOE inputs to individual necklace glomeruli and the intrabulbar relationships among the various glomerular necklaces – and suggest models for how sensory information within the GC-D subsystem may be encoded in the periphery. We have also identified downstream targets of the GC-D subsystem, which include brain regions that were not previously thought to receive direct OB innervation but which are critical for many odor-driven behaviors. These data suggest unique roles for the GC-D necklace subsystem in olfactory perception.

The Peripheral Anatomy of the GC-D Subsystem is Built for Integration

Molecularly, individual GC-D cells appear *a priori* better suited to act as coincidence detectors than to mediate odor discrimination, based on their expression of multiple MS4A chemoreceptors with different ligand specificities. Furthermore, the GC-D subsystem is not constrained in its projections to only a few glomeruli within the OB. Thus, the concomitant existence of multiple necklace glomeruli provides a structural framework that could facilitate either the segregation or integration of signals corresponding to the activation of different receptors, based on known spatial biases of odor binding within the MOE.

Odorant molecules exhibit great diversity in chemical properties that affect odorant binding within a mucus-lined epithelial environment, and differences in airflow velocity also exist within the complex rodent nasal cavity. As a result, odorants can elicit distinct neural responses at different locations within the epithelial zone corresponding

to their cognate OR (Johnson and Leon, 2007; Scott et al., 2000; 2007). Chemical properties like the hydrophobicity and volatility of odorants also affect odorants' relative ability to activate cells within the MOE via orthonasal (through the nose) versus retronasal (through the mouth) olfaction, respectively (Gautam and Verhagen, 2012; Scott et al., 2007). The odorants that activate GC-D cells (either via GC-D or the MS4A proteins) are quite diverse in chemical structures, hydrophobicity, and volatility, ranging from a gas (CO_2) to hydrophobic polyunsaturated fatty acids (Gao et al., 2010; Greer et al., 2016; Hu et al., 2007). Different necklace ligands might, then, preferentially bind within different sub-regions of the MOE, and such effects may be more pronounced by the fact that GC-D cells are particularly sequestered within the MOE relative to OR-expressing cells. GC-D cells within spatially segregated cul-de-sacs may therefore only be activated by some subset of GC-D ligands, despite expressing receptors to detect all of them.

Thus, one possibility is that the existence of multiple glomeruli within the necklace subsystem serves to retain and reinforce any segregation of various olfactory signals introduced by differences in ligand binding across different cul-de-sacs. This would be achieved if each necklace glomerulus were innervated by GC-D cells located within only a sub-region of the MOE, such as a particular cul-de-sac. Accordingly, each GC-D glomerulus would represent some portion of "olfactory space" – as defined by MOE-induced constraints on ligand binding – and together the necklace glomeruli would completely tile that space. Alternatively, the necklace glomeruli may be organized to actively combat variability in odor binding within the MOE so as to faithfully transmit

signals within the subsystem. For example, if the GC-D subsystem acts as a coincidence detector – requiring the simultaneous binding of multiple ligands for activation – but each ligand has only limited accessibility to specific groups of GC-D cells, then each glomerulus should be innervated by OSNs that are widely distributed within the MOE so as to sample all of MOE "olfactory space." This organization maximizes the odds of subsystem activation – at the level of the OB – by the coincident presence of multiple necklace ligands. It also may increase the fidelity of information transfer within the circuit through the introduction of redundancy, as individual glomeruli within the necklace in this model exist as identical information processing channels.

Our data argue for the latter model, as the cells that innervate an individual GC-D glomerulus are broadly distributed across multiple cul-de-sacs and exhibit a range across all aspects (dorsal-ventral, medial-lateral, anterior-posterior) of the MOE. Thus, regardless of the extent to which necklace ligands exhibit region-specific binding within the MOE due to differences in chemical properties, the GC-D necklace is organized to broadly pool sensory signals from across the entirety of the epithelial space that is populated by GC-D cells. As we were only able to trace from ventrolateral necklace glomeruli, there may be subtle differences among necklace glomeruli that we were unable to detect in our experiments. However, the general pattern of innervation that we observe suggests that individual GC-D glomeruli are likely to be fairly equivalent to one another.

The redundant organization of OSN inputs to each GC-D glomerulus, coupled with the expression of multiple receptors in each GC-D OSN, provide anatomical and

molecular evidence that the GC-D subsystem is organized for the integration of olfactory signals as opposed to odor discrimination. This hypothesis is further substantiated by our intrabulbar tracing data, which reveal strong interconnectivity of GC-D glomeruli postsynaptic to the OSN axons that appears to be mediated at least in part by multiglomerular M/T cells. Dense connections also exist between the GC-D necklace and two other olfactory necklaces corresponding to the GG subsystem and the atypical ChAT glomeruli. An analogous convergence is observed within the AOB, as individual mitral cells integrate information from homotypic glomeruli expressing the same VR as well as from across glomeruli expressing different VRs; as such, the organization of the necklaces may serve similar functions as those postulated for glomeruli within the AOB.

The divergence of VR input across multiple glomeruli and subsequent re-pooling by mitral cells in the AOB is thought to recruit a higher degree of lateral inhibition than would be achieved if the VR population projected to just a single glomerulus, since lateral inhibition depends upon the degree of mitral cell activation (Cleland, 2014; Ennis and Holy, 2015). The proposed functional effect of increased lateral inhibition is to increase the signal-to-noise for individual VR channels, while integration across glomeruli corresponding to different VRs is thought to facilitate the coincident detection of odorants that together comprise a pheromonal signal (Del Punta et al., 2002; Luo and Katz, 2004).

Thus, the GC-D subsystem (along with the GG and ChAT subsystems) may use a necklace of multiple glomeruli to similarly increase the signal-to-noise of ethologically relevant olfactory signals and facilitate the detection of behaviorally meaningful odor

blends. Notably, GC-D glomeruli alone (without integrating GG or ChAT inputs) are in theory capable of detecting odor blends due to the multiple receptors expressed in all GC-D cells, and at least one known function of the GC-D subsystem – mediating socially transmitted food preference (STFP) – requires the coincident presence of food that is paired with odorants present on rodent breath or in their feces. Intriguingly, GC-D cells are activated by both the rodent-derived odorants required for STFP and odorants that are found in natural food sources of mice (Arakawa et al., 2013; Greer et al., 2016; Munger et al., 2010).

Similarly, the connections among GC-D glomeruli and glomeruli within the GG and ChAT subsystems could mediate the processing of yet-to-be-defined odor blends that rely upon concomitant activation of multiple necklace subsystems by different compounds. Alternatively, this anatomical arrangement may be a parsimonious solution to process behaviorally important odorants that simultaneously activate multiple necklace subsystems, as a common pool of M/T cells could easily forward signals from the different subsystems to common downstream processing centers.

For example, the closely related predator-derived odorants 2,5-dimethylpyrazine (2,5-DMP) and 2,3-DMP both activate cells within the GC-D and the GG subsystems, and presumably these olfactory signals are relayed to common circuits mediating defensive behaviors and innate avoidance (Greer et al., 2016; Mamasuew et al., 2011; Osada et al., 2015; Zhang et al., 2007). The function of the ChAT necklace is completely unknown, as the sensory afferents have not been identified; however, based on our data we hypothesize that this necklace will also either directly detect behaviorally

relevant odorants similar to the GC-D and GG necklaces, or it will play a role in the neuromodulatory regulation of GC-D and GG signals.

GC-D Glomeruli are Homogeneously Innervated by GC-D Cells

In contrast to an earlier report (Cockerham et al., 2009), we fail to find evidence for the co-innervation of GC-D glomeruli by populations of GC-D and non-GC-D cells, suggesting that despite the multiple mechanisms for integration across necklace glomeruli, the GC-D necklace may not integrate information from the main olfactory system to the same degree as previously thought. This discrepancy may be due to methodological differences between our study – in we which labeled OSN inputs to a GC-D glomerulus in an unbiased manner – and the earlier study, which argued for heterogeneous innervation based on a lack of overlap between fluorescence resulting from IHC with anti-PDE2A (a marker of GC-D cells) and fluorescence in the OMP-GFP mouse line, which labels all OR-expressing cells based on their expression of OMP. Illustrating the difficulty in interpreting such experiments, however, a study using a different combination of antibodies and genetically encoded fluorescence – using antisera to OMP and the GCD-IRES-GFP mouse line – yielded the opposite result. In those experiments, a complete overlap of the two fluorescent signals was observed (Walz et al., 2007), suggesting that GC-D cells may express OMP at a low enough level that it is not sufficient to drive strong GFP fluorescence in the OMP-GFP line.

Alternatively, our approach could fail to identify a population of non-GCD cells if those cells were located substantially anterior to the GC-D population within the MOE,

due to differences in diffusion time required for the dye to reach the cell bodies or the amount of dye required to strongly label cell bodies located a great distance from the site of electroporation. As the proposed second population of OSNs innervating the GC-D necklace has been defined only by the expression of OMP, it is also formally possible that the cells do not reside within the MOE but within a separate sensory epithelium like the septal organ. Additional tracing experiments – in conjunction with transcriptional profiling of GC-D cells – will further illuminate the relationship between GC-D and OMP cells within the necklace subsystem.

The co-innervation of GC-D glomeruli by GC-D cells and OR-expressing cells has been proposed as a mechanism by which the necklace subsystem coordinates the detection and association of the unconditioned stimuli (carbon disulfide or uroguanylin) and the conditioned stimuli (typically cinnamon or cocoa) in STFP, as these stimuli activate GC-D cells and OR-expressing cells, respectively. Our results suggest that coincident detection of the unconditioned and conditioned stimuli in STFP is not mediated at early processing stages but is instead effected by downstream brain regions that receive common input from both the main olfactory and GC-D subsystems, such as a cortical region like the PCtx.

This latter organization – in which inputs from main olfactory OSNs are excluded from necklace glomeruli – makes sense in light of the projections from GC-D glomeruli to unique targets like the septal nuclei in additional to “normal” MOB targets like the PCtx. That is, by excluding OR-expressing OSNs from necklace glomeruli, the activation of those cells by general odorants like cinnamon or cocoa – which occurs under normal

circumstances beyond STFP – does not recruit the specialized circuitry downstream of the necklace that may be reserved for ethologically important odorants. In contrast, activation of GC-D cells concurrently recruits activity in specialized septal regions and MOB targets because both regions are innervated by necklace M/T cells. Thus, only if an OR-activating odorant like cocoa was presented with a GC-D cell ligand could an MOB target like the PCtx encode the resulting cortical activity pattern as an odor object for STFP, as the specialized necklace circuits mediating STFP would be obligately co-activated under those circumstances.

Unique Downstream Circuitry of the GC-D Necklace: Possible Functional Roles

Glomeruli of the GC-D necklace subsystem are interconnected via putative M/T projection neurons with glomeruli of two other specialized necklaces, the GG and the ChAT subsystem, and the M/T cells innervating GC-D glomeruli project both to regions innervated by the main olfactory system and to specialized targets that are selectively innervated by the necklace. This anatomical arrangement suggests that the three necklaces in aggregate may comprise a functional subsystem with specialized anatomy. We would thus predict that the GG and ChAT necklaces also project to the septal targets innervated by the GC-D necklace, as the necklaces share at least a partly common pool of M/T cells. We did observe a small number of non-GC-D glomeruli that were innervated by virally infected cells in our retrograde tracing experiments from the LSr/NDB, and some of these may belong to other necklace subsystems.

As described above, the particular anatomical organization of the GC-D subsystem appears to facilitate the segregation of the combined necklace inputs to unique downstream circuits, while simultaneously permitting integration of main olfactory system inputs downstream of the OB. In this way, the necklaces are given direct access to higher order main olfactory system circuitry, but OR-expressing cells are not given access to necklace-specific circuits.

The unique projections to the LSr/NDB suggest that the GC-D necklace subsystem serves a specialized role in olfactory perception. The LSr is a central node of neural circuits regulating affect and motivation, fear and anxiety, aggression, social behaviors, feeding, and cognition (Anthony et al., 2014; Bielsky et al., 2005; Endres and Fendt, 2008; Li et al., 2015; Sheehan et al., 2004; Sweeney and Yang, 2015; Talishinsky and Rosen, 2012; Wong et al., 2016; Zahm et al., 2013); as such, the structure is well positioned to direct appropriate behavioral responses to specific environmental stimuli in a context-dependent manner.

The LSr projects to regions within the medial hypothalamus involved in defensive and social behaviors that are also innervated by the MeA (Cádiz-Moretti et al., 2014; Sheehan et al., 2004). The direct projection from the AOB to the MeA is considered a major mechanism by which the vomeronasal olfactory system is specialized to mediate innate behaviors because the MeA strongly projects to the abovementioned hypothalamic nuclei; thus, the necklace projection to the LSr may be an equivalent specialization within the necklace subsystem to generate pheromone and predator odor-evoked behaviors.

While the GC-D necklace subsystem seems poised to mediate a range of odor-evoked behaviors, the molecular and anatomical features of the subsystem suggest that it is not optimized to discriminate the various behaviorally important cues that activate GC-D cells. Thus, selection of an appropriate behavioral response would likely require additional context regarding external sensory cues and information about internal state. The LSr is also suited to manage the integration of those contextual cues, as it receives tertiary input from the main (via the Ent) and vomeronasal (via the MeA and BNST) olfactory systems, and also has numerous connections to various cortical and neuromodulatory centers (Cádiz-Moretti et al., 2014; Risold and Swanson, 1997; Sheehan et al., 2004; Swanson and Cowan, 1979).

On its own, the GC-D necklace subsystem may not function to discriminate odors but may instead serve a particular role in olfactory perception: to alert the organism of the general presence of ethologically salient stimuli, regardless of their specific identities. Expression of multiple chemoreceptors in each GC-D cell – and the fact that all of their ligands that have been identified thus far carry innate ethological meaning to the mouse – supports the hypothesis that the GC-D subsystem could act as a "salience detector." This proposed function is further supported by the other downstream target uniquely innervated by the GC-D necklace, the NDB. The NDB is a neuromodulatory region that provides broad cholinergic input (from the vNDB) to the hippocampus, and to olfactory regions including the PCtx, Ent, and the OB via cells in the hNDB. Notably, cholinergic bulbar projections from the hNDB include the dense projections that define the ChAT necklace (D'Souza and Vijayaraghavan, 2014; Zaborszky et al., 2012).

Broadly, cholinergic signaling enhances learning, attention, and arousal; in the OB, optogenetic activation of cholinergic axons results in an increase in excitation of M/T cells (Rothermel et al., 2014), and increasing cholinergic signaling sharpens the receptive fields of M/T cells (D'Souza and Vijayaraghavan, 2012; Nunez-Parra et al., 2013). Both of these effects are consistent with a role in increasing the salience of olfactory cues. Thus, the GC-D necklace subsystem may act as a general “alerting” system by increasing attention and arousal of the animal through the recruitment of cholinergic activity via excitatory M/T inputs to the NDB. We have some evidence from our trans-synaptic rabies experiments that necklace M/T cells synapse onto cholinergic neurons within the basal forebrain; however, it remains to be seen whether necklace M/T cells specifically target cells within the hNDB that provide centrifugal cholinergic modulation within the OB.

Together, our data define an anatomical framework for the GC-D necklace olfactory subsystem that generates new and specific hypotheses regarding the necklace subsystem’s role in olfactory perception. In particular, the unique anatomy of this subsystem – including the presence of parallel, interconnected information channels and privileged access to downstream targets with known functions in arousal and sensory salience – suggests that the GC-D necklace may uniquely act in olfactory processing to signal the general presence of ethologically salient stimuli to the animal. Future experiments to functionally dissect the architecture of the necklace subsystem will reveal further insight into the specific role of this subsystem in olfactory perception.

EXPERIMENTAL METHODS

Ventrolateral Surgical Preparation

All animal procedures were done in accordance with Harvard Medical School's Institutional Animal Care and Use Committee (IACUC). A cranial window over the ventrolateral portion of the right OB of GCD-IRES-GFP (Greer et al., 2016) and OMP-GFP mice (Potter et al., 2001) was made as described below. For the control 174-9 electroporations, a standard dorsal craniotomy above the OB of 174-9-IRES-GFP mice was made (Sosulski et al., 2011). All mice were aged 2-4 months, and male and female mice were used indiscriminately. For the ventrolateral surgical exposure, mice were anesthetized with an intraperitoneal injection of a cocktail of ketamine (100 mg/kg); xylazine (10 mg/kg); acepromazine (3 mg/kg) and given a subcutaneous injection of dexamethasone (0.2 mg/kg); carprofen (5 mg/kg) to minimize brain inflammation.

The skin overlying the dorsal skull was removed and a steel head-post was affixed to the posterior skull with Rely-X luting cement. Anti-coagulant Gel-foam was carefully packed into the orbital socket to compress the optic nerve before removing the eye. A portion of the orbital bone was removed to provide access to the ventrolateral aspect of the OB. Kwik-Sil was used to construct an imaging well. A craniotomy overlying the posterior OB and anterior ventral forebrain was made using an air drill, while the well was frequently flushed with cold lactated Ringer's solution to prevent thermal damage. The bone and dura were carefully removed and the well was filled with lactated Ringer's solution for electroporation and imaging. After imaging, moist Gel-foam was placed over the exposed brain. The well was filled with 2% low-melt agarose and

covered with Kwik-Cast silicone sealant. The head post was removed and the exposed skin was also covered with Kwik-Cast. The mouse was given buprenorphine (0.05 mg/kg), placed in a clean cage, and monitored during recovery.

Electroporations

The electroporation procedure was modified from (Sosulski et al., 2011). The exposed mouse was placed under a two-photon microscope (Prairie Technologies microscope with a Ti:Sapphire Coherent Chameleon laser) and a wire connected to the anode of a Grass SD 9 stimulator was clamped to the mouse's rear paw with an alligator clip. A glass pipette (1.0mm x 0.78mm borosilicate, pulled to a 5 μm outer diameter) attached to the stimulator cathode and filled with anionic, lysine-fixable 3 kDa TMR-dextran (ThermoFisher D-3308, 12.5mg/mL in 1x PBS) was lowered into the center of aGFP+ glomerulus under two-photon guidance using PrairieView software for image acquisition. *In vivo* imaging was performed at 860-880 nm with a 16x objective (0.8 N.A., Nikon).

Electroporation stimulation conditions were as follows: 20 volts, 30 msec pulses, 2 pulses per second, 0 sec delay, monophasic output, reverse polarity. A few test pulses from the stimulator were applied to ensure labeling of the glomerulus. The glomerulus was electroporated for bouts of 30-60 seconds, repeated up to 3 times with breaks of 10-20 minutes in between. For some anterograde tracing experiments, a second GC-D+ glomerulus was electroporated if cleanly accessible. For electroporations using the 174-9-IRES-GFP mouse line to retrogradely label 174-9

OSNs, modified stimulation conditions previously optimized for robust labeling of OSNs from that glomerulus were used: 50V instead of 20V, and the glomerulus was stimulated for 3x15 minutes. For retrograde tracing to the MOE, mice were recovered for 1-3 days before tissue processing; for anterograde tracing of M/T cell axons, mice were recovered for 2-7 days.

Stereotactic Viral Injections

AAV experiments: 6-10 week old male and female mice harboring the protocadherin 21-Cre transgene (Pcdh21-Cre, MMRRC #030952-UCD, (Wachowiak et al., 2013)) were used. Mice were anesthetized with isoflurane and head-fixed into a stereotax with accompanying software (Angle 2, Leica Biosystems). After removing the skin overlying the skull, the skull was aligned to bregma and lambda and straightened. A small hole was drilled above the bilateral target coordinates using an air drill, and virus (50-200 nL, depending on the target region) was slowly delivered bilaterally via a glass pipette pulled to an outer diameter of ~10 μm.

The viruses used were AAV1-hSyn-FLEX-GCaMP-WPRE-SV40 (three different GCaMP viruses were used, due to changing availability from the vector core: GCaMP3, GCaMP5, GCaMP6S), from the University of Pennsylvania Perelman School of Medicine Vector Core. The following coordinates were used (given as ML/AP/DV): piriform cortex (3.1/1.25/-4.2), olfactory tubercle (1.15/1.55/-5.5), posteromedial cortical amygdala (2.75, -2.88, -5.8), and lateral septum/nucleus of the diagonal band (0.2, 1.45, -4.2). Mice were recovered for 3-4 weeks before tissue processing.

Rabies experiments: 6-10 week old male and female ChAT-IRES-Cre mice (The Jackson Laboratory #006410) were used. Stereotactic surgery was performed as described above, but injections were made unilaterally. The helper AAVs were as follows: AAV9-CAG-DIO-TCB (stock diluted 1:100 in 1x PBS) and AAV9-CAG-DIO-RVG (stock diluted 1:10 in 1x PBS). The diluted AAVs were mixed together in a 1:1 ratio and 50 nL of the mixed virus was injected into the lateral septum/nucleus of the diagonal band (ML/AP/DV = 0.2, 1.45, -4.2). AAV stocks were packaged by the Boston Children's Hospital Viral Core; aliquots generously donated by the Sabatini Lab, Harvard Medical School. Following AAV injection, mice were recovered for 2-4 weeks to allow for viral expression and then a second injection of pseudotyped, G-deleted rabies virus encoding EGFP (EnvA G-deleted rabies EGFP, The Salk Institute) was delivered to the same coordinates. 100 nL of undiluted rabies virus was injected. Mice were recovered for 5-7 days before tissue processing.

Tissue Processing / Image Acquisition

Mice were perfused with 1xPBS followed by 4% paraformaldehyde (PFA), and the dissected tissue (brain and/or main olfactory epithelium (MOE)) was post-fixed in 4% PFA overnight at 4ºC. Tissue was then transferred to a 20% sucrose solution (brains) or 0.45 M EDTA (MOE) for an overnight incubation at 4ºC prior to being embedded in tissue freezing medium and cryosectioned.

Electroporation experiments: Tissue processing was modified from (Sosulski et al., 2011). For brain sections (to trace M/T axons), 50 μm coronal cryosections were

collected onto Superfrost Plus glass slides. Slides were incubated with rb-anti-TMR (ThermoFisher A-6397, 1:500) and NeuroTrace 435/455 (1:100) diluted in block solution (1x PBS + 2% TX-100 + 0.5% BSA + 0.02% NaN3) overnight at room temperature, followed by a 1-hour incubation at room temperature with an AlexaFluor-conjugated secondary antibody (e.g. dk-a-gt-AF555) diluted 1:250 in block solution. Slides were mounted in VectaShield mounting medium. For OB sections (to assess intrabulbar connectivity), tissue was coronally cryosectioned at 50 μm as described above. The TMR signal was not amplified by antibody staining, but IHC using antibodies against PDE2A (gt-a-PDE2A (N-20), Santa Cruz sc-17227, 1:50 in block solution) or ChAT (gt-a-ChAT, Millipore AB144P, 1:100 in block solution) was performed.

Slides were incubated in primary antibody overnight at room temperature, followed by incubation with an AlexaFluor-conjugated secondary antibody (dk-a-gt-AF647, diluted 1:250 in block solution) for 1 hour at room temperature, and mounted in VectaShield+DAPI mounting medium. For MOE sections (to assess retrograde label of OSNs), the decalcified nose and epithelium were coronally sectioned at 30 μm and slides were mounted in VectaShield+DAPI mounting medium without any IHC. All slides were imaged with an Olympus VS120 slide scanning system (10x magnification); for MOE slides, tiled Z-stacks were collected.

AAV experiments: Tissue was cryosectioned at 50 μm (brain) or 20 μm (OB). IHC was performed as described above (overnight primary antibody incubation, 1-hour secondary antibody incubation, both at room temperature). Brain slides were stained with NeuroTrace 433/435 (1:100, diluted in block solution) and mounted in VectaShield

mounting medium. Slides containing OB were co-stained with an antibody against CAR2 (rb-a-CAR2, 1:1000, Abcam ab191343) to label the GC-D glomeruli and an antibody against GFP (ch-a-GFP, 1:500, Abcam ab13970) to amplify the viral GCaMP signal, and were mounted in VectaShield+DAPI mounting medium. Slides were imaged using an Olympus VS120 Slide Scanner (10x magnification). High-resolution images were collected with an Olympus FV1000 or FV1200 confocal microscope at 20-60x magnification (20x air = 0.75NA; 40x oil = 1.3NA; 60x oil = 1.42NA, Olympus) and processed in Imaris software (Bitplane).

Rabies experiments: Brain and OB tissue was processed the same as above, but OB tissue was sectioned at 50 μm and only stained for anti-CAR2.

Data Analysis

Electroporations: Slide scanner images collected at 10x magnification were viewed in OlyVia software. Labeled fibers throughout the brain were manually identified from these images and maps depicting the approximate extent of those labeled fibers in specific brain regions were manually constructed. For labeled OSNs in the MOE, the slide scanner Z-stacks were viewed in OlyVia to manually identify the labeled cells and annotate their positions on the images. Cells were tallied for each mouse and the percentage of yellow cells across all mice was calculated. The schematic depicting the approximate range of yellow cells within the MOE was manually constructed from the annotated slide scanner images.

AAV experiments: For each brain region targeted with AAV injections, the numbers of innervated GC-D versus non GC-D glomeruli were counted and expressed

as a percentage of the total respective glomerular population (GC-D or non-GC-D). To quantify the number of non-GCD glomeruli innervated by fibers labeled by retrograde infection, glomeruli in every other section were counted to minimize the number of double-counted glomeruli, but also to minimize the number of "missed" glomeruli due to sparse labeling. (Due to the number of non-GC-D glomeruli it is not feasible to follow the same glomerulus from section to section). The "percentage of non-GC-D glomeruli" was calculated by dividing the number of innervated glomeruli by a scaled version of the total estimated number of glomeruli within the MOB (~1800,(Royet et al., 1988)), based on how much of the OB was sectioned and counted. For most samples only the posterior third of the OB was collected and counted, so we divided by 600 to get the percentage; for a few samples the posterior half of the OB was collected and accordingly, the total number of glomeruli was divided by 900.

To quantify the number of innervated GC-D glomeruli (labeled by anti-CAR2), individual glomeruli could be unambiguously followed across sections and therefore the total number of "unique" glomeruli was assessed. (This therefore eliminated the risk of either double counting or missing labeled glomeruli.) The number of innervated GC-D glomeruli was divided by 40 (the upper estimate of GC-D glomeruli per OB, (Walz et al., 2007)) to calculate the percentage of innervated GC-D glomeruli. Percentages of GC-D and non-GC-D glomeruli were statistically compared using a one-tailed paired t-test.

Rabies experiments: All possible starter cells were identified by their co-expression of mCherry (from AAV9-CAG-DIO-TCB) and EGFP (from the RABV-EGFP), counted according to their anatomical position, and grouped as follows: "non-olfactory"

targets = MA/Hy/miscellaneous posterior targets; “septal targets” = MS/NDB, LSr; “olfactory targets” = OT/AON/TT/miscellaneous anterior targets. To quantify the number of glomeruli (GC-D versus non-GC-D) innervated by fibers labeled by trans-synaptic retrograde infection (i.e. EGFP+), glomeruli in every other section spanning the entire OB were counted to minimize both the number of double counted glomeruli and the number of “missed” glomeruli. Note that because LSr injections were targeted close to the midline, starter cells and labeled glomeruli were observed in both hemispheres of the brain and were counted together. To express the numbers as a percentage of the glomerular population (GC-D vs. non-GC-D), the number of innervated GC-D glomeruli was divided by 80 (2x the upper estimate of GC-D glomeruli per OB to account for both bulbs, (Walz et al., 2007)), and the number of non-GC-D glomeruli was divided by 3600 (accounting for both OBs, (Royet et al., 1988)). Percentages of GC-D and non-GC-D glomeruli were statistically compared using a one-tailed paired t-test.

REFERENCES

Anthony, T.E., Dee, N., Bernard, A., Lerchner, W., Heintz, N., and Anderson, D.J. (2014). Control of stress-induced persistent anxiety by an extra-amygdala septohypothalamic circuit. Cell *156*, 522–536.

Arakawa, H., Kelliher, K.R., Zufall, F., and Munger, S.D. (2013). The Receptor Guanylyl Cyclase Type D (GC-D) Ligand Uroguanylin Promotes the Acquisition of Food Preferences in Mice. Chem Senses *38*, 391–397.

Belluscio, L., Koentges, G., Axel, R., and Dulac, C. (1999). A map of pheromone receptor activation in the mammalian brain. Cell *97*, 209–220.

Bergan, J.F., Ben-Shaul, Y., and Dulac, C. (2014). Sex-specific processing of social cues in the medial amygdala. Elife *3*, e02743.

Bielsky, I.F., Hu, S.-B., Ren, X., Terwilliger, E.F., and Young, L.J. (2005). The V1a Vasopressin Receptor Is Necessary and Sufficient for Normal Social Recognition: A Gene Replacement Study. Neuron *47*, 503–513.

Buck, L., and Axel, R. (1991). A novel multigene family may encode odorant receptors: A molecular basis for odor recognition. Cell *65*, 175–187.

Cádiz-Moretti, B., Otero-García, M., Martinez-Garcia, F., and Lanuza, E. (2014). Afferent projections to the different medial amygdala subdivisions: a retrograde tracing study in the mouse. Brain Struct Funct *221*, 1033–1065.

Chess, A., Simon, I., Cedar, H., and Axel, R. (1994). Allelic inactivation regulates olfactory receptor gene expression. Cell *78*, 823–834.

Cleland, T.A. (2014). Construction of odor representations by olfactory bulb microcircuits. Prog. Brain Res. *208*, 177–203.

Cockerham, R.E., Puche, A.C., and Munger, S.D. (2009). Heterogeneous sensory innervation and extensive intrabulbar connections of olfactory necklace glomeruli. PLoS ONE *4*, e4657.

D'Souza, R.D., and Vijayaraghavan, S. (2012). Nicotinic receptor-mediated filtering of mitral cell responses to olfactory nerve inputs involves the α3β4 subtype. Journal of Neuroscience *32*, 3261–3266.

D'Souza, R.D., and Vijayaraghavan, S. (2014). Paying attention to smell: cholinergic signaling in the olfactory bulb. Front Synaptic Neurosci *6*, 21.

Dalton, R.P., and Lomvardas, S. (2015). Chemosensory receptor specificity and regulation. Annu Rev Neurosci *38*, 331–349.

Del Punta, K., Puche, A., Adams, N.C., Rodriguez, I., and Mombaerts, P. (2002). A divergent pattern of sensory axonal projections is rendered convergent by second-order neurons in the accessory olfactory bulb. Neuron *35*, 1057–1066.

Devor, M. (1976). Fiber trajectories of olfactory bulb efferents in the hamster. J Comp Neurol *166*, 31–47.

Dulac, C., and Axel, R. (1995). A novel family of genes encoding putative pheromone receptors in mammals. Cell *83*, 195–206.

Endres, T., and Fendt, M. (2008). Inactivation of the lateral septum blocks fox odor-induced fear behavior. NeuroReport *19*, 667–670.

Ennis, M., and Holy, T.E. (2015). Anatomy and Neurobiology of the Main and Accessory Olfactory Bulbs. Doty/Handbook of Olfaction and Gustation 157–182.

Gao, L., Hu, J., Zhong, C., and Luo, M. (2010). Integration of CO2 and odorant signals in the mouse olfactory bulb. Nsc *170*, 881–892.

Gautam, S.H., and Verhagen, J.V. (2012). Retronasal odor representations in the dorsal olfactory bulb of rats. Journal of Neuroscience *32*, 7949–7959.

Greer, P.L., Bear, D.M., Lassance, J.-M., Bloom, M.L., Tsukahara, T., Pashkovski, S.L., Masuda, F.K., Nowlan, A.C., Kirchner, R., Hoekstra, H.E., et al. (2016). A Family of non-GPCR Chemosensors Defines an Alternative Logic for Mammalian Olfaction. Cell *165*, 1734–1748.

Haberly, L.B., and Price, J.L. (1977). The axonal projection patterns of the mitral and tufted cells of the olfactory bulb in the rat. Brain Res *129*, 152–157.

Haga, S., Hattori, T., Sato, T., Sato, K., Matsuda, S., Kobayakawa, R., Sakano, H., Yoshihara, Y., Kikusui, T., and Touhara, K. (2010). The male mouse pheromone ESP1 enhances female sexual receptive behaviour through a specific vomeronasal receptor. Nature *466*, 118–122.

Herrada, G., and Dulac, C. (1997). A novel family of putative pheromone receptors in mammals with a topographically organized and sexually dimorphic distribution. Cell *90*, 763–773.

Hu, J., Zhong, C., Ding, C., Chi, Q., Walz, A., Mombaerts, P., Matsunami, H., and Luo, M. (2007). Detection of near-atmospheric concentrations of CO2 by an olfactory subsystem in the mouse. Science *317*, 953–957.

Ihara, S., Yoshikawa, K., and Touhara, K. (2013). Chemosensory signals and their receptors in the olfactory neural system. Neuroscience *254*, 45–60.

Johnson, B.A., and Leon, M. (2007). Chemotopic odorant coding in a mammalian olfactory system. J Comp Neurol *503*, 1–34.

Juilfs, D.M., Fülle, H.J., Zhao, A.Z., Houslay, M.D., Garbers, D.L., and Beavo, J.A. (1997). A subset of olfactory neurons that selectively express cGMP-stimulated phosphodiesterase (PDE2) and guanylyl cyclase-D define a unique olfactory signal transduction pathway. Proc Natl Acad Sci USA *94*, 3388–3395.

Kang, N., Baum, M.J., and Cherry, J.A. (2009). A direct main olfactory bulb projection to the “vomeronasal” amygdala in female mice selectively responds to volatile pheromones from males. European Journal of Neuroscience *29*, 624–634.

Kay, L.M., and Sherman, S.M. (2007). An argument for an olfactory thalamus. Trends Neurosci *30*, 47–53.

Larriva-Sahd, J. (2012). Cytological organization of the alpha component of the anterior olfactory nucleus and olfactory limbus. Front Neuroanat *6*, 23.

Li, W., Motelow, J.E., Zhan, Q., Hu, Y.-C., Kim, R., Chen, W.C., and Blumenfeld, H. (2015). Cortical Network Switching: Possible Role of the Lateral Septum and Cholinergic Arousal. Brain Stimulation *8*, 36–41.

Liberles, S.D. (2014). Mammalian pheromones. Annu. Rev. Physiol. *76*, 151–175.
Luo, M. (2008). The Necklace Olfactory System in Mammals. J Neurogenet *22*, 229–238.

Luo, M., and Katz, L.C. (2004). Encoding pheromonal signals in the mammalian vomeronasal system. Curr Opin Neurobiol *14*, 428–434.

Mamasuew, K., Hofmann, N., Kretzschmann, V., Biel, M., Yang, R.-B., Breer, H., and Fleischer, J. (2011). Chemo- and Thermosensory Responsiveness of Grueneberg Ganglion Neurons Relies on Cyclic Guanosine Monophosphate Signaling Elements. Neurosignals *19*, 198–209.

Matsuo, T., Rossier, D.A., Kan, C., and Rodriguez, I. (2012). The wiring of Grueneberg ganglion axons is dependent on neuropilin 1. Development *139*, 2783–2791.

Miyamichi, K., Amat, F., Moussavi, F., Wang, C., Wickersham, I., Wall, N.R., Taniguchi, H., Tasic, B., Huang, Z.J., He, Z., et al. (2011). Cortical representations of olfactory input by trans-synaptic tracing. Nature *472*, 191–196.

Mombaerts, P. (2006). Axonal wiring in the mouse olfactory system. Annu. Rev. Cell Dev. Biol. *22*, 713–737.

Munger, S.D., Leinders-Zufall, T., McDougall, L.M., Cockerham, R.E., Schmid, A., Wandernoth, P., Wennemuth, G., Biel, M., Zufall, F., and Kelliher, K.R. (2010). An olfactory subsystem that detects carbon disulfide and mediates food-related social learning. Curr Biol *20*, 1438–1444.

Nagayama, S. (2010). Differential Axonal Projection of Mitral and Tufted Cells in the Mouse Main Olfactory System. Frontiers in Neural Circuits *4*, 120

Nagayama, S., Homma, R., and Imamura, F. (2014). Neuronal organization of olfactory bulb circuits. Frontiers in Neural Circuits *8*, 98.

Nunez-Parra, A., Maurer, R.K., Krahe, K., Smith, R.S., and Araneda, R.C. (2013). Disruption of centrifugal inhibition to olfactory bulb granule cells impairs olfactory discrimination. Proc Natl Acad Sci USA *110*, 14777–14782.

Osada, K., Miyazono, S., and Kashiwayanagi, M. (2015). The scent of wolves: pyrazine analogs induce avoidance and vigilance behaviors in prey. Front. Neurosci. *9*, 2147–11.

Potter, S.M., Zheng, C., Koos, D.S., Feinstein, P., Fraser, S.E., and Mombaerts, P. (2001). Structure and emergence of specific olfactory glomeruli in the mouse. Journal of Neuroscience *21*, 9713–9723.

Ring, G., Mezza, R.C., and Schwob, J.E. (1997). Immunohistochemical identification of discrete subsets of rat olfactory neurons and the glomeruli that they innervate. J Comp Neurol *388*, 415–434.

Risold, P., and Swanson, L. (1997). Connections of the rat lateral septal complex. Brain Res Rev *24*, 115–195.

Rodriguez, I., Feinstein, P., and Mombaerts, P. (1999). Variable patterns of axonal projections of sensory neurons in the mouse vomeronasal system. Cell *97*, 199–208.

Rothermel, M., Carey, R.M., Puche, A., Shipley, M.T., and Wachowiak, M. (2014). Cholinergic Inputs from Basal Forebrain Add an Excitatory Bias to Odor Coding in the Olfactory Bulb. Journal of Neuroscience *34*, 4654–4664.

Royet, J.P., Souchier, C., Jourdan, F., and Ploye, H. (1988). Morphometric study of the glomerular population in the mouse olfactory bulb: numerical density and size distribution along the rostrocaudal axis. J Comp Neurol *270*, 559–568.

Salcedo, E., Tran, T., Ly, X., Lopez, R., Barbica, C., Restrepo, D., and Vijayaraghavan, S. (2011). Activity-Dependent Changes in Cholinergic Innervation of the Mouse Olfactory Bulb. PLoS ONE *6*, e25441.

Scalia, F., and Winans, S.S. (1975). The differential projections of the olfactory bulb and accessory olfactory bulb in mammals. J Comp Neurol *161*, 31–55.

Scott, J.W., Brierley, T., and Schmidt, F.H. (2000). Chemical determinants of the rat electro-olfactogram. J Neurosci *20*, 4721–4731.

Scott, J.W., Acevedo, H.P., Sherrill, L., and Phan, M. (2007). Responses of the Rat Olfactory Epithelium to Retronasal Air Flow. J Neurophysiol *97*, 1941–1950.

Sheehan, T.P., Chambers, R.A., and Russell, D.S. (2004). Regulation of affect by the lateral septum: implications for neuropsychiatry. Brain Res Rev *46*, 71–117.

Shinoda, K., Ohtsuki, T., Nagano, M., and Okumura, T. (1993). A possible functional necklace formed by placental antigen X-P2-immunoreactive and intensely acetylcholinesterase-reactive (PAX/IAE) glomerular complexes in the rat olfactory bulb. Brain Res *618*, 160–166.

Shinoda, K., Shiotani, Y., and Osawa, Y. (1989). “Necklace olfactory glomeruli” form unique components of the rat primary olfactory system. J Comp Neurol *284*, 362–373.

Sosulski, D.L., Bloom, M.L., Cutforth, T., Axel, R., and Datta, S.R. (2011). Distinct representations of olfactory information in different cortical centres. Nature *472*, 213–216.

Stowers, L., and Logan, D.W. (2010). Olfactory mechanisms of stereotyped behavior: on the scent of specialized circuits. Curr Opin Neurobiol *20*, 274–280.

Su, C.-Y., Menuz, K., and Carlson, J.R. (2009). Olfactory Perception: Receptors, Cells, and Circuits. Cell *139*, 45–59.

Swanson, L.W., and Cowan, W.M. (1979). The connections of the septal region in the rat. J Comp Neurol *186*, 621–655.

Sweeney, P., and Yang, Y. (2015). An excitatory ventral hippocampus to lateral septum circuit that suppresses feeding. Nat Commun *6*, 10188.

Talishinsky, A., and Rosen, G.D. (2012). Systems Genetics of the Lateral Septal Nucleus in Mouse: Heritability, Genetic Control, and Covariation with Behavioral and Morphological Traits. PLoS ONE *7*, e44236.

Tirindelli, R., Dibattista, M., Pifferi, S., and Menini, A. (2009). From Pheromones to Behavior. Physiological Reviews *89*, 921–956.

Vassar, R., Chao, S.K., Sitcheran, R., Nun, J.M., and Vosshall, L.B. (1994). Topographic organization of sensory projections to the olfactory bulb. Cell *79*, 981–991.

Vassar, R., Ngai, J., and Axel, R. (1993). Spatial segregation of odorant receptor expression in the mammalian olfactory epithelium. Cell *74*, 309–318.

Wachowiak, M., Economo, M.N., Díaz-Quesada, M., Brunert, D., Wesson, D.W., White, J.A., and Rothermel, M. (2013). Optical dissection of odor information processing in vivo using GCaMPs expressed in specified cell types of the olfactory bulb. Journal of Neuroscience *33*, 5285–5300.

Wagner, S., Gresser, A.L., Torello, A.T., and Dulac, C. (2006). A multireceptor genetic approach uncovers an ordered integration of VNO sensory inputs in the accessory olfactory bulb. Neuron *50*, 697–709.

Walz, A., Feinstein, P., Khan, M., and Mombaerts, P. (2007). Axonal wiring of guanylate cyclase-D-expressing olfactory neurons is dependent on neuropilin 2 and semaphorin 3F. Development *134*, 4063–4072.

Wong, L.C., Wang, L., D'Amour, J.A., Yumita, T., Chen, G., Yamaguchi, T., Chang, B.C., Bernstein, H., You, X., Feng, J.E., et al. (2016). Effective Modulation of Male Aggression through Lateral Septum to Medial Hypothalamus Projection. Current Biology.

Zaborszky, L., van den Pol, A., and Gyengesi, E. (2012). The Basal Forebrain Cholinergic Projection System in Mice. In The Mouse Nervous System, (Elsevier), pp. 684–718.

Zahm, D.S., Parsley, K.P., Schwartz, Z.M., and Cheng, A.Y. (2013). On lateral septum-like characteristics of outputs from the accumbal hedonic "hotspot" of Peciña and Berridge with commentary on the transitional nature of basal forebrain "boundaries". J Comp Neurol *521*, 50–68.

Zhang, J.-X., Sun, L., and Novotny, M.V. (2007). Mice Respond Differently to Urine and Its Major Volatile Constituents from Male and Female Ferrets. J Chem Ecol *33*, 603–612.

Zheng, L.M., Ravel, N., and Jourdan, F. (1987). Topography of centrifugal acetylcholinesterase-positive fibres in the olfactory bulb of the rat: evidence for original projections in atypical glomeruli. Neuroscience *23*, 1083–1093.

CHAPTER 4

Conclusions and Future Directions

As described in the previous chapters, we have developed experimental approaches that provide unprecedented access to the GC-D necklace olfactory subsystem *in vivo*, and we have used them to better define the subsystem's anatomical architecture from sensory epithelium to higher brain. Our results suggest that 1) GC-D glomeruli are homogeneous, redundant information channels that pool sensory information from across the epithelial sheet; 2) the GC-D subsystem may – like the vomeronasal subsystem – be specialized to encode ethologically salient stimuli via atypical features of glomerular organization; 3) GC-D glomeruli integrate information from two other specialized "necklace" subsystems within the olfactory bulb (OB); 4) information from the GC-D subsystem is integrated with sensory signals from the main olfactory system in downstream brain areas via commonly projecting M/T cells from each subsystem, but not within the OB within heterogeneous glomeruli innervated by OSNs from each subsystem; and 5) the GC-D subsystem is poised to serve a unique role in olfactory perception by virtue of its privileged access to downstream brain regions that mediate odor-evoked behaviors and general arousal state.

We are now pursuing some of the many lines of investigation that have been opened by this work (described below), with a focus on functional interrogation of the GC-D subsystem. Through such experiments we will gain insights into the specific mechanisms by which the mammalian brain converts sensory signals into appropriate, context-dependent behavioral outputs.

Identification of the Postsynaptic Targets of Necklace M/T Cells

All brain regions innervated by GC-D necklace M/T cells – both classic olfactory regions (e.g. the olfactory tubercle (OT) and piriform cortex (PCTx)) and novel septal targets (the lateral septum (LSr) and nucleus of the diagonal band (NDB)) – are heterogeneous structures comprised of multiple cell types. As such, the postsynaptic targets of the M/T cells within each region must be identified if we are to fully understand the functional effects of activation of the GC-D necklace, the role of each downstream target in processing olfactory signals from this subsystem, and the similarities and differences between the GC-D subsystem and the canonical main olfactory system. Trans-synaptic tracing from various genetically identified starter cell populations in each brain target using modified rabies virus will identify the cell types that receive direct synaptic contacts from M/T cells.

We found that necklace M/T cells synapse onto cholinergic cells within the medial septum (MS)/NDB complex; however, it is likely that M/T cells also target other cell types within the heterogeneous septal nuclei. In addition to a large population of long-range GABAergic projection neurons (Sheehan et al., 2004), the LSr and NDB include many genetically distinguishable cell populations based on expression of neuropeptides (e.g. neuropeptide Y (NPY) and somatostatin) (Risold and Swanson, 1997), hormones (e.g. gonadotropin-releasing hormone (GnRH)) (Zaborszky et al., 2012), or hormone receptors (e.g. type 2 corticotropin-releasing factor receptor (CRFR2, (Anthony et al., 2014)) the oxytocin receptor (OTR), and vasopressin receptor 1a (V1aR) (Talishinsky and Rosen, 2012)). Fortunately, Cre mouse lines exist for many of the genes expressed

within the septal nuclei, so we can easily query many potential postsynaptic targets of necklace M/T cells. These Cre lines will also be essential after postsynaptic cell identities have been assigned to dissect the functional contribution of those cells and their projections to the larger circuits mediating odor-evoked behaviors, as was recently done to demonstrate the involvement of CRFR2+ cells within the LSr in stress-induced anxiety (Anthony et al., 2014).

Similarly, within brain regions that are co-innervated by both the main and GC-D necklace subsystems, the projections from each subsystem may have distinct functional roles due to differences in features such as the identities of the postsynaptic cells or density of projections. Data from our retrograde AAV tracing experiments suggest that inputs from the GC-D subsystem may be underrepresented in the PCtx relative to those from the main olfactory system, and the two subsystems may also differ with regards to other metrics – like the identity of the postsynaptic targets within the PCtx – that could not be deduced from those experiments. M/T cells from the main olfactory system synapse onto both glutamatergic and GABAergic cells within the PCtx (Miyamichi et al., 2011); however, the GC-D subsystem may preferentially or exclusively target one population over the other. Trans-synaptic tracing from each cell population using Cre lines for excitatory versus inhibitory cells could reveal these differences. Thus, even in the absence of atypical projections to unique brain regions like the LSr/NDB, differences in postsynaptic cellular targets between the main and GC-D subsystems in canonical downstream regions like the PCtx could endow the GC-D necklace subsystem with specialized functions in olfactory processing.

The OT is even more diverse in its cellular composition than the PCtx, and to date the exact postsynaptic cellular targets within the OT for M/T cells of even the main olfactory system have not been identified. Canonical M/T cells are thought to synapse onto medium spiny neurons (MSNs) within the dense-cell layer of the OT (Wesson and Wilson, 2011). As in the rest of the striatum, OT MSNs are GABAergic cells that express either the type 1 or type 2 dopamine receptor. Thus, M/T cells of different olfactory subsystems could differentially target specific MSN cell types.

The OT and a contiguous region, the ventral pallidum (VP), also contain cholinergic cells, which are interesting candidates as the postsynaptic targets of necklace M/T cells since the OT and VP are densely interconnected with the septal nuclei (Risold and Swanson, 1997; Wesson and Wilson, 2011), and the VP is even considered a component of the “basal cholinergic system” that encompasses the septal nuclei (Zaborszky et al., 2012). Thus, the GC-D necklace subsystem could gain further access to septal-related neural circuits mediating affect, hedonics, and motivation (Ikemoto, 2007; Sheehan et al., 2004) via projections to cholinergic cells within the OT/VP.

In anterograde tracing experiments we often observe labeled fibers within deep portions of the OT and occasionally even within the VP (data not shown), a region not known to receive direct M/T cell innervation that would therefore represent a third unique target of the necklace subsystem. Due to the contiguous nature of the VP/OT – and given that we were unable to assess the extent of the viral infection – we were unable to verify the VP projections via retrograde AAV tracing. However, we will be able

to verify whether necklace M/T cells project to the VP via rabies tracing, as we can unambiguously identify the positions of the starter cells and can therefore be assured of the specificity of our tracing.

Assessment of Septal Activity Following Activation of the GC-D Subsystem

We hypothesize that activation of the GC-D necklace subsystem may increase the animal's arousal and attention by recruiting cholinergic activity via either direct or indirect (relayed by the LSr) M/T projections to the NDB. In this way, the GC-D subsystem could serve as a general alerting system that conveys the presence of a wide variety of ethologically salient stimuli detected by the various olfactory receptors expressed in GC-D cells. To test this hypothesis, we must assess the effects of activating the GC-D subsystem (and specifically, the M/T cells that project to septal regions) on the LSr/NDB.

We could indirectly assess neural activity within the LSr/NDB following activation of the GC-D subsystem by analyzing the expression of activity-dependent immediate early genes (IEGs) in the septal nuclei following exposure of the mouse to GC-D or MS4A ligands. Odor-evoked IEG mapping is a standard technique in the field to implicate specific brain regions and downstream circuits in the detection of particular ligands (Carvalho et al., 2015; Haga et al., 2010; Kobayakawa et al., 2007; Matsuo et al., 2015; Papes et al., 2010; Pérez-Gómez et al., 2015).

However, while this approach likely would reveal activation of cells within the septal nuclei, such data could not distinguish between primary activation of the regions

(by direct projections of M/T cells, a unique feature of the GC-D subsystem) and indirect activation of the regions (via downstream circuits that are accessible to many olfactory subsystems). For example, direct targets of both the main olfactory system (e.g. the OT and the entorhinal cortex (Ent)) and the accessory olfactory system (e.g. the medial amygdala (MeA) and the bed nucleus of the stria terminalis (BNST)) project to the septal nuclei (Risold and Swanson, 1997; Sheehan et al., 2004; Wesson, 2010), and problematically, almost all of the ligands identified for the GC-D subsystem activate at least one other olfactory system (Brechbühl et al., 2013; Chamero et al., 2012; Isogai et al., 2011; Lin et al., 2007).

Thus, to definitively attribute IEG induction to the GC-D subsystem, one would have to compare the patterns of odor-evoked IEG expression in wild-type mice and in mice that are functionally deficient in one or more olfactory subsystems due to the genetic deletion of required signal transduction proteins like the CNGA2 subunit in the main olfactory system (Brunet et al., 1996) and the TRPC2 receptor in the vomeronasal olfactory system (Lucas et al., 2003). We have recently acquired *Cnga3* deletion mice, in which signaling within the Grueneberg ganglion (GG) and the GC-D subsystem – at least, downstream of GC-D activation – is ablated (Hanke et al., 2013; Leinders-Zufall et al., 2007), and we will soon have *Gucy2d* (GC-D) knock-out mice (Leinders-Zufall et al., 2007) within our laboratory. As we do not yet know whether activation of GC-D cells by ligand binding to MS4A proteins requires CNGA3, we have also recently generated mice in which the *Ms4a* gene cluster is deleted as a further comparison. These mice will be useful for IEG experiments, as well as for behavioral experiments.

While the abovementioned genetic reagents will be useful to tease apart the relative activation of septal regions that occurs via indirect circuits accessible by different olfactory subsystems, odor-evoked IEG experiments cannot attribute induction of IEG expression within the septal nuclei to the direct septal projections of GC-D necklace M/T cells since the necklace subsystem could activate the LSr/NDB indirectly as well (e.g. via M/T → Ent → LSr/NDB). Instead, we can specifically query the changes in activity of septal cells induced by the activation of direct M/T projections to those regions using approaches that combine optogenetics with either electrophysiology or fiber photometry.

Bulk infection of the OB of Pcdh21-Cre mice by a Cre-dependent AAV that encodes the light-gated cation channel channelrhodopsin (ChR2) will result in the restricted expression of ChR2 to M/T cells. (Alternatively, we can cross the Pcdh21-Cre mice to a Cre-dependent ChR2 reporter like the Ai32 strain.) Subsequently, physiological recordings can be performed on tissue slices through the LSr/NDB to record changes in electrical activity within septal cells that occur upon activation of the innervating M/T axon terminals via illumination of the slice with blue light. Alternatively, we could use a fiber photometry set-up our lab recently established to simultaneously activate M/T cell afferents expressing a red-shifted ChR2 and record activity-dependent calcium transients in cells within the LSr/NDB that express GCaMP *in vivo*. Both of these approaches will be most fruitful when paired with the knowledge of specific cell types within the LSr/NDB that receive direct synaptic input from M/T cells, which we plan to acquire using approaches described in the preceding section.

Functional Dissection of GC-D Subsystem-Mediated Behaviors

To elucidate the functional consequences of the necklace subsystem's unique projections to the septal nuclei – and to ultimately test our hypotheses regarding the subsystem's specific roles in olfactory perception – we require behavioral assays. As an initial investigation, we plan to use the optogenetic set-up described above (infection of M/T cells with a ChR2-expressing virus or Pcdh21-Cre;ChR2 mice, and fiber placement within the LSr/NDB) to record and analyze mouse behavior in an open-field assay. Our laboratory has developed a machine learning-based computational pipeline that extracts information about fine aspects of a mouse's three-dimensional behavior recorded by a Microsoft Kinect camera (Wiltschko et al., 2015). With this approach we can – in an unbiased manner – identify subtle behavioral features that emerge following optogenetic stimulation of M/T axons within the septal nuclei.

As we hypothesize that a behavioral outcome of GC-D necklace activation is increased attention or arousal, we also need to test specific behavioral correlates of attention/arousal in the context of our optogenetic manipulations. Some potential readouts of enhanced attention or arousal – such as increased investigation time – may be evident from our open-field assay and Kinect data analyses; however, other metrics of attention and arousal – such as increased sniffing or pupil dilation – will not be detectable from these experiments. Therefore, we will need to employ alternative assays. For example, we could place an awake, head-fixed mouse on a Styrofoam ball and use a regular video camera to record changes in sniffing and eye dilation induced by optogenetic stimulation of M/T axons. Under our hypothesis, we would expect the

activation of M/T projections within the septal nuclei to induce an increase in the frequency of sniffing, which is an active sensing strategy (Wachowiak, 2011), and in the extent of pupil dilation, which is a corollary to periods of increased cortical responsiveness to external stimuli (Reimer et al., 2014).

The above experiments are aimed at directly testing our "alerting system" hypothesis, but the GC-D subsystem and its unique projections to the septal region may instead serve other functions. As a more general inquiry into the behavioral effects mediated by the GC-D subsystem, we can analyze odor-evoked behaviors in wild-type, *Gucy2d*-/-, *Cnga3*-/-, and *Ms4a*-/- mice in an "odor box" behavioral assay. For this assay we use a square box that is divided into quadrants by vacuum lines drilled into its bottom and which contains odor delivery ports at each corner. Due to the vacuum lines, an odorant can be selectively delivered to a single corner without contaminating the rest of the box (Wiltschko et al., 2015). We can analyze the fine details of the mouse's behavior using the computational pipeline described above.

As mentioned previously, odor-evoked experiments using GC-D/MS4A ligands are difficult to interpret due to the fact that most odorants that activate GC-D cells also activate other olfactory subsystems. The loss-of-function mouse lines will thus be useful towards disentangling the specific behavioral effects mediated by each subsystem that is activated by these cues. Gain-of-function manipulations to specifically target the GC-D necklace will also be valuable. Toward that end, we have generated BAC transgenic GC-D-Cre mice that will allow us to optogenetically activate just the GC-D subsystem through select expression of ChR2 in GC-D OSNs and placement of an optical fiber in

the OB.

Apart from its potential role as an “alerting signal” – or any other specific functions that the GC-D necklace subsystem may serve in olfactory processing – a role for GC-D cells (and in particular, GC-D itself) in mediating socially transmitted food preference (STFP) has been firmly established. In STFP, mice learn to prefer a food scented with a particular odor if that food was previously paired with different GC-D ligands – carbon disulfide or uroguanylin – that are naturally found in rodent breath or urine/feces, respectively (Arakawa et al., 2013; Munger et al., 2010). STFP does not occur in *Gucy2d*-/- or *Cnga3*-/- mice (Munger et al., 2010), though the mechanisms downstream of odor detection by which the GC-D subsystem mediates this form of olfactory learning are unknown.

Research on the neural mechanisms of STFP has revealed that the hippocampus is important for STFP performance, specifically over longer (i.e. not immediate) intervals of STFP memory retrieval. Induction of the IEG c-Fos occurs within the hippocampus during STFP retrieval (Countryman et al., 2005; Munger et al., 2010), and intact c-Fos and CREB levels within the hippocampus prior to STFP training are required for long-term, but not immediate, STFP memory (Countryman et al., 2005). Intact cholinergic signaling in cortical, amygdalar, and hippocampal regions is also crucial for different aspects of STFP memory (Berger-Sweeney et al., 2000; Gold et al., 2011; van der Kooij and Sandi, 2012). In particular, cholinergic signaling within the septohippocampal circuit – which involves the MS/vNDB – is required for the retrograde retrieval of STFP memories (Martínez and Baxter, 2002). Importantly, this result does

not rule out a role for non-cholinergic septohippocampal projections in the initial STFP acquisition and immediate retrieval of the olfactory memory. Finally, arginine-vasopressin (AVP) and oxytocin signaling facilitates STFP (particularly in the natural expression of STFP, which typically involves physical interaction with another animal), and STFP is generally improved upon exogenous application of AVP or oxytocin (Gabor et al., 2012). As mentioned above, the LSr is a key brain region for oxytocin and AVP signaling, as evidenced by the strong expression of the corresponding receptors – OTR and V1aR – within that region (Talishinsky and Rosen, 2012). Thus, the LSr is likely recruited to facilitate as least some aspects of STFP.

Combining the existing body of work with our data, we propose the following model for STFP: convergent cortical projections (e.g. to PCtx or Ent) of the GC-D necklace and the main olfactory system allow cortical regions to encode the activity pattern induced by coincident detection of the unconditioned GC-D ligands and the conditioned main olfactory system ligand as the odor object that will be linked to the appetitive association that defines STFP. Specialized LSr/NDB necklace projections recruit activity in septal regions that enables learning processes in cortical and hippocampus areas and assigns the appetitive valence of the association by recruiting highly interconnected striatal circuits involved in hedonics and reward. Cholinergic septohippocampal circuits, meanwhile, mediate consolidation and longer term retrieval of the STFP memory.

We can test a number of explicit predictions that follow from this model using optogenetic and behavioral approaches. First, from our model we posit that the GC-D

ligands that induce STFP are only important in the sense that their binding results in the activation of M/T projections to septal nuclei that underlie the formation of the STFP appetitive association. We accordingly predict – assuming comparable activation of GC-D cells by MS4A ligands – that any of our recently identified MS4A ligands could substitute for carbon disulfide or uroguanylin as the unconditioned stimulus of STFP. We can test this in wild-type mice using the STFP paradigm.

A negative result could reflect differences in the degree of cellular activation of GC-D OSNs by GC-D versus MS4A ligands, or could be caused by confounding factors related to the stimuli, such as the fact that all the MS4A ligands identified thus far convey various ethological meanings to the animal – such as the presence of predators – that could interfere with STFP. If we are able to induce STFP with GC-D cell ligands as both the unconditioned and conditioned stimuli, then we could repeat the experiment in a *Cnga2*-/- mouse that lacks a functional main olfactory system as a way to further establish whether olfactory signaling through the GC-D system alone (which projects to both cortical and septal targets) is sufficient to mediate STFP.

Similarly, a second prediction from our model is that we could use optogenetic activation as the unconditioned stimulus to induce STFP if we activated M/T afferents in the septal nuclei (e.g. via ChR2) during training. Technically this is quite challenging to do, as it is unclear that we would be able to achieve widespread illumination and optogenetic activation of M/T afferents within the septal nuclei. We could alternatively optogenetically simulate activation of the GC-D system via a fiber placed in the OB of a GC-D-Cre mouse that selectively expresses ChR2 in GC-D OSNs. We expect that we

could induce STFP in this way, substituting the GC-D ligand with an optogenetic surrogate unconditioned stimulus; however, this experiment does not directly test our hypothesis that the septal projections in particular underlie the STFP phenomenon.

Third, we predict that we could block STFP under normal conditions (e.g. coincident presentation of a GC-D ligand and a novel main olfactory system odorant) through select inhibition of the septal necklace M/T projections (e.g. via expression of the chloride pump, halorhodopsin (Halo)) during odor presentation. Again, this is a technically challenging experiment. An alternate approach would be to bulk inhibit cells within the septal region during the initial odor training via bulk infection by a Cre-independent, Halo-expressing virus. The cellular effects would be non-specific (affecting cholinergic and non-cholinergic cells alike), but this approach should increase our chances of interfering with STFP acquisition and would establish a role (albeit indirectly) of septal necklace M/T projections in that process.

In the end, the null hypothesis – that the septal projections from the GC-D subsystem do not mediate STFP – might prevail. In this case, we would look to identify subtle differences between M/T projections of the GC-D and the main olfactory subsystems in common targets, as GC-D necklace M/T cells could exert unique influence in “canonical” olfactory regions in a number of ways such as by synapsing onto different cell types than those targeted by the main olfactory system. Whatever the outcome, our anatomical data have provided a conceptual framework to think critically about the neural mechanisms underlying STFP and to test specific hypotheses designed to further our understanding of this particular form of social learning and the

functions of the GC-D subsystem.

The ChAT Necklace and a Potential Cholinergic Circuit

Beyond determining the functional significance of the newly described projections from GC-D necklace glomeruli to higher brain regions, an equally interesting avenue of investigation is to determine the functional implications of the atypical peripheral anatomy of this subsystem. In particular, the dense interconnections of GC-D glomeruli with two other "necklaces" in the OB that correspond to the Grueneberg ganglion and the mysterious "atypical" cholinergic glomeruli suggest that the multiple necklaces may together comprise a unique processing center for olfactory information. Dissecting the function of this atypical "organizing center" for olfactory signals within the posterior OB – as well as the functional significance of the glomerular necklace motif in general – will be critical to ultimately understand how the mammalian brain integrates olfactory information from various specialized subsystems.

We are particularly keen to investigate the ChAT necklace. Beyond the strikingly dense innervation by centrifugal cholinergic (ChAT+) afferents that defines this ring of glomeruli, almost nothing is known about the ChAT necklace. The specific population(s) of primary sensory neurons that innervate these glomeruli has not yet been identified; however, ultrastructural analyses have revealed that the axon terminals of the presumptive sensory neurons within the ChAT glomeruli are atypical and contain dense-core vesicles (Zheng and Jourdan, 1988), indicative of a possible neuropeptide-mediated neuromodulatory function. We are currently performing transcriptional profiling

of single cells from the MOE in expectation of identifying atypical subpopulations of OSNs that may innervate the ChAT glomeruli.

Given our anterograde tracing results, the ChAT necklace is of particular interest because the source of the cholinergic fibers innervating these glomeruli (and indeed, all glomeruli within the OB) is the horizontal limb of the NDB, one of the septal targets of necklace M/T cells. The cholinergic nature of the ChAT necklace implies that the sensory signals associated with this necklace (coming either directly, from OSNs, or indirectly, via interconnected necklace glomeruli) are subject to heavy neuromodulation. In general, acetylcholine (ACh) release in the OB increases sensory perception and attention (D'Souza and Vijayaraghavan, 2014); therefore, the close association of GC-D necklace glomeruli with ChAT glomeruli may serve to further increase the salience of odorants that activate GC-D necklace.

Our anatomical results may thus describe a novel, septal-bulbar neuromodulatory circuit: activation of the GC-D necklace leads to activation of cholinergic cells within the NDB via direct M/T cell projections. This results in increased ACh release by centrifugal NDB fibers within the OB, which increases the salience of incoming sensory signals by establishing a “filter” by which weakly activating sensory signals aren’t propagated beyond the OB. The increased cholinergic signaling preferentially affects the ChAT necklace due to the density of cholinergic afferents.

Likewise, the specific mechanism by which the “salience filter” is established – via activation of glomerular nicotinic ACh receptors (nAChRs) that ultimately leads to increased inhibition of M/T cells through an excitation-inhibition mechanism (D'Souza

and Vijayaraghavan, 2012; Nunez-Parra et al., 2013) – implies that the signal filtering mechanism will be propagated from the ChAT necklace to glomeruli within the other necklaces due to the multiglomerular mitral cells that connect them. Thus, sensory responses passing through the GC-D necklace will also be thresholded and sharpened, consistent with its hypothesized role of conveying the presence of behaviorally relevant stimuli during a heightened attentional state. We will therefore ultimately want to characterize the centrifugal arm of this circuit to fully understand the mechanisms of olfactory processing mediated by the necklace subsystems.

In opening many exciting avenues of investigation, the work described in this dissertation thus establishes a critical foundation upon which we can build an understanding of the neural mechanisms employed by the GC-D subsystem to process sensory information.

REFERENCES

Anthony, T.E., Dee, N., Bernard, A., Lerchner, W., Heintz, N., and Anderson, D.J. (2014). Control of stress-induced persistent anxiety by an extra-amygdala septohypothalamic circuit. Cell *156*, 522–536.

Arakawa, H., Kelliher, K.R., Zufall, F., and Munger, S.D. (2013). The Receptor Guanylyl Cyclase Type D (GC-D) Ligand Uroguanylin Promotes the Acquisition of Food Preferences in Mice. Chem Senses *38*, 391–397.

Berger-Sweeney, J., Stearns, N.A., Frick, K.M., Beard, B., and Baxter, M.G. (2000). Cholinergic basal forebrain is critical for social transmission of food preferences. Hippocampus *10*, 729–738.

Brechbühl, J., Moine, F., Klaey, M., Nenniger-Tosato, M., Hurni, N., Sporkert, F., Giroud, C., and Broillet, M.-C. (2013). Mouse alarm pheromone shares structural similarity with predator scents. Proc Natl Acad Sci USA *110*, 4762–4767.

Brunet, L.J., Gold, G.H., and Ngai, J. (1996). General Anosmia Caused by a Targeted Disruption of the Mouse Olfactory Cyclic Nucleotide–Gated Cation Channel. Neuron *17*, 681–693.

Carvalho, V.M.A., Nakahara, T.S., Cardozo, L.M., Souza, M.A.A., Camargo, A.P., Trintinalia, G.Z., Ferraz, E., and Papes, F. (2015). Lack of spatial segregation in the representation of pheromones and kairomones in the mouse medial amygdala. Front. Neurosci. *9*, 283.

Chamero, P., Leinders-Zufall, T., and Zufall, F. (2012). From genes to social communication: molecular sensing by the vomeronasal organ. Trends Neurosci *35*, 597–606.

Countryman, R.A., Kaban, N.L., and Colombo, P.J. (2005). Hippocampal c-fos is necessary for long-term memory of a socially transmitted food preference. Neurobiol Learn Mem *84*, 175–183.

D'Souza, R.D., and Vijayaraghavan, S. (2012). Nicotinic receptor-mediated filtering of mitral cell responses to olfactory nerve inputs involves the α3β4 subtype. Journal of Neuroscience *32*, 3261–3266.

D'Souza, R.D., and Vijayaraghavan, S. (2014). Paying attention to smell: cholinergic signaling in the olfactory bulb. Front Synaptic Neurosci *6*, 21.

Gabor, C.S., Phan, A., Clipperton-Allen, A.E., Kavaliers, M., and Choleris, E. (2012). Interplay of oxytocin, vasopressin, and sex hormones in the regulation of social recognition. Behavioral Neuroscience *126*, 97–109.

Gold, P.E., Countryman, R.A., and Dukala, D. (2011). Acetylcholine release in the hippocampus and prelimbic cortex during acquisition of a socially transmitted food preference. Neurobiol Learn Mem *96*, 498–503.

Haga, S., Hattori, T., Sato, T., Sato, K., Matsuda, S., Kobayakawa, R., Sakano, H., Yoshihara, Y., Kikusui, T., and Touhara, K. (2010). The male mouse pheromone ESP1 enhances female sexual receptive behaviour through a specific vomeronasal receptor. Nature *466*, 118–122.

Hanke, W., Mamasuew, K., Biel, M., Yang, R.-B., and Fleischer, J. (2013). Odorant-evoked electrical responses in Grueneberg ganglion neurons rely on cGMP-associated signaling proteins. Neuroscience Letters *539*, 38–42.

Ikemoto, S. (2007). Dopamine reward circuitry: two projection systems from the ventral midbrain to the nucleus accumbens-olfactory tubercle complex. Brain Res Rev *56*, 27–78.

Isogai, Y., Si, S., Pont-Lezica, L., Tan, T., Kapoor, V., Murthy, V.N., and Dulac, C. (2011). Molecular organization of vomeronasal chemoreception. Nature *478*, 241–245.

Kobayakawa, K., Kobayakawa, R., Matsumoto, H., Oka, Y., Imai, T., Ikawa, M., Okabe, M., Ikeda, T., Itohara, S., Kikusui, T., et al. (2007). Innate versus learned odour processing in the mouse olfactory bulb. Nature *450*, 503–508.

Leinders-Zufall, T., Cockerham, R.E., Michalakis, S., Biel, M., Garbers, D.L., Reed, R.R., Zufall, F., and Munger, S.D. (2007). Contribution of the receptor guanylyl cyclase GC-D to chemosensory function in the olfactory epithelium. Proc Natl Acad Sci USA *104*, 14507–14512.

Lin, W., Margolskee, R., Donnert, G., Hell, S.W., and Restrepo, D. (2007). Olfactory neurons expressing transient receptor potential channel M5 (TRPM5) are involved in sensing semiochemicals. Proc Natl Acad Sci USA *104*, 2471–2476.

Lucas, P., Ukhanov, K., Leinders-Zufall, T., and Zufall, F. (2003). A diacylglycerol-gated cation channel in vomeronasal neuron dendrites is impaired in TRPC2 mutant mice: mechanism of pheromone transduction. Neuron *40*, 551–561.

Martínez, A.V., and Baxter, M.G. (2002). Selective lesions of basal forebrain cholinergic neurons produce anterograde and retrograde deficits in a social transmission of food preference task in rats. European Journal of Neuroscience *16*, 983–998.

Matsuo, T., Hattori, T., Asaba, A., Inoue, N., Kanomata, N., Kikusui, T., Kobayakawa, R., and Kobayakawa, K. (2015). Genetic dissection of pheromone processing reveals main olfactory system-mediated social behaviors in mice. Proc Natl Acad Sci USA *112*, E311–E320.

Miyamichi, K., Amat, F., Moussavi, F., Wang, C., Wickersham, I., Wall, N.R., Taniguchi, H., Tasic, B., Huang, Z.J., He, Z., et al. (2011). Cortical representations of olfactory input by trans-synaptic tracing. Nature *472*, 191–196.

Munger, S.D., Leinders-Zufall, T., McDougall, L.M., Cockerham, R.E., Schmid, A., Wandernoth, P., Wennemuth, G., Biel, M., Zufall, F., and Kelliher, K.R. (2010). An olfactory subsystem that detects carbon disulfide and mediates food-related social learning. Curr Biol *20*, 1438–1444.

Nunez-Parra, A., Maurer, R.K., Krahe, K., Smith, R.S., and Araneda, R.C. (2013). Disruption of centrifugal inhibition to olfactory bulb granule cells impairs olfactory discrimination. Proc Natl Acad Sci USA *110*, 14777–14782.

Papes, F., Logan, D.W., and Stowers, L. (2010). The Vomeronasal Organ Mediates Interspecies Defensive Behaviors through Detection of Protein Pheromone Homologs. Cell *141*, 692–703.

Pérez-Gómez, A., Bleymehl, K., Stein, B., Pyrski, M., Birnbaumer, L., Munger, S.D., Leinders-Zufall, T., Zufall, F., and Chamero, P. (2015). Innate Predator Odor Aversion Driven by Parallel Olfactory Subsystems that Converge in the Ventromedial Hypothalamus. Curr Biol 1–8.

Reimer, J., Froudarakis, E., Cadwell, C.R., Yatsenko, D., Denfield, G.H., and Tolias, A.S. (2014). Pupil fluctuations track fast switching of cortical states during quiet wakefulness. Neuron *84*, 355–362.

Risold, P., and Swanson, L. (1997). Connections of the rat lateral septal complex. Brain Res Rev *24*, 115–195.

Sheehan, T.P., Chambers, R.A., and Russell, D.S. (2004). Regulation of affect by the lateral septum: implications for neuropsychiatry. Brain Res Rev *46*, 71–117.

Talishinsky, A., and Rosen, G.D. (2012). Systems Genetics of the Lateral Septal Nucleus in Mouse: Heritability, Genetic Control, and Covariation with Behavioral and Morphological Traits. PLoS ONE *7*, e44236.

van der Kooij, M.A., and Sandi, C. (2012). Social memories in rodents: Methods, mechanisms and modulation by stress. Neuroscience & Biobehavioral Reviews *36*, 1763–1772.

Wachowiak, M. (2011). All in a Sniff: Olfaction as a Model for Active Sensing. Neuron *71*, 962–973.

Wesson, D.W. (2010). Sniffing out the contributions of the olfactory tubercle to the sense of smell: hedonics; sensory integration; and more? Neuroscience & Biobehavioral Reviews.

Wesson, D.W., and Wilson, D.A. (2011). Sniffing out the contributions of the olfactory tubercle to the sense of smell: Hedonics, sensory integration, and more? Neuroscience & Biobehavioral Reviews *35*, 655–668.

Wiltschko, A.B., Johnson, M.J., Iurilli, G., Peterson, R.E., Katon, J.M., Pashkovski, S.L., Abraira, V.E., Adams, R.P., and Datta, S.R. (2015). Mapping Sub-Second Structure in Mouse Behavior. Neuron *88*, 1121–1135.

Zaborszky, L., van den Pol, A., and Gyengesi, E. (2012). The Basal Forebrain Cholinergic Projection System in Mice. In The Mouse Nervous System, (Elsevier), pp. 684–718.

Zheng, L.M., and Jourdan, F. (1988). Atypical olfactory glomeruli contain original olfactory axon terminals: An ultrastructural horseradish peroxidase study in the rat. Neuroscience *26*, 367–378.